DEVELOPMENT OF NOVEL HOLLOW FIBER MEMBRANES FOR FORWARD OSMOSIS APPLICATIONS

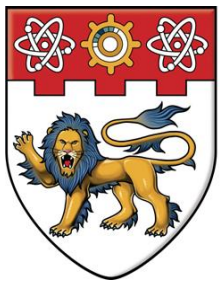

NANYANG TECHNOLOGICAL UNIVERSITY

DEVELOPMENT OF NOVEL HOLLOW FIBER MEMBRANES FOR FORWARD OSMOSIS APPLICATIONS

LAURENTIA E.K. SETIAWAN

SCHOOL OF CIVIL AND ENVIRONMENTAL ENGINEERING

2012

LAURENTIA E.K. SETIAWAN

2012

DEVELOPMENT OF NOVEL HOLLOW FIBER MEMBRANES FOR FORWARD OSMOSIS APPLICATIONS

LAURENTIA E.K. SETIAWAN

SCHOOL OF CIVIL AND ENVIRONMENTAL ENGINEERING

A thesis submitted to the Nanyang Technological University
in partial fulfillment of the requirement for the degree of
Doctor of Philosophy

2012

ACKNOWLEDGEMENTS

This thesis would not have been possible without the guidance and help of many people who contributed and extended their valuable assistance in the preparation and completion of this study.

First of all, it is my great pleasure writing this acknowledgement to express my gratitude to my supervisor, Associate Professor Wang Rong, for the support, guidance and advice she has extended to me throughout my study. I am sincerely and heartily grateful to her for her encouragements and patience. It would not have been possible without her help.

I would like to acknowledge the Environment and Water Industry Programme Office (EWI) of Singapore for funding the project (#EWI RFP 08/01). I am also grateful to Nanyang Technological University for providing my scholarship and to the Singapore Membrane Technology Centre (SMTC) for providing the necessary facilities.

I sincerely thank Prof. Li Kang (Imperial College London) for the constructive comments and discussions, Prof. William B. Krantz (visiting professor in SMTC) for the helpful workshops and suggestions, Prof. Anthony G. Fane as the SMTC director, and qualification exam reviewer committee, Prof. Chiew Yee Meng, Assistant Prof. Philip Wong and Associate Prof. Wang Kean, for their kind suggestions and comments.

It is a pleasure to thank everyone for their help, support and sharing throughout my research work. I would like to thank Dr. Shi Lei for his guidance in various instruments' trainings, Mr. Chou Shuren for his help in experiments, Ms. Susan Sulaiman Lay for her kind assistance, Dr. Filicia Wicaksana for many advices and microscope training, Dr. Qiu Changquan for his advices and SMTC Laboratory Manager Dr. Chong Tzyy Haur for his involvement and guidance in laboratory safety and equipment purchasing.

Many thanks are also due to FYP/NEMS Students: Mr. Jackson Cwa Xing Long (2010), Miss Cheryl Raditya Tanardi (2010), Mr. Chow Chee Chong (2011) and Miss Tan Si Hui (2012) for their diligent assistance.

I am thankful to Mr. Aidil Bin Md Idris, Mr. Yong Fook Yew, Mr. Tan Han Khiang, Mrs. Koh Tang Lai Sim, Ms Maria Chong and other staff in CEE Environment Laboratory for helping me out with various purchasing and equipment usage. Many thanks are due to Mr. Gabriel Goh from NEWRI office for his kind assistance in purchasing and admin works.

It is difficult to find words to express my appreciation to my friends and colleagues for their lovely companionships and helps. Special thanks to my office and lab buddies as well as my group mates: Goh Shuwen, Wei Jing, Stannislaus Raditya Soewarno, Amir Hooshang Taheri, Ebrahim Akhondi, Zhou Jin, Yang Xing, Loh Chun Heng, Zhang Yuan, Li Xue Song, Zuo Guangzhi, Dr. Rajabzadeh K.Saeid, Dr. Yogesh B. Singh, Dr. Yelyzaveta Arkhangelsky, Sunee Wongchitphimon, Liu Chang, Fang Wangxi, Liao Yuan, Tian Miao. It is my pleasure to be part of SMTC family so that I have had an enjoyable PhD life.

Last but not least, this thesis is dedicated to my beloved parents and godmother who always support me in my endeavors, always give me strength and encouragement to pursue my dreams and never leave me in doubt of their love for me.

Laurentia E.K. Setiawan

LIST OF PUBLICATIONS

- *Journals*

1. **L. Setiawan**, R. Wang, S.H. Tan, L. Shi, A.G. Fane, Fabrication of poly(amide-imide)-polyethersulfone dual layer hollow fiber membranes applied in forward osmosis by combination of polyelectrolyte cross-linking and depositions, Desalination, submitted (2012)
2. **L. Setiawan**, L. Shi, W.B. Krantz, R. Wang, Explorations of delamination and irregular structure in poly(amide-imide)-polyethersulfone dual layer hollow fiber membranes, Journal of Membrane Science (2012) http://dx.doi.org/10.1016/j.memsci.2012.07.030
3. **L. Setiawan**, R. Wang, L. Shi, K. Li, A.G. Fane, Novel dual-layer hollow fiber membranes applied for forward osmosis process, Journal of Membrane Science 421-422 (2012) 238-246
4. **L. Setiawan**, R. Wang, K. Li, A. G. Fane, Fabrication and characterization of forward osmosis hollow fiber membranes with antifouling NF-like selective layer, Journal of Membrane Science, 394-395 (2012) 80-88
5. **L. Setiawan**, R. Wang, K. Li, A. G. Fane. Fabrication of novel poly(amide–imide) forward osmosis hollow fiber membranes with a positively charged nanofiltration-like selective layer, J Membrane Sci. 369 (2011) 196-205
6. C. Qiu, **L. Setiawan**, R. Wang, CY Tang, A.G. Fane, High performance flat sheet forward osmosis membrane with an NF-like selective layer on a woven fabric embedded substrate, Desalination, 287 (2012) 266–270
7. W. Fang, R. Wang, S. Chou, **L. Setiawan**, A.G. Fane, Composite forward osmosis hollow fiber membranes: Integration of RO- and NF-like selective layers to enhance membrane properties of anti-scaling and anti-internal concentration polarization, Journal of Membrane Science, 394-395 (2012) 140-150

8. Y. Zhang, R. Wang, SL Yi, **L. Setiawan**, X Hu, A.G. Fane, Novel chemical surface modification to enhance hydrophobicity of polyamide-imide (PAI) hollow fiber membranes, Journal of Membrane Science, 380 (2011), 241-250

- *Conferences*

1. **Laurentia Setiawan**, Shi Lei, William B. Krantz, Wang Rong, 'Exploration of delamination in dual-layer hollow fiber membranes', The 22nd Annual Meeting North American Membrane Society (NAMS), New Orleans, LA – USA, 9-13 June 2012 (Oral presentation)
2. **Laurentia Setiawan**, Rong Wang, 'Development of novel dual layer hollow fiber membranes applied for forward osmosis application', The Asia-Oceania Top University League on Engineering (AOTULE) - 2011, Beijing – China, 10−12 October 2011 (Oral presentation)
3. **Laurentia Setiawan**, Rong Wang, Anthony G. Fane. 'Development of poly(amide-imide) nanofiltration hollow fiber membrane applied in forward osmosis application', The 6th conference of the Aseanian Membrane Society/The 7th International Membrane Science and Technology Conference (AMS6/IMSTEC10), Sydney – Australia, 22-26 November 2010 (Oral presentation)
4. **Laurentia Setiawan**, Rong Wang. 'Polyelectrolyte modification of poly(amide-imide) hollow fiber membrane for nanofiltration', Young Water Talents Symposium, Singapore, 28 June 2010 (Oral presentation)
5. Lei Shi, **Laurentia Setiawan**, Rong Wang, Anthony G. Fane, 'Development of novel composite dual-layer nanofiltration hollow fiber membranes for water softening at low operation pressure', The 22nd Annual Meeting North American Membrane Society (NAMS), New Orleans, LA – USA, 9-13 June 2012

- *Patents*

1. R. Wang, **L. Setiawan**, L.Shi, A.G. Fane (2012). "Novel dual-layer forward osmosis hollow fiber membranes with a positively charged nanofiltration-like selective layer", NTU Technical Disclosure, #TD/045/12, March 2012.
2. R. Wang, W. Fang, S. Chou, **L. Setiawan**, A.G. Fane (2011). "Composite forward osmosis hollow fiber membranes: integration of RO- and NF-like two selective skins for high performance", NTU Technical Disclosure # TD/169/11, Application number 61/607,180, Oct. 2011.
3. R. Wang, **L. Setiawan**, A.G. Fane (2010). "Poly(amide-imide) forward osmosis hollow fiber membranes with a positively charged nanofiltration-like selective layer". US provisional number: 61/417,758, TD/138/10

TABLE OF CONTENTS

LIST OF TABLES

LIST OF FIGURES

LIST OF SYMBOLS

A	Water permeation coefficient of the membrane (l/m^2.h.bar)
B	Solute permeation coefficient of the membrane (g/m^2.h)
C	Concentration of all solutes (mol/l)
i	Number of ions produced during dissociation of solute, called dissociation factor of Van't Hoff
J_s	Salt permeability (g/m^2.h)
J_v, J_w	Water permeability (l/m^2.h)
ΔG_{mix}	Gibbs free energy of mixing
P	Pressure (bar)
PWP	Pure water permeability (l/m^2.h.bar)
ΔP	Hydrostatic pressure difference across the membrane, bar
R	Universal gas constant, 8.314 x 10^{-2} (l bar/K.mol)
S	Structural parameter
T	Absolute temperature (K)

Greek

δ	Total solubility parameter (MPa)$^{1/2}$
$\Delta\delta$	Total solubility parameter difference (MPa)$^{1/2}$
ε	Porosity of the membrane
ϕ	Osmotic coefficient which distinguishes the difference of solvent from ideal behavior referenced to Raoult's law
ϕ_2	Volume fraction of polymer
π	Osmotic pressure (bar)
$\Delta\pi$	Osmotic pressure gradient across the membrane (bar)
π_{DS}	Osmotic pressure of the draw solution
$\Delta\pi_{eff}$	Effective osmotic pressures difference
π_F	Osmotic pressures of the feed solution
$\Delta\pi_m$	Membrane (bulk) osmotic pressures difference
τ	Tortuosity of the support layer

ABSTRACT

Forward osmosis (FO) process has been gaining popularity in recent years as a potential alternative to pressure-driven membrane processes such as reverse osmosis (RO) for water desalination and wastewater reclamation. However, the main drawback of FO system is permeate flux decline due to internal concentration polarization (ICP) when conventional RO membranes are used. The only commercially available FO flat sheet membrane developed by Hydration Technologies Inc (HTI) presented low water permeation flux. Therefore, the development of novel FO membranes with optimized structure to reduce ICP has become a critical issue to facilitate FO practical applications.

In this study, single layer asymmetric microporous hollow fiber membranes were fabricated using Torlon polyamide-imide (PAI) material as the porous support followed by a simple polyelectrolyte cross-linking using polyethyleneimine (PEI) to produce hollow fiber membranes with a positively charged nanofiltration (NF)-like selective layer. The newly developed PAI hollow fiber membranes show a pure water permeability of 2.19-2.25 l/m^2.h.bar and reasonable NaCl and $MgCl_2$ rejections of 49% and 94% at 1 bar, respectively. It is also found that in FO processes, when using 0.5 M $MgCl_2$ as a draw solution and de-ionized (DI) water as the feed in the active layer facing feed water (AL-FW) configuration at 23°C, the water fluxes of two PAI FO hollow fiber membranes are 8.36 and 9.74 l/m^2.h, respectively, and the salt to water flux ratio (J_s/J_v) of the two membranes is smaller than 0.4 g/l, which is lower than the data of 0.85 g/l for commercial HTI FO membrane. Different from a neutral membrane, the positively charged FO membrane provides double electric repulsions to the salt transfer through the membrane in the AL-FW configuration, leading to a reduction of salt penetration, while in the active layer facing draw solution (AL-DS) configuration, the positive charges facilitate salt transportation. This study provides a simple and effective approach to make hollow fibers with a NF-like skin suitable for FO applications.

An improvement for the single layer PAI hollow fiber membranes has been carried out by incorporating a negatively charged polyelectrolyte layer on the selective skin, aiming to enhance membrane antifouling property. This new type of PAI FO membrane possesses pure water permeability of 3.7-4.3 $l/m^2.h.bar$ and Na_2SO_4 rejection up to 85% at 1 bar. In the FO process, the membranes can achieve water flux of 17 and 12 $l/m^2.h$ for the AL-DS and AL-FW configurations, respectively, using a 2000 ppm Na_2SO_4 aqueous solution as the feed and 0.5 M Na_2SO_4 as the draw solution. When the feed contained 1000 ppm bovine serum albumin (BSA) and 2000 ppm Na_2SO_4, a steady water flux of 11 $l/m^2.h$ can be maintained using 0.5 M Na_2SO_4 as the draw solution at ambient temperature of 23 °C. The approach of making FO membranes developed in this study offers the advantages of simple fabrication process, tailorable selective layer and promising membrane performance for protein-contained wastewater treatment by FO process.

Despite the fact that the membranes developed by means of simple post-chemical treatments exhibited a high water flux and high salt rejection in the FO process, the chemical cross-linking through entire PAI substrate still resulted in a dense structure which adversely affected the water flux. To overcome the drawback of cross-linking modification on entire PAI membrane, a dual-layer hollow fiber with PAI polymer as the outer layer, supported by an inner layer made of other material inert to PEI polyelectrolyte, was designed and fabricated.

However, obtaining a good lamination between the two layers as well as a regular morphology is critical to fabricate a usable dual layer hollow fiber membrane. Simultaneous extrusion of PAI and polyethersulfone (PES) dope solutions was carried out by using a triple orifice spinneret. Thermodynamic properties and phase separation kinetics of the polymer dopes as well as various spinning parameters were carefully tailored in order to investigate the evolution of the membrane morphology and structure. A series of experiments have confirmed that when the external coagulant (water) has a higher diffusion rate in the outer layer than in the inner layer, the outer layer tends to expand to form large macrovoids and to hold more water at the interface. As a result, the accumulated water probably impedes the adhesion of the two layers, leading to a delamination of two layers. On the other hand, if water has a slower penetration rate through the outer layer dope than the inner layer dope, a good

adhesion between these two layers is expected. Under this scenario, since macrovoids may form in the inner layer leading to the expansion of the inner layer, a distortion of the finger-like structure/macrovoids in the inner and an irregularity of the inner contour may occur. This study provides a solid foundation to develop superior dual layer hollow fiber membranes with an inter-penetrating dual layer structure.

After obtaining good asymmetric microporous PAI/PES dual-layer hollow fibers, PEI modification on the outer PAI layer was applied to produce a NF-like thin layer, while the PES porous inner layer remained intact as PES is inert to PEI. It was found that the resultant dual-layer NF hollow fiber membrane can achieve pure water permeability of 15.9 l/m^2.h.bar and a high rejection to divalent cations up to 89%. In FO process, the dual-layer hollow fiber exhibited a water flux of 40 l/m^2.h and J_s/J_v of 0.35 g/l in the orientation of active layer facing draw solution by using 0.5M $MgCl_2$ as draw solution and DI water as feed at room temperature. The newly developed dual layer hollow fibers outperform all the single layer and dual-layer NF hollow fibers reported in the literature for FO applications.

In conclusion, this thesis presents the development of novel FO hollow fiber membranes based on the studies of the fundamental mechanisms of membrane chemical treatments, dual-layer membrane formation and mass transfer across charged FO membranes with a NF-skin layer. This work contributes to the development of membrane fabrication technology and facilitates the practical applications of forward osmosis membrane processes.

CHAPTER 1

Introduction

1.1. Background

Water is one of the most essential elements for all living organisms on earth. For example, 55-60% of human body is water. With just a 2 liter loss of water, we can suffer from dehydration. It is very important to manage our water needs wisely for human health, environment, agriculture and industries. With water scarcity that has already affected many countries and the prediction of the world's population growth from 6.1 billion in 2000 to 8.9 billion in 2050 (United-Nations 2004), the existing water supply may not be sufficient to fulfill the world's demand. Ironically, 70% of the earth surface is covered by water, but 97% of this water is in the ocean (salt water) and only 3% is fresh water. Two-third of the planet's fresh water is locked up in the glacier and polar ice caps. Another one-third comprises underground water in aquifers and wells, and surface water in rivers and lakes. Therefore, only less than 1% of naturally-available fresh water can be used for daily life, environments, industries and agricultures, etc. Nowadays, our water resources have been contaminated and continuously being depleted. These water problems have stimulated people to discover alternative water production means, such as wastewater reclamation and seawater desalination. Innovative membrane-based technologies show the most potential in solving the water scarcity problems (McGinnis and Elimelech 2007).

A membrane, essentially defined as a barrier, separates two phases and restricts the transport of various particles, molecules, or substances in a selective manner. Membranes have been used for more than three decades especially for water treatment and water production including wastewater treatment and reclamation as well as desalination for seawater and brackish water. They can be made in different configurations such as flat-sheet, tubular and hollow fiber membranes. Among these, hollow fibers are the most efficient configuration with a large surface area per volume, suggesting that they can handle a large volume of water while utilizing a minimum

space (Mulder 1996; Veríssimo, Peinemann *et al.* 2005b). Also, hollow fiber membranes are mechanically self-supporting while flat sheet membranes require extra support materials (Liu, Xu *et al.* 1991). Moreover, due to their structural integrity and construction, hollow fiber membranes can withstand certain permeate back pressures thus allowing flexibility in system design and operation. In addition, the advantage of the hollow fiber geometry over flat sheet membranes includes that it is easy to produce modules containing thousands of fibers, which can then be assembled as required in a large-scale set-up with a less demanding of pretreatment and maintenance than the spiral wound module (Veríssimo, Peinemann *et al.* 2005a).

Hollow fiber membrane fabrication via phase inversion, especially non-solvent induced phase separation (NIPS) technique, is an area that has been widely explored by many researchers (Cabasso, Klein *et al.* 1976; Chung, Kafchinski *et al.* 1992; Wienk, Teunis *et al.* 1993; Niwa, Kawakami *et al.* 2000; Albrecht, Weigel *et al.* 2001; Khayet, Feng *et al.* 2002; Nijdam, De Jong *et al.* 2005; Shi, Wang *et al.* 2007; Setiawan, Wang *et al.* 2011). Good membranes have to meet a number of criteria. They should present high water permeability, high solute rejection, good thermal stability, high resistance to a wide variety of chemical substances over a wide pH range, and high mechanical strength to withstand pressure during long term processes. The membranes should also exhibit appropriate features of surface chemistry to minimize the tendency of various fouling and scaling.

Conventional desalination and reclamation, based on reverse osmosis (RO), requires substantial energy to push the pure water from seawater or wastewater through a semi-permeable membrane. In recent years, a new desalination process which is potentially more efficient and requires less energy as compared to RO has drawn much attention (Cath, Childress *et al.* 2006). This so-called forward osmosis (FO) is a natural process, where water moves automatically from a low concentration side to the high concentration side through a semi-permeable membrane under the driving force of osmotic pressure difference across the membrane.

Presently, most available membranes used in the FO process are dense semi-permeable membranes that were originally designed for pressure driven RO process (Cath, Childress *et al.* 2006). These RO membranes have an asymmetric structure, typically

consisting of a thin selective active layer supported by thick layers of porous polymer and fabric. There is only one commercialized FO membrane developed by Osmotek Inc. (now known as Hydration Technologies Inc. (HTI)) (Herron 2008). This proprietary membrane is made of cellulose triacetate with a thickness of less than 50 μm supported by embedded polyester mesh. In 2007, a polybenzimidazole (PBI) nanofiltration (NF) hollow fiber membrane has been tested for its performance in forward osmosis (Wang, Chung *et al.* 2007). Research interest in forward osmosis (FO) membrane development has been rising steadily in recent years (Tang and Ng 2008; Garcia-Castello, McCutcheon *et al.* 2009; Chou, Shi *et al.* 2010; Yip, Tiraferri *et al.* 2010; Tiraferri, Yip *et al.* 2011; Wei, Qiu *et al.* 2011; Zhang, Wang *et al.* 2011; Fang, Wang *et al.* 2012; Su, Chung *et al.* 2012).

The commercial FO flat sheet membrane is able to achieve better performance than RO membranes, but it exhibits flux reductions. The lower-than-expected flux is attributed to the presence of internal and external concentration polarization (CP) during the mass transport process, which significantly reduces the effective osmotic driving force. The CP phenomena are associated with solute physical properties, fluid dynamics and, most significantly, the membrane structure. The external CP can be controlled hydrodynamically but the internal CP occurs in the porous support layer of the membrane, making it difficult to handle. Thus, the key challenge is to produce a membrane that can minimize the internal CP - the main cause of the substantial flux decline. Therefore, a desirable FO membrane should have (i) a dense active layer for high solute rejection, (ii) hydrophilic surface for flux enhancement and fouling reduction, and (iii) high porosity of the thin support layer to reduce internal concentration polarization (Cath, Childress *et al.* 2006; Wang, Shi *et al.* 2010).

1.2. Objectives

This study aims at developing an enabling technology to fabricate hollow fiber membranes for FO applications. The primary objectives are to

- develop a simple and effective method to make single-layer hollow fiber membranes with a nanofiltration (NF)-like selective layer as a basic step for forward osmosis application:

- to synthesize and characterize asymmetric ultrafiltration (UF) hollow fiber membranes as the substrate with an optimal structure
- to perform chemical modification on the substrate in order to form a charged NF-like selective layer by cross-linking and multilayer polyelectrolyte deposition

➢ fabricate and characterize dual layer hollow fiber membranes in order to elucidate the mechanisms associated with the lamination/delamination of outer and inner layers as well as regular/irregular cross-section and macrovoids morphology

➢ develop dual layer hollow fiber membranes with a NF-like selective layer intended for use in FO process

➢ assess the FO performance of dual layer hollow fiber membrane with a NF-like selective layer

1.3. Thesis outline

This thesis includes 7 chapters, which are highlighted as follows:

Chapter 1: ***Introduction*** - Background information and the objectives of the study are provided.

Chapter 2: ***Literature review*** - This chapter is divided into two parts. The first part is the review of FO technology. It starts with the introduction of FO concept followed by its potential applications and the challenges for developments. The current status of FO membrane fabrication is also reviewed. The second part of the literature study is the development of FO hollow fiber membranes with a NF-like selective layer. In this part, the fundamental study of phase inversion method for asymmetric membrane preparation is provided. This is then followed by a more specific review concerning fabrication of asymmetric hollow fiber substrates via dry jet-wet spinning technique. Development of NF-like selective layer, subsequently, was followed to end this chapter.

Chapter 3: ***Fabrication of novel PAI FO hollow fiber membranes with a positively charged NF-like selective layer*** - This chapter begins with a brief review of the FO membranes with NF-like skin. Single layer PAI hollow fiber membranes were fabricated followed by a simple cross-linking modification to impart positive charges on the membrane surface. The discussion on the effects of cross-linking modification conditions on the membrane intrinsic properties such as pure water permeanility (PWP) and salt rejections, as well as FO performance were conducted based a series of experimental results.

Chapter 4: ***Fabrication and characterization of FO hollow fiber membranes with antifouling NF-like selective layer*** - Single layer PAI hollow fiber substrates were modified by chemical cross-linking and multilayer polyelectrolyte deposition. The additional step of the polyelectrolyte deposition aims to enhance membrane antifouling property. The FO performance for the feed containing protein foulant was evaluated to observe the effect of the modification.

Chapter 5: ***Explorations of delamination and irregular structure in PAI-PES dual layer hollow fiber membranes*** - A fundamental study of PAI-PES dual layer hollow fiber fabrication was presented in this chapter. A series of experiments was performed and the results were discussed on how to eliminate delamination and irregular structure, which are the main challenges in order to obtain a good dual layer hollow fiber membrane.

Chapter 6: ***Novel dual-layer hollow fiber membranes applied for FO process*** - Based on the understanding of the delamination mechanism, a good dual layer PAI-PES UF hollow fiber was fabricated and used for PEI polyelectrolyte modification. Since the chemical cross-linking only occurred on the thin outer PAI layer, while the inner layer made of PES is inert to PEI polyelectrolyte, a high water flux in the FO process is anticipated. FO experiments were performed to confirm the merit of the dual-layer membranes.

Chapter 7: ***Conclusions and recommendations*** - The important findings of this study and recommendations for future work are made in this chapter.

CHAPTER 2

Literature Review

This review begins with the theoretical background of forward osmosis process, the applications and the challenges, followed by the current status of FO membranes in terms of characteristics and performance. After this, the preparation of asymmetric membranes by phase inversion specifically for hollow fiber membrane fabrications via dry jet-wet spinning technique has been discussed in details. In the final section, a review of selective membrane surface preparation is provided.

2.1. Forward osmosis

2.1.1. Concept of forward osmosis

Nowadays, water desalination and waste water reclamation have become an appealing method to produce fresh water due to water shortage. Reverse osmosis (RO), at present, is one of the most commonly used technologies for desalination and reclamation as it is a more economical process when compared to the traditional thermal process of distillation. However, in RO process, high hydraulic pressure is required to oppose and exceed the osmotic pressure, leading to high energy requirement and consequently, high operational cost. As shown in Figure 2.1, the energy needed for RO is much higher than forward osmosis for seawater desalination.

Osmosis is a natural phenomenon, known as direct osmosis (DO) or forward osmosis (FO) which can be defined as the net movement of water molecules across a semi-permeable membrane from a less concentrated solution to a more concentrated solution. FO process utilizes an osmotic pressure gradient ($\Delta\pi$) as a driving force instead of hydraulic pressure (ΔP). Hence, FO is able to produce water at a reduced cost with high recovery. This phenomenon is the basis of food preservation (Cath, Childress *et al.* 2006).

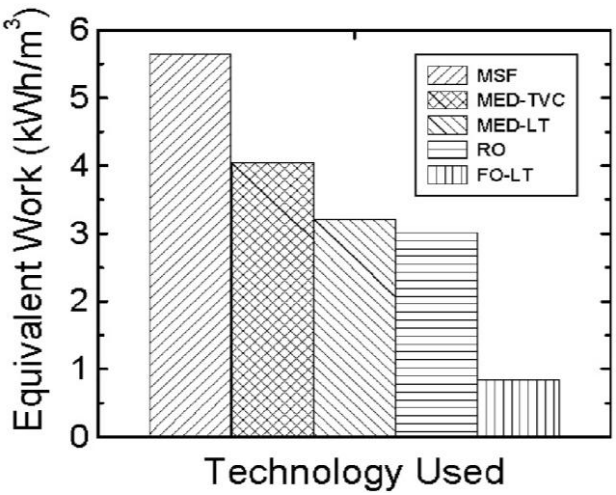

Figure 2.1. Comparison of equivalent work for seawater desalination using various technologies. (MSF: multi-stage flash distillation; MED-TVC: multi effect distillation using thermal vapor compression; MED-LT: multi effect distillation-low temperature; RO: reverse osmosis; FO-LT: single column low temperature vacuum forward osmosis). Adapted from (McGinnis and Elimelech 2007).

Theoretically, osmotic pressure (π) can be calculated (Wilkinson 1997):

$$\pi = i\phi C R T \tag{2.1}$$

where i is the number of ions produced during dissociation of solute, called dissociation factor of Van't Hoff, ϕ is osmotic coefficient which distinguishes the difference of solvent from ideal behavior referenced to Raoult's law, C is concentration of all solutes, R is gas constant, T is absolute temperature. Based on Equation 2.1, it is important to note that the osmotic pressure depends on the molar concentration.

Figure 2.2 shows membrane classification based on osmotic power. Membrane filtration can be classified as follows: (a) Forward osmosis (FO) which uses osmotic pressure gradient ($\Delta\pi$) as the driving force (hydraulic pressure (ΔP) = 0). Product water thus flows from a less concentrated feed (F) to a more concentrated draw solution (DS); (b) Pressure retarded osmosis (PRO) which applies a hydraulic pressure lower than the osmotic pressure to the draw solution side. The net water flux is in the direction toward the draw solution (same as FO) (Lee, Baker *et al.* 1981; Achilli, Cath *et al.* 2009a); (c) Reverse osmosis (RO) that utilizes hydraulic pressure to overcome the osmotic pressure difference ($\Delta P > \Delta\pi$). Consequently, the net water flux flows from

a concentrated feed (F) to the permeate (P) side. The net water flux, J_v, across a membrane is given by (Lee, Baker *et al.* 1981):

$$J_v = A(\Delta\pi - \Delta P) \tag{2.2}$$

where A is water permeation coefficient of the membrane, $\Delta\pi$ is the osmotic pressure gradient across the membrane and ΔP is the hydrostatic pressure difference across the membrane.

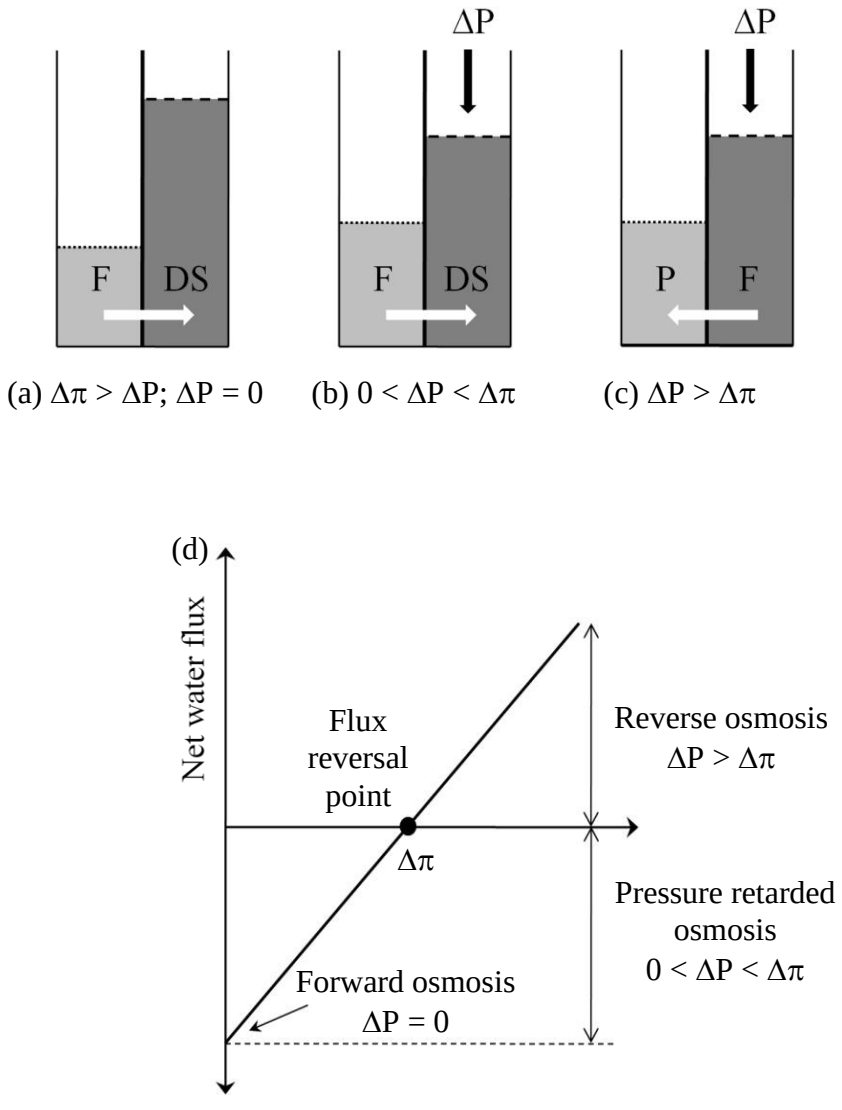

Figure 2.2. Membrane classification based on osmotic power: (a) FO; (b) PRO; (c) RO (arrow indicates the direction of solvent flow); (d) The relationship between FO, PRO, and RO for an ideal semi permeable membrane. Figure was adapted from (Lee, Baker *et al.* 1981).

2.1.2. FO applications and challenges

FO has been utilized in many areas from water production and water treatment to pharmaceutical and food industries as well as hybrid system of FO and other technologies (i.e. membrane bioreactor, RO) to achieve a better performance. For instance, a novel membrane bioreactor (MBR) system which utilizes a submerged FO membrane in the bioreactor, called osmotic membrane bioreactor (OMBR) has been developed (Achilli, Cath *et al.* 2009b). Results demonstrated that OMBR required substantially less backwashing and has higher total organic carbon (TOC) removal efficiencies as compared to conventional MBRs. Moreover, McGinnis introduced a closed cycle osmotic heat engine based on the principles of natural osmosis for renewable power generation (McGinnis, McCutcheon *et al.* 2007). The system uses an ammonia-carbon dioxide as draw solution (DS) and deionized water as working fluid (feed).

There are two major challenges in FO. One is the suitable draw solution. FO uses a particular draw solution to generate an osmotic pressure gradient across a semi-permeable membrane. Water will naturally diffuse through the membrane from the feed side into the draw solution side. The next challenging step is how to separate the clean water from the draw solution. There are some criteria for an ideal draw solution: (i) It should have a significantly higher osmotic pressure than feed water on the opposite side. Thus, the system will possess high water flux and high feed water recoveries (McCutcheon, McGinnis *et al.* 2005); (ii) The separation of water from the draw solution should be easy (McCutcheon, McGinnis *et al.* 2005); (iii) The draw solution must be able to be re-generated and reused easily and economically (Cornelissen, Harmsen *et al.* 2008); (iv) The draw solution should be non-toxic and chemically compatible with membrane materials (Cornelissen, Harmsen *et al.* 2008); (v) The Solutes in the draw solution must have high diffusivity in liquids and low permeability through the selective layer of the membrane (Hancock and Cath 2009). Several solutions have been considered as draw solutions such as magnesium chloride, sodium chloride, sucrose, ammonium bicarbonate, etc. Among these solutions, magnesium chloride has the highest osmotic pressure for the same concentration as shown in Figure 2.3.

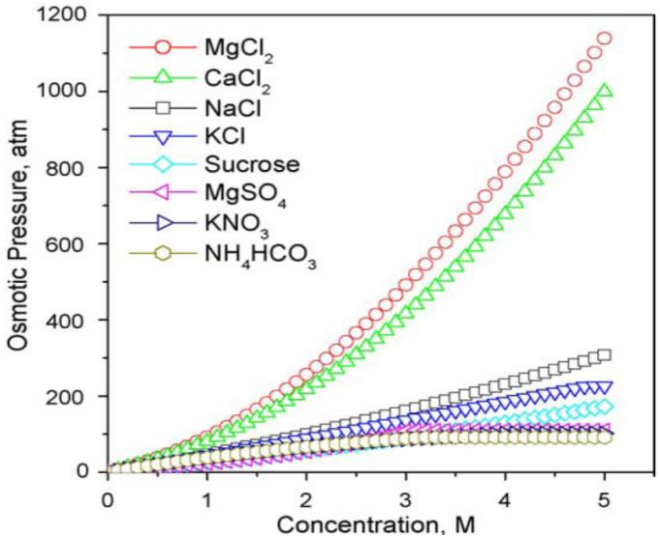

Figure 2.3. Osmotic pressure generate from various salt as draw solution as a function of concentration. Adapted from (Cath, Childress *et al.* 2006).

The development of suitable draw solutions for FO process has been carried out as early as 1965 by Batchelder who employed a volatile solute (e.g. sulfur dioxide, ammonia, sodium sulfite). The product water could be recovered by heating and/or air stripping of the volatile solute (Batchelder 1965). Moreover, in 1972, Frank used chemically precipitable soluble salts (e.g. aluminium sulfate, magnesium sulfate, manganese sulfate) as the draw solution (Frank 1972). Hypertonic glucose solution (Kravath and Davis 1975) and concentrated fructose solution (Stache 1989) have been used as the draw solution intended for emergency water supplies in the life boat. McGinnis in 2002 utilized a combination of hot saturated potassium nitrate (KNO_3) and dissolved sulfur dioxide (SO_2) at a pressure of 15 atm as the draw solutions (McGinnis 2002). The recovery of the draw solution can be done by crystallization and heating. Furthermore, FO desalination process by using a concentrated ammonium bicarbonate solution as the draw solution has been designed (McCutcheon, McGinnis *et al.* 2005; 2006). In 2010, highly water-soluble magnetic nanoparticles have been used as draw solutes (Ling, Wang *et al.* 2010).

The other challenge is the appropriate membrane which can reduce the effect of concentration polarization (CP). CP is defined as the accumulation of the solutes near the membrane surface as water permeates through a membrane. CP and fouling are the main reasons for flux decline in membrane separation process. CP reduces not only the

net water flux (or increasing trans-membrane pressure) but also the solute retention and leads to fouling. CP is reversible and can be controlled hydro-dynamically (e.g. by velocity adjustment or by closing off the permeate outlet, the accumulated solutes should diffuse back to the bulk). Fouling, on the other hand, is an irreversible deposition or adsorption of solutes onto the membrane surface or into the pores of the membrane. Therefore, fouling can only be removed by cleaning.

Equation 2.2 shows the net water flux in osmotic-driven membrane processes. Concentration buildup near membrane surface during filtration process causes the effective osmotic pressure gradient lower than the bulk osmotic pressure gradient. From this equation, the water flux decreases as the osmotic pressure gradient ($\Delta\pi$) decreases (Sablani, Goosen *et al.* 2001). Based on the location, there are two types of CP: external CP (ECP), which occurs on the outside of membrane, and internal CP (ICP) which occurs within the porous support layer.

Osmotic driven membrane processes (e.g. FO) has both ECP and ICP which is different from reverse osmosis process. Since the driving force of FO process is based on the osmotic pressure gradient ($\Delta P = 0$), membrane fouling led by ECP has a milder effect on net water flux as compared to pressure driven membrane processes. The unfavorable outcome of ECP, nevertheless, can be minimized by increasing the turbulence at the membrane surface (Sablani, Goosen *et al.* 2001; Cath, Childress *et al.* 2006; McCutcheon and Elimelech 2006). However, the adverse effect of ICP (i.e. net water flux decline), which is exclusive to FO process, cannot be minimized by altering hydrodynamic conditions since ICP takes place within the membrane (Gray, McCutcheon *et al.* 2006). Based on membrane orientation, there are two types of ICP: (1) concentrative ICP and (2) dilutive ICP.

Concentrative ICP, as illustrated in Figure 2.4-a, occurs when the active layer is placed against the draw solutions. This orientation is also known as 'PRO mode'. Since the feed is facing the porous support layer, the solute in the feed water goes through the open structure of the porous support when it is carried on by convective water flow that diffuses across the active layer into the draw solutions side. The solute cannot penetrate into the active layer, instead, it will accumulate and lead to a concentration build up within the porous support layer. Dilutive ICP, on the other hand, occurs when

the active layer is placed against the feed water. The pure water that diffuses through the membrane dilutes the draw solution inside the porous support layer (Figure 2.4-b). Therefore, the development of the proper membrane structure which can reduce the effect of ICP is essential.

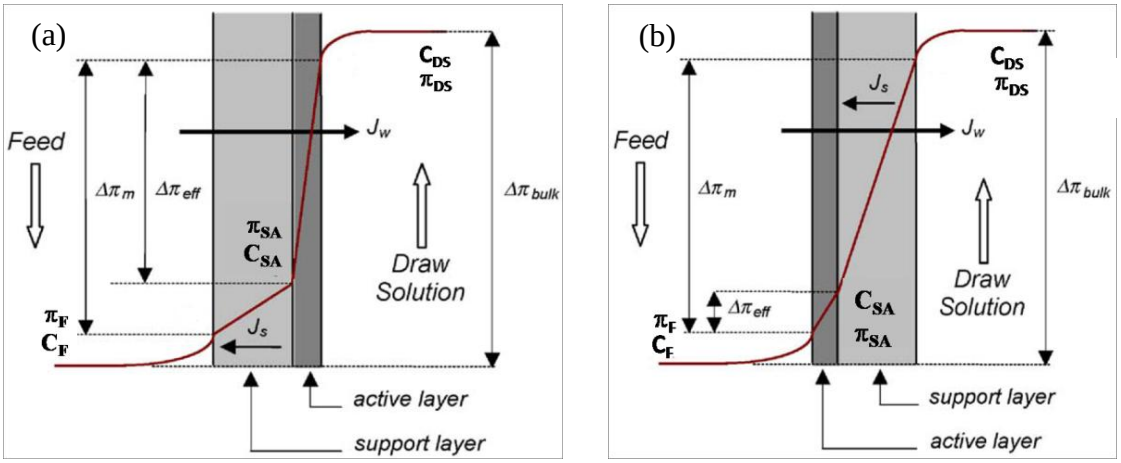

Figure 2.4. Illustration of concentration profile across a composite or asymmetric membrane for internal concentration polarization (ICP) adapted from (Cath, Childress *et al.* 2006) corresponding to membrane orientation: (a) active layer facing draw solution (AL-DS), also known as PRO mode; (b) active layer facing feed water (AL-FW), also known as FO mode.

2.1.3. Current status of FO membranes

Since Loeb-Sourirajan initiated membrane synthesis via phase inversion in 1960s, membrane development is mainly for pressure driven processes (not for osmosis driven). RO membrane, which has a thin selective layer to reject undesired solutes and a thick porous support to give mechanical strength to withstand high pressure and long term operation, is not suitable to be applied in osmosis driven process (McCutcheon, McGinnis *et al.* 2005; Elimelech and Mc Cutcheon 2008; Herron 2008). In RO, mass transfer takes place in the selective layer only. Therefore the possible concentration polarization is ECP as described in Section 2.1.1. In an osmosis driven process (FO), however, mass transfer occurs in both side of the membrane causing ECP and ICP. To overcome this problem, membranes with a new structure should be re-designed. Loeb *et al.* pioneered the investigation of the effect of a support fabric, that was attached at the commercial Loeb-Sourirajan (L-S) type asymmetric membrane, on the osmotic

water flux (Loeb, Titelman *et al.* 1997). It was found that water flux increased in an order of 6 folds for the membranes with the absence of a support fabric.

Furthermore, two RO membranes from GE osmonic (AG and CE) has been compared to FO membranes produced by HTI (CTA) in FO process (McCutcheon, McGinnis *et al.* 2005). Under the same experimental conditions, the CTA membrane had a notably higher water flux than either GE RO membrane. The structure of two RO membranes differed significantly as compared to the FO membrane. AG membrane was made from interfacial polymerization of polyamide on a polysulfone porous support layer (thickness of 50 μm) which was casted on a porous fabric (thickness of 90μm). CE is an integral asymmetric membrane made from cellulose acetate (thickness of 50 μm) supported by a porous fabric (thickness of 90μm). CTA, on the other hand, has an overall thickness of 50 μm which consists of two thin layers of cellulose triacetate on the top and bottom of polyester fabric. In addition to the porous support for FO membranes, the hydrophobicity of the membrane support layer and its effect on water flux in FO and PRO processes has been studied (McCutcheon and Elimelech 2008). The results showed that hydrophobicity of membrane support layer significantly hindered the water flux because of insufficient wetting leading to disruption of water continuity.

Moreover, a proper substrate for FO membrane should have high porosity and excellent pore interconnectivity. Elimelech and McCutcheon utilized nanofiber electrospinning technique to fabricate the support layer of flat sheet FO membranes with high porosity (>80%), good pore interconnectivity (the tortuosity of ~1), and high degree of fiber interconnectivity which increased the mechanical strength (Elimelech and Mc Cutcheon 2008). Therefore, the thickness of the porous layer can be reduced. In addition, nanoparticles has been employed to strengthen the thin porous support layer (Kurth and Burk 2009).

In the past few years, many researchers have worked on fabrication and characterization of forward osmosis membranes. FO membranes, both in hollow fiber and flat sheet configurations, reported in the literature have a dense selective layer and a porous support layer. The selective layer can be RO-like skin or NF-like skin.

- *RO-like skin*

In 2008, Herron invented an integral asymmetric structure of osmosis driven flat sheet membrane (the first commercial FO membrane produced by Hydration Technologies). The membrane consisted of three layers: (1) a skin layer, with a density of > 50% polymer by volume and an average thickness of 8-18 μm; (2) a porous layer made from the same polymeric material as the skin layer, with density of 15-30% by volume and a thickness of 25-75 μm; (3) a hydrophilic support fabric embedded in the porous layer. The skin and porous layers were made from cellulosic material. The resultant membrane had a FO water flux of 22 l/m^2.h (experiment conditions – draw solution: ammonium bicarbonate 6 M, feed: 0.5 M sodium chloride, temperature of 50°C), and salt rejection of 99% (Herron 2008).

Wang *et al.* worked on thin film composite (TFC) FO hollow fiber membranes, made of polyamide on the top of a polyethersulfone (PES) UF substrate. The substrate characteristics were described as follows: (1) molecular weight cut off (MWCO) of 83-88KDa; (2) mean pore size of 12.7 nm; (3) porosity of 75%; (4) pure water permeability (PWP) of 266-271 l/m^2.h.bar. Polyamide as the selective layer (thickness ~600nm) was synthesized on the inner surface of PES hollow fiber substrate. The resulting membrane had the structural parameter (S) of 5.95 x 10^{-4} m, the water permeability (*A*) of 2.19 l/m^2.h.bar and NaCl permeability (*B*) of 0.2 l/m^2.h. During FO process using 0.5 M NaCl as a draw solution and DI-water as the feed, the membranes exhibited water flux of 32.2 l/m^2.h and salt flux of 3.5 g/m^2.h for AL-DS configuration (Wang, Shi *et al.* 2010). Chou *et al.* from the same group further improved the FO hollow fiber membrane by adjusting the substrate and the active layer. The substrate had an UF-like skin in the lumen side (MWCO of 39KDa, mean pore size of 9.6 nm) without an outer skin (MWCO >500KDa). The thickness of the RO-like skin at the lumen side was reduced by half (~300nm). The resulting membrane had improved the water permeability of 3.45 l/m^2.h.bar while the salt permeability remained unchanged and the structural parameter (S) of 5.5 x 10^{-4} m. FO water flux increased to 42.6 l/m^2.h under the same FO experiment conditions (Chou, Shi *et al.* 2010).

Yip *et al.* studied the fabrication of a TFC flat sheet membrane tailored for FO operation. The TFC-FO membrane, which had an overall thickness of 96μm, consisted

of a thin active selective layer supported by a microporous polymer layer. The result showed that making a support membrane with a thin layer of the sponge-like morphology on the top of a finger-like layer favored to be applied in FO process. The FO membranes have a structural parameter (S) of 4.92 x 10^{-4} m, water permeability of 1.14 l/m^2.h.bar and NaCl rejection of 97.4%. FO process was carried out by employing 1.5M NaCl as the draw solution and DI-water as the feed. The measured FO water flux was 18 l/m^2.h (Yip, Tiraferri *et al.* 2010). Similarly, Tiraferri *et al.* fabricated a composite FO membranes made from polyamide as the active layer supported by a polysulfone support layer. The resultant membranes have water fluxes ranging from 4 to 25 l/m^2.h using 1 M NaCl as the draw solution and DI- water as the feed (Tiraferri, Yip *et al.* 2011).

Zhang *et al.* compared single-skin and double-skin of integral asymmetric flat sheet FO membranes made from cellulose acetate. The overall thickness of the membranes was 35 μm and the thickness of the top skin (for both single and double-skin) was 1μm while the bottom skin was 95 nm. The single skinned membrane had water permeability (*A*), NaCl permeability (*B*) and structural parameter (*S*) of 0.13 l/m^2.h.bar, 0.09 g/m^2.h, and 5.1 x 10^{-5} m, respectively, while the double skinned membrane possessed *A* value of 0.17 l/m^2.h.bar, *B* value of 0.07 g/m^2.h and *S* value of 5.4 x 10^{-5} m. During the FO process where 1.0 M NaCl was employed as the draw solution and DI-water as the feed, the double skin membrane had a higher water flux and salt flux (6.2 l/m^2.h and 4.2 g/m^2.h, top layer facing DS) as compared to the single skin membrane (4.9 l/m^2.h and 3.5 g/m^2.h, top layer facing DS) (Zhang, Wang *et al.* 2010).

Wei *et al.* prepared TFC FO membranes with tailored support structure. The resultant membranes can achieve FO water flux of 54 l/m^2.h with a 2 M NaCl as draw solution in the configuration of AL-DS (Wei, Qiu *et al.* 2011).

- *NF-like skin*

Chung's group has been working on single and dual layer NF hollow fiber membranes utilized in FO process (Wang, Chung *et al.* 2007; Wang, Yang *et al.* 2009; Yang, Wang *et al.* 2009b; a; Su, Yang *et al.* 2010). Wang *et al.* fabricated single layer polybenzimidazole NF hollow fiber membrane and examined its performance in FO.

The fibers had inner diameter/outer diameter (ID/OD) of 0.17/0.27 mm and mean effective pore radius of 0.32 nm. Using a 2 M $MgCl_2$ solution as draw solution and DI water as the feed, the water flux was 9 $l/m^2.h$ when applied in the active layer facing draw solution configuration (Wang, Chung *et al.* 2007). In later publication, Wang *et al.* further chemically modified PBI membrane surface by using p-xylylene dichloride to adjust effective mean pore size and pore size distribution. The 4h modified membrane showed water flux of 11 $l/m^2.h$ based on 1M $MgCl_2$ as draw solution and DI water as the feed operating in the configuration of the active layer facing draw solution (Wang, Yang *et al.* 2009). Furthermore, Yang *et al.* developed dual-layer hollow fiber NF membranes utilized in FO process for concentration of protein solutions (Yang, Wang *et al.* 2009b) as well as water production (Yang, Wang *et al.* 2009a). PBI was employed as the outer selective layer while PES-polyvinylpyrrolidone (PVP) was used to form the inner support layer. The resultant fibers had an average pore radius of 0.4 nm, ID/OD of 0.54/0.95 mm and an outside layer thickness of 10 μm. The membranes showed water flux of 33.8 $l/m^2.h$ using $MgCl_2$ draw solution of 5M facing the outer active layer and feed DI water facing the inner support layer. Recently, Su and coworkers reported the fabrication of cellulose acetate hollow fiber NF membrane for FO purposes. The mean pore radius of resultant membrane was 0.3 nm and the fiber dimension of ID/OD was 0.35/0.55 mm/mm. Under FO test using 0.5M $MgCl_2$ as draw solution and DI water as feed, the water flux of 2.7 $l/m^2.h$ and 1.8 $l/m^2.h$ was obtained in the orientation of active layer facing draw solution and feed water, respectively (Su, Yang *et al.* 2010).

Wang *et al.* developed very thin integral asymmetric FO flat sheet membranes from cellulose acetate with an overall thickness of 36 μm. The membrane had double skins with a porous structure in the middle. The top and bottom skin layers had a thickness of 150 nm and 50 nm, respectively. Pure water permeability, A, is 0.78 $l/m^2.h.bar$ while salt permeability, B, for $MgCl_2$ is 0.25 $l/m^2.h$. In FO process using 5 M $MgCl_2$ as draw solution and DI water as feed, the resulting membrane exhibited water flux of 48 $l/m^2.h$ and salt flux of 6.5 $g/m^2.h$ for draw solution facing bottom layer configuration. When the configuration was switched to draw solution facing top layer, there was water flux reduction to 27.4 $l/m^2.h$ and salt flux of 3.9 $g/m^2.h$ (Wang, Ong *et al.* 2010).

2.2. Development of FO hollow fiber membranes with a NF-like selective layer

This part of review begins with an overview of various polymer materials used for membrane preparation, and the understanding of phase inversion mechanism of the asymmetric membranes preparation in general, followed by the discussion of the fabrication conditions and parameters involved in making asymmetric hollow fiber substrates via dry jet-wet spinning technique. Last section is the preparation of selective membrane surfaces.

2.2.1. Membrane materials and phase inversion technique for asymmetric membrane preparation

Generally, suitable materials used for membrane application should have high mechanical strength, good thermal stability over a wide range of temperature, good chemical stability over a wide range of pH and ability to form films and hollow fibers easily (Petersen 1993; Ulbricht 2006). In addition, the material should be less susceptible to bacterial and colloidal-particle attachments. The common membrane materials include cellulose acetate (Herron 2008), polysulfone (Wijmans, Kant *et al.* 1985), polyethersulfone (Chou, Shi *et al.* 2010; Shi, Chou *et al.* 2012), polybenzimidazole (Wang and Chung 2006), and polyetherimide (Shen, Xu *et al.* 2004). Hollow fiber NF membranes can be constructed from various polymers which have their own pros and cons. The challenge is how to select an appropriate material for desirable processes (Frank, Bargeman *et al.* 2001; Wang and Chung 2006; Yang, Jian *et al.* 2006; Liu, Xu *et al.* 2007).

Loeb and Sourirajan in 1960 initiated the fabrication of asymmetric flat sheet membranes by phase inversion using cellulose acetate (Loeb and Sourirajan 1963). Since then membrane fabrication via phase inversion has grown rapidly. Asymmetric membranes are commonly prepared by immersion precipitation process, known as non-solvent induced phase separation (NIPS). The mechanism behind relies on induced thermodynamic demixing of a homogeneous polymer-solvent solution into a polymer-rich phase and a polymer-lean phase by exposure of the solution to the non-solvent. One of the significant advantages of this technique over other membrane

manufacturing techniques is that various porous structures can be easily controlled by adjusting various fabrication parameters. However, the mechanism of membrane formation through phase inversion is a complex process which involves thermodynamic and kinetic parameters such as Gibb's free energy of mixing, and diffusivities and chemical potentials of each component (Strathmann and Kock 1977). In the membrane formation, the thermodynamic properties of the polymer solution can be determined by cloud point measurement (Wijmans, Kant *et al.* 1985). There are several ways to observe the kinetics of the phase inversion: (1) light transmission on immersed casting solution (the light transmittance decreases when phase separation occurs) (Reuvers and Smolders 1987); (2) the length of precipitation front which is related to the diffusion of non-solvent into the casting solution (Kang, Kim *et al.* 1987; Kang and Lee 2002); (3) viscosity measurement of the casting solution (Ohya, Shiki *et al.* 2009).

Thermodynamic properties of a polymer/solvent/non-solvent system can be represented by a ternary phase diagram shown in Figure 2.5. The phase diagram consists of four regions. The first region (region I) is the stable region or a homogenous region with one-phase liquid state. The initial dope solution prior to spinning is situated in this region. Region II, located in between the binodal curve and gelation boundary, is a liquid-liquid two-phase solution. This region consists of two curves: binodal and spinodal. The spinodal line separates the two-phase region into metastable (between binodal and spinodal curves: ABD and ACE) and unstable regions (under spinodal curve: ADE). A metastable region occurs if $\left(\partial^2 \Delta G_{mix} / \partial \phi_2^{\,2}\right)_{T,P} > 0$ and an unstable region occurs if $\left(\partial^2 \Delta G_{mix} / \partial \phi_2^{\,2}\right)_{T,P} < 0$. The boundary, where $\left(\partial^2 \Delta G_{mix} / \partial \phi_2^{\,2}\right)_{T,P} = 0$, is called the spinodal point obtained for each tie line, and a collection of these points becomes the spinodal line (where ΔG_{mix} is Gibbs free energy of mixing and ϕ_2 is volume fraction of polymer at certain temperature (T) and pressure (P)). Region III, confined to the gelation and swelling boundary, is liquid-solid two-phase swelling. The last region is region IV. In a ternary phase diagram, region IV is separated from region I and III by the vitrification boundary and swelling boundary, respectively. In this region, a polymer solution reaches its glass state or swelling state (one-phase glass) (Ren and Wang 2010).

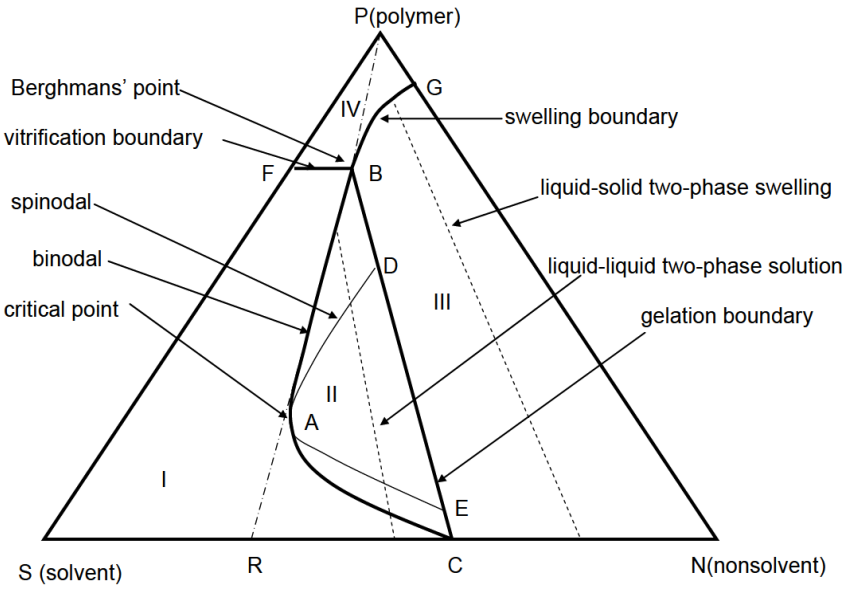

Figure 2.5. Phase diagram of a ternary system in diffusion induced phase separation (DIPS) method. Adapted from (Ren and Wang 2010).

Various morphological structures of the membranes fabricated by NIPS are strongly affected by gelation and demixing. A dense membrane structure can be obtained when a homogeneous polymer solution reaches the vitrification boundary directly and goes into region IV. A porous membrane is formed if a homogeneous polymer solution crosses the binodal/spinodal curve. In a metastable area, the polymer solution will phase separate into a polymer-rich phase and a polymer-lean phase based on the nucleation and growth (NG) mechanism. As shown in Figure 2.5, there are two metastable areas. One is ABD region which is NG of polymer-lean phase and the other one is ACE region which is NG of polymer-rich phase. If demixing is situated in ABD region, closed-cell membrane morphology will be developed in the beginning and afterward, nuclei will grow sufficiently and finally touch each other, creating an interconnected structure. If demixing occurs in ACE region, on the other hand, it is not favored for membrane formation since it will lead to low-integrity powdery agglomerates. If demixing turns out crossing the spinodal curve into the unstable ADE region, two separate phases appear following the tie-lines to form two co-continuous phases instead of well defined nuclei. An interconnected pore structure will be developed but it might evolve into a closed cell structure later (Mulder 1996; Schafer, Fane *et al.* 2005; Ren and Wang 2010).

There are two mechanisms for membrane formation in terms of demixing process: instantaneous liquid-liquid demixing and delayed onset of liquid-liquid demixing. Instantaneous demixing occurs when the polymer system gels and solidifies immediately after immersion resulting in a membrane with a fine pore skin or surface structure. The layer beneath the surface, however, is porous and has macrovoids (Schafer, Fane *et al.* 2005; Barzin and Sadatnia 2008; Ren and Wang 2010). For the delayed demixing, the composition of the entire solution remains in the homogeneous region for a certain period of time (Ren and Wang 2010). As a result, the membrane skin becomes thinner and the macrovoids are significantly reduced. Instead, sponge-like structures are observed in the membrane structure (Mulder 1996; Barzin and Sadatnia 2008). Experimental results conducted by Tasselli and Drioli (Tasselli and Drioli 2007) have shown that utilizing water as the bore fluid resulted in a less porous skin due to rapid demixing as water is a strong coagulant for polyetheretherketone (PEEK) (water solubility parameter, δ, is 47.9 $(MPa)^{1/2}$ and PEEK solubility parameter is 22.0 $(MPa)^{1/2}$). The resulting membrane has water flux of 158 $l/m^2.h.bar$. However, when n-butanol was utilized as the bore fluid, the water flux increased dramatically to 1209 $l/m^2.h.bar$. N-butanol has a solubility parameter of 23.3$(MPa)^{1/2}$. A small difference in solubility between n-butanol and the polymer dope indicates that n-butanol is a poor coagulant for PEEK. Therefore, delayed demixing occurred and consequently, a more open and porous skin was formed.

2.2.2. Asymmetric hollow fiber membranes via dry jet – wet spinning technique

A number of parameters have to be considered in the fabrication of hollow fiber membranes via dry jet-wet spinning technique. These include solvent type, polymer concentration, external and internal coagulants, air gap, non-solvent additive, viscosity of the dope solution and take-up speed, etc.

- *Choice of solvents*

Solvents play an important role in membrane fabrication via phase inversion method. A polymer has to be able to dissolve in a solvent and remains uniform and stable prior to precipitating in a coagulation bath. Also, the solvent and non-solvent should be completely miscible with each other. Common organic solvents used include N,N-

dimethylacetamide (DMAc), N,N-dimethylformamide (DMF), N-methyl-2-pyrrolidone (NMP), hexamethylphosphoramide (HMPA), tetramethylurea (TMU), triethyl phosphate (TEP) and trimethyl phosphate (TMP) (Bottino, Camera-Roda *et al.* 1991; Yeow, Liu *et al.* 2003; Barzin and Sadatnia 2008). Barzin *et al.* compared DMAc and NMP as a solvent for the PES-water system. Non-solvent/solvent interaction parameter of water/DMAc is smaller than that of water/NMP, suggesting that water and DMAc has better miscibility as compared to water and NMP. The solvent/polymer interaction parameter of NMP/PES is smaller than that of DMAc/PES. This means that NMP is a better solvent for PES as compared to DMAc. Therefore, in the ternary phase diagram, the binodal curve of H_2O/NMP/PES system is closer to the polymer-solvent axis than that of H_2O/DMAc/PES system. Consequently, the membrane prepared by using DMAc as a solvent had more sponge-like structures compared to that prepared by NMP due to a higher mutual affinity between H_2O and DMAc. Delayed demixing in H_2O/DMAc/PES system suppresses the formation of macrovoids (Barzin and Sadatnia 2008).

- *Polymer concentration*

Several studies reported that increasing initial polymer concentration in a solution can slow down the non-solvent inward diffusion resulting in a denser and thicker skin, lower porosity and subsequently lower water flux (Kneifel and Peinemann 1992; Xu, Shen *et al.* 2003; Shi, Wang *et al.* 2007). Shi and co-workers studied the effect of polymer concentration on the polyvinylidene fluoride (PVDF) hollow fiber structure and performance. When the polymer concentration increased from 13 to 17 wt.%, the macrovoids were reduced significantly and the sponge-like structure sandwiched in the middle became thicker. Consequently, pure water permeability as well as MWCO decreased (Shi, Wang *et al.* 2007). Furthermore, Bonyadi *et al.* observed the effect of initial polymer concentrations on the corrugation phenomenon in the inner contour of hollow fiber membranes. An increase in the dope concentration from 13 to 22 wt.% resulted in gradual elimination of the inner contour deformation. A higher dope concentration might have a higher rigidity and chain orientation of the inner precipitated shell. Thus, there was less hydrodynamic instability. The inner shell with a higher rigidity will be more resistant to buckling (Bonyadi, Chung *et al.* 2007).

- *Addition of non-solvent additives*

A number of studies have been carried out to fabricate porous hollow fiber membranes using different non-solvent additives to obtain an optimal membrane structure. The addition of non-solvent additives affects the thermodynamic properties of polymer solution as well as the solution viscosity which has an effect on the phase inversion kinetics as it changes the solvent and non-solvent diffusion (Yeow, Liu *et al.* 2003). There are many additives commonly used including polymeric additives (e.g. polyethylene glycol (PEG), poly(vinyl pyrrolidone) (PVP)), organic acids (e.g. acetic acid, propionic acid), inorganic salts (e.g. lithium chloride (LiCl), lithium nitrate ($LiNO_3$) and lithium perchlorate ($LiClO_4$)), weak co-solvents (e.g. methanol, ethanol, 2-propanol, n-butanol and acetone), and weak non-solvents (e.g. glycerol, ethylene glycol, diethylene glycol, and γ-butyrolactone) (Bottino, Camera-Roda *et al.* 1991; Boom, Wienk *et al.* 1992; Kneifel and Peinemann 1992; Liu, Koops *et al.* 2003; Yeow, Liu *et al.* 2003; Xu and Qusay 2004; Mansourizadeh and Ismail 2010).

The addition of non-solvent additives in the initial dope solution normally enhances the thermodynamic instability of the system made the solution closer to the phase separation point (Wang, Li *et al.* 2000). In a ternary phase diagram, it shifts the isothermal precipitation curve toward polymer-solvent axis, indicating that less non-solvent is needed for precipitation in the thermodynamic equilibrium. Since it will reduce the miscibility area of the system and increase the precipitation rate of polymer solutions, macrovoids with finger-like structure are likely to be developed.

The addition of different molecular weights of PEG (from 200 to 10,000) into the PES-NMP systems has been investigated (Xu and Qusay 2004). The membrane structures were changed from a double-layer finger-like structure to sphere or ellipsoids macrovoids with an increase in PEG molecular weights from 200 to 10,000 Da in the dope solution. As a result, PWP increased from 22 to 64 $l/m^2.h.bar$ and mechanical properties were decreased. Furthermore, Shi and coworkers studied the effect of PVP (Shi, Wang *et al.* 2007) as well as glycerol and LiCl (Shi, Wang *et al.* 2008) on the formation of poly(vinylidene fluoride-co-hexafluropropylene) (PVDF-HFP) asymmetric hollow fiber membranes. From the isothermal phase diagram, it was found that the addition of glycerol made the binodal line shifted further towards the

polymer-solvent axis followed by LiCl and PVP (15,000 Da). When water was used as bore fluid, larger and longer macrovoids can be observed in the fibers as the concentration of LiCl increased. This was because LiCl has a good affinity with water. However, when a weak bore fluid was used, the size of macrovoids decreased as the concentration of LiCl increased. The addition of LiCl or glycerol made the resultant membranes presenting a narrow pore size distribution compared to the addition of PVP. In addition, Mansourizadeh and Ismail also looked at the effect of various additives (i.e. PEG 200, ethanol, glycerol, acetic acid) on the polysufone hollow fiber membrane morphology. Their results showed that the effect of the additives used in reducing miscibility area of the system followed the trend of glycerol > acetic acid > PEG200 > ethanol. Furthermore, the addition of non-solvent additives has increased the surface porosity, and subsequently increased the permeability of the membranes (Mansourizadeh and Ismail 2010).

Loh *et al.* investigated the effect of pluronic (additive) concentration on the viscosity, and cross-section morphology of PES membranes. It was found that increasing the pluronic concentration increased the viscosity of polymer solution. As a result, the finger-like macrovoids became narrower when the concentration increased from 5% (viscosity 2.8 Pa.s) to 10% (viscosity 4.3 Pa.s). A further increase of the pluronic concentration to 15% (viscosity 7.0 Pa.s) resulted in a more sponge-like structure. This is due to the increase in viscosity leading to a delayed diffusion of the non-solvent through the polymer solution (Loh, Wang *et al.* 2011).

- *External coagulant and internal coagulant (bore fluid)*

The ideal external and internal coagulants, which depend on the system, can fine tune the final membrane structure and performance such as suppressing the formation of macrovoids, etc (Tasselli and Drioli 2007; Barzin and Sadatnia 2008). Water is commonly used as an external and internal coagulant. However, since water is a strong non-solvent to the polymer, instantaneous demixing could occur during precipitation in water. The resultant membranes usually have a dense skin with big macrovoids underneath.

Kong and Li investigated the effect of external and internal coagulants using a mixture of water and ethanol. If water, a strong coagulant, was used as both external and

internal coagulants, instantaneous demixing due to rapid precipitation would occur. The resultant membranes had both inner and outer skins. When a mixture of ethanol-water (1:1) was used as the external coagulant, the outer skin disappeared due to the slow precipitation rate which may lead to the formation of dead pores. Increasing the ethanol concentration in the coagulation bath led to a shift in membrane morphology from large cavities to a sponge-like structure (Kong and Li 2001). Increasing the concentration of NMP and PEG in the internal coagulant reduced the outward diffusion rate of the solvent and additives from the dope into the coagulant as well as inward diffusion of water from the coagulation bath to the dope. As a result, the skin gradually disappears while the skin pore size increased due to delayed demixing (Liu, Koops *et al.* 2003). Furthermore, by varying the strength of the internal coagulant, the phase separation mechanism can be changed. Moriya *et al.* examined the effect of internal coagulant composition on poly(lactic acid) hollow fiber membranes by varying the weight ratio of dimethyl sulfoxide (DMSO) and water. As the internal coagulant became weaker, the water permeability was improved (from 10 to 320 $l/m^2.h.bar$) while tensile stress at break of the membrane was maintained constant at 3.5 MPa. The structure of hollow fiber inner surface changed from a microporous to a spherulite structure as the internal coagulant grew weaker. At a low concentration of DMSO, the liquid-liquid phase separation took place. However, when pure DMSO was used as the internal coagulant, the solid-liquid phase separation occurred on the inner surface of the membrane. Since there was no penetration of non-solvent (water), the liquid-liquid phase separation was not induced at the inner surface resulting in a hollow fiber membrane with a spherulite structure in the inner skin (Moriya, Maruyama *et al.* 2009).

- *Air gap*

The air gap between the spinneret and coagulation bath has an effect on the evaporation of solvent and the penetration of moisture into the nascent fiber during the dry period in the dry jet-wet spinning process. Therefore, the skin pore size and porosity can be controlled by varying the air gap. At a long air gap, for instance, the nascent fibers are exposed longer in the air, facilitating the moisture from air to penetrate into the fibers. Thus nuclei form and grow until the phase separation freeze the structure when the fibers enter the coagulation bath (Niwa, Kawakami *et al.* 2000;

Khulbe, Feng *et al.* 2004). The effect of various air gap from 10 to 90 cm on the performance and morphology of polyetherimide hollow fiber membranes has been reported. As the air gap increases, the pure water permeability and molecular weight cut off (MWCO) increase while the pore size distribution become broader (Khulbe, Feng *et al.* 2004).

Bonyadi *et al.* investigated the corrugation phenomenon in the inner contour of polyacrylonitrile (PAN) hollow fibers prepared by NIPS. The results showed that increasing air gap can eliminate the deformation of the inner contour due to a longer contact time and faster solvent exchange between the internal coagulant and the dope solution before entering the coagulation bath (Bonyadi, Chung *et al.* 2007). In addition, Shi *et al.* also experienced the deformation of the inner contour of PVDF-HFP membrane during wet spinning process (zero air gap). PVDF-HFP material, which shows strong viscoelastic property, entered the coagulation bath directly, and in an instant it froze by a strong external coagulant such as water. An increase in air gap to 15 cm was able to eliminate the inner contour deformation as there was an extra time for the polymer chains to relax and re-arrange. By using a softer internal coagulant to delay the precipitation, it is possible to spin hollow fibers with perfect annular structure at a lower air gap (Shi, Wang *et al.* 2007).

- *Take up speed*

In commercial hollow fiber membrane manufacture, high-speed spinning is more favorable in order to increase the production efficiency. Several studies have been conducted to observe the effect of take-up speed on membrane structure and morphology (Wang, Fei Li *et al.* 2004; Santoso, Chung *et al.* 2006). Wang and co-workers have reported that increasing take-up speed can eliminate the formation of macrovoids in the cross section of single layer PES hollow fiber membranes as well as matrimid-PEI double layer hollow fiber membranes. The macrovoids disappear completely at a take-up speed about 5-6 times of the free fall speed (Wang, Fei Li *et al.* 2004). There were several factors responsible for this result such as the induced elongational stresses which affected instability of polymer dope solution, polymer chain packing, nascent membrane deformation and outflow of spinning solvents.

- *Temperature*

The spinning temperature includes the temperatures of dope solution, external and internal coagulants as well as the spinneret (Cheng 1999; Yeow, Liu *et al.* 2004; Yu, Chou *et al.* 2006; Widjojo, Chung *et al.* 2007; Wongchitphimon, Wang *et al.* 2011). Simply by varying the system temperature, membrane structures can be tailored into either more cellular or particulate morphologies. For semi-crystalline polymers, the role of dominance by either liquid-liquid (L-L) demixing or crystallization can be reverted depending on the precipitation temperature. The L-L demixing, for instance, can be suppressed and crystallization will dominate using a weak coagulant at a low temperature. Therefore, the resultant membrane has particulate morphology (spherulite). At a high precipitation temperature, on the other hand, the L-L phase separation will dominate the precipitation process, resulting in a membrane with cellular morphology (Cheng 1999). Yeow *et al.* also obtained similar results that gelation induced by crystallization favored at a lower precipitation temperature while elevated temperature suppressed gelation and L-L demixing dominated the mechanism of phase separation process (Yeow, Liu *et al.* 2004).

Yu *et al.* varied the temperature of the internal coagulant from 20 to 60°C while the dope solution (PAN/DMF) was maintained at 60°C. Experiments showed that the fiber spun using 60°C internal coagulant had a smaller inner diameter than those using 20 and 40°C internal coagulants due to the fact that the rapid solidification at a high temperature restricts die swelling (Yu, Chou *et al.* 2006). Moreover, membrane porosity increased with temperature increase of the internal coagulant, because instantaneous demixing occurred as the solubility and diffusivity increased. The water permeability of the resultant membranes increased greatly with the increase of internal coagulant temperature. However, in a different system of PVDF-HFP/NMP, increasing the external coagulant temperature to 40°C resulted in an increases in the thermodynamic stability of the dope resulting in a more sponge-like structures in the membrane matrix because of delayed demixing (Wongchitphimon, Wang *et al.* 2011).

2.2.3. Development of NF-like selective layer

In recent years, nanofiltration (NF) processes have drawn much attention because of their merits such as low operating pressure, high water flux, high retentions to multivalent ions and organic materials with low molecular weights as well as low operating and maintenance costs (Yang, Jian *et al.* 2006). The idea of NF membranes came from reverse osmosis membrane operating at a low pressure. NF membrane is classified between UF and RO. The unique characteristic of NF is the selectivity between monovalent and multivalent ions while UF has zero ions rejections and RO retains ions completely. Principles for the rejections of multivalent ions and neutral organic molecules in NF membranes are based on charge interactions and size exclusion. As for uncharged molecules, the rejections of inorganic NF membrane are basically determined by sieving effect (Schafer, Fane *et al.* 1998; Schafer, Fane *et al.* 2005).

In general, a NF membrane consists of a selective skin layer supported by a porous substrate which provides necessary mechanical strength. There are several ways to construct the selective layer for a NF membrane. Firstly, an active layer can be fabricated by integrally connecting it to the support layer. Such examples include integral asymmetric PBI and cellulose acetate NF hollow fiber membranes (Wang, Chung *et al.* 2007; Su, Yang *et al.* 2010), and recently reported NF membranes using torlon® 4000TF poly(amide-imide) (Sun, Wang *et al.* 2010b). This method requires a delicate polymer dope formula and a precise control of spinning conditions to avoid defect formation. The most important factor to obtain integrally skinned asymmetric membrane is the speed of demixing (Mulder 1996).

Secondly, the selective layer can be made based on the composite membrane concept – the active layer and porous substrate are fabricated separately using different materials. Typically, the porous nonselective layer is formed in the first step, followed by the synthesis of a thin selective layer on the top of the porous surface. The selective layer, which provides the selective properties, can be in either lumen side or outer side. There are some advantages of composite membranes: (1) the selective layer, either inside or outside, can be synthesized easily; (2) since each layer is made separately, it is easier to optimize the individual layer structures. The selective layer can be customized to

enhance the solvent flux and solute/ions rejections while the structure of the support layer can be tailored for maximum strength and compression resistance as well as decreasing the resistance to permeate flow. Verissimo *et al.* described that the composite membranes offer higher water permeability and higher salt rejections as compared to integral asymmetric membranes (Veríssimo, Peinemann *et al.* 2005a). (3) the modification of the selective layer can be done easily, such as by using cross-linking method (Petersen 1993). The composite membranes also have the disadvantages of being a more expensive method of membrane fabrication and time consuming as compared to the integral asymmetric membranes (Petersen 1993). In addition, the composite membranes produced by these processes may experience failure and poor performance due to an increased risk of introducing defects in the substrate and separating layer with increasing the number of processing steps involved (He, Mulder *et al.* 2002).

Several processes have been reported for the preparation of composite NF membranes. Polyamide thin film composite (TFC) by interfacial polymerization is the most commonly used technique (Veríssimo, Peinemann *et al.* 2005a; Liu, Xu *et al.* 2007; Yoon, Hsiao *et al.* 2009). Petersen has conducted an excellent review on TFC membranes for flat sheet NF and RO membranes (Petersen 1993). Multilayer polyelectrolyte coating has also gained attention for the preparation of charged NF membranes. Nevertheless, most of literatures involved flat sheet NF membranes (Jin, Toutianoush *et al.* 2003; Malaisamy and Bruening 2005; Hong and Bruening 2006; Ouyang, Malaisamy *et al.* 2008). By using chemical treatment, the surface pores of the membrane can be tightened and charge-contained functional groups can also be easily attached to the membrane surface (Ba, Langer *et al.* 2009). Other techniques for composite NF membrane fabrication include dual layer (Yang, Wang *et al.* 2009a), polyelectrolyte dip-coating (He, Frank *et al.* 2008), and UV-photografting (Akbari, Desclaux *et al.* 2007).

- *Interfacial polymerization*

Basically, interfacial polymerization is the polymerization that takes place at the interfacial boundary of two immiscible solutions between two different monomers. Polyamides (PA) are commonly used in the fabrication of composite membranes via

interfacial polymerization as the selective layer. It is formed from amide monomers which link together by peptide bonds or amide link. Amide link is a covalent bond between carboxyl group (–COOH) from acyl halides (e.g. trimesoyl chloride, *iso*-phthloyl chloride) and amine group ($–NH_2$) from amine solutions (e.g. piperazine, *m*-phenylenediamine). The amide group makes PA polar and very sensitive to water. The amide groups may form hydrogen bonding with water molecule which weakens the adhesion of the active layer to the support layer during membrane fabrication. In addition, PA can be easily attacked by chlorine in water/wastewater treatment which causes degradation of amide group (Yang, Jian *et al.* 2006). Therefore, pretreatment for chlorine removal is needed.

Verissimo and co-workers performed interfacial polymerization of N,N'-diaminopiperazine (DAP) and trimesoyl chloride (TMC) to prepare the lumen selective layer on polyetherimide UF membranes. The final membrane had PWP of 6 l/m^2.h.bar, NaCl, Na_2SO_4, glucose, sucrose, and lactose rejections of 14%, 87%, 57%, 77%, and 91%, respectively (Veríssimo, Peinemann *et al.* 2005a). Similar works have been done by Yang *et al.* A polyamide hollow fiber composite membrane was prepared by interfacial polymerization using piperazine (PIP) as the aqueous phase monomer and TMC as the organic phase monomer on the lumen side of PPESK UF membrane. The membrane had PWP of 12.8 l/m^2.h.bar, while the rejections of Na_2SO_4, sucrose, and raffinose were more than 99% (Yang, Zhang *et al.* 2007). Furthermore, Verissimo *et al.* prepared composite membranes by interfacial polymerization of piperazine (PIP), DAP, 1,4-bis(3-aminopropyl)-piperazine (DAPP) and N-(2-aminoethyl)-piperazine (EAP) with TMC separately. The investigation proved that the amine structure affected the membrane performance, membrane surface charge and morphology (Veríssimo, Peinemann *et al.* 2006). To increase the rejection performance of the resulting membrane, three-step interfacial polymerization had been carried out by Liu *et al.* The substrate was contacted with the aqueous phase monomer followed by the organic phase, and the aqueous phase for a second time. This method produced a denser selective layer compared to conventional interfacial polymerization. The resulting membrane had PWP of 5.3 l/m^2.h.bar, and Na_2SO_4 rejection of 96% (Liu, Xu *et al.* 2007).

- *Multilayer polyelectrolyte deposition*

The word 'polyelectrolyte' originally comes from 'polymer' and 'electrolyte'. It can be described as a polymer which has (an) electrolyte group(s) in each repeating unit. Since it contains electrolyte compounds, polyelectrolyte is able to dissociate in water or an aqueous solution, and therefore, presents charge property. Table 2.1 provides the list of commonly used polyelectrolytes from various literatures (Decher 1997; Krasemann and Tieke 2000; Jin, Toutianoush *et al.* 2003; Stanton, Harris *et al.* 2003; Klitzing and Tieke 2004; Lajimi, Abdallah *et al.* 2004; Miller and Bruening 2004; Malaisamy and Bruening 2005; Miao, Chen *et al.* 2005; Tieke, Toutianoush *et al.* 2005; Hong and Bruening 2006; Hong, Malaisamy *et al.* 2006; Hong, Malaisamy *et al.* 2007; Bruening, Dotzauer *et al.* 2008; Nanda, Tung *et al.* 2008; Ouyang, Malaisamy *et al.* 2008; Hoffmann and Tieke 2009; Hong, Ouyang *et al.* 2009; Wang, Yao *et al.* 2009; Zhang, Ruan *et al.* 2009; Li, Goyens *et al.* 2010; Shan, Bacchin *et al.* 2010). A strong polyelectrolyte is fully charged in water while a weak polyelectrolyte is partially charged.

Table 2.1. List of polyanions and polycations commonly used for polyelectrolyte membranes.

Polyanions	Polycations
Poly(acrylic acid) (PAA) 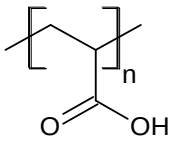	Poly(diallyldimethyl ammonium chloride) (PDADMAC) 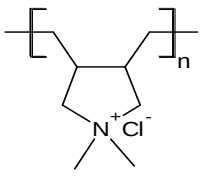
Poly(styrene sulfonate) (PSS) sodium salt 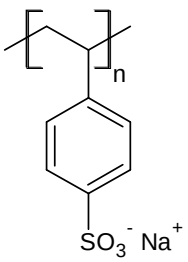	poly(allylamine hydrochloride) (PAH) 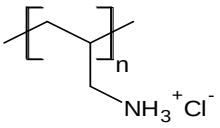

(Continued)

Polyanions	Polycations
Poly(vinyl sulfonic acid) sodium salt (PVSu) 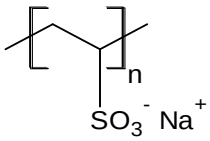	Polyvinylamine (PVA) 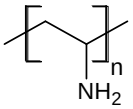
Poly(vinyl sulfate) (PVS) potassium salt 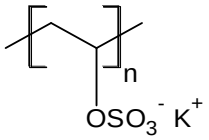	Poly(4-vinylpyridine) (P4VP) 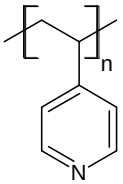
Sulfated chitosan 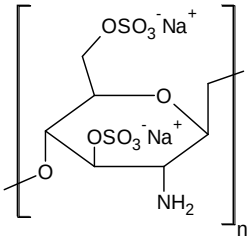	Poly(4-vinylbenzyl trimethyl ammonium chloride) (PVTAC) 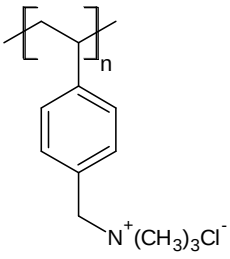
	Chitosan 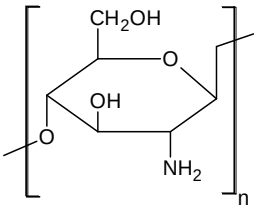 Polyethylenimine 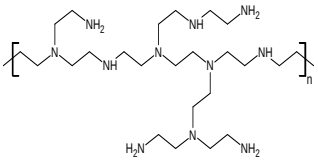

Recently, polyelectrolyte membranes gain more and more interests due to their high selectivity and very thin skin thickness (in the range of nm). They have wide applications in water treatment (Suryanarayan, Mika *et al.* 2006), pervaporation

(Zhang, Song *et al.* 2008; Zhang, Gao *et al.* 2009) and gas separation (Van Ackern, Krasemann *et al.* 1998; Krasemann and Tieke 1999). Fabrication of polyelectrolyte membranes is basically a coating process of PE solutions on a porous support layer. A support layer that is suitable for PE coating is a UF-type support with a MWCO of ~50 kDa (Malaisamy and Bruening 2005). After PE coating, the membrane pore size will become denser with a MWCO reduced to < 500 Da (Malaisamy and Bruening 2005).

A polyelectrolyte membrane with an ultrathin skin (at nanometer scale) can be made by layer-by-layer deposition of aqueous polyelectrolyte solutions onto the porous substrate which is based on the electrostatic interaction of oppositely charged molecules. A minimum of two oppositely charged molecules is required here. By using this method the thickness of membrane skin could be easily adjusted (for example thickness of 4.5-bilayer polystyrene sulfonate (PSS)/poly(allylamine hydrochloride) (PAH) is 20 nm). In addition, the charge of the outer layer depends on the last polyelectrolyte used. It can be positive if the last one is a polycation or negative if a polyanion is the last one (Stanton, Harris *et al.* 2003; Hong and Bruening 2006; Hong, Malaisamy *et al.* 2006; Ouyang, Malaisamy *et al.* 2008; Zhang, Song *et al.* 2008). By varying the PE, the membrane can be constructed for specific applications such as the separation of monovalent and divalent ions, phosphate/chloride separation, fluoride/bromide/chloride separation, separation of protein and amino acids, etc.

In the formation of polyelectrolyte membranes, the solid substrate commonly used could be (1) a UV/O_3-cleaned porous alumina with 0.02 μm-diameter surface pores (Miller and Bruening 2004; Hong and Bruening 2006; Hong, Malaisamy *et al.* 2006; Hong, Malaisamy *et al.* 2007), (2) a plasma-treated porous polyacrylonitrile (PAN) layer on poly(ethylene terephthalate) (PET) fleece (Krasemann and Tieke 2000; Jin, Toutianoush *et al.* 2003), (3) polyethersulfone (PES) UF membrane, (4) cellulose acetate (Lajimi, Abdallah *et al.* 2004). Porous alumina is attractive as a support layer for polyelectrolyte membranes since it has positive charges. Therefore, polyanion should be deposited first. Plasma-treated PAN and cellulose acetate, on the other hand, possess negative charges. Hence, for polyelectrolyte adsorption, the supporting membrane is immersed in a polycation solution. Even though PES is quite neutral, it is possible to use PES as a supporting material to make polyelectrolyte membranes. The attachment of polyelectrolyte layer is based on hydrophobic interaction.

The morphology and the capability of the polyelectrolyte film will be dependent on several variables, including: (i) molecular structure and molecular weight of polyelectrolyte; (ii) number of deposited layers; (iii) pH and ionic strength of the deposition solution.

The molecular structure of polyelectrolyte affects its charge density. Charge density of polyelectrolyte can be defined as the ratio of the number of ion pairs to the total carbon atoms in a repeat unit (Krasemann and Tieke 2000), For example, PAH/PSS has a charge density of 0.09 (total ion pair = 1; total carbon = 8 + 3 = 11). The higher the charge density the more effective the membrane in ion repulsion and it increases the separation factor. 5 layers of PSS/PAH on the top of a porous alumina support gave a rejection to Mg^{2+} ions of 95%, PWP of 7.4 l/m^2.h.bar, and separation factor (Na^+/Mg^{2+}) of 22.5. On the other hand, 5 layers of PSS/PDADMAC, which has charge density of 0.06, gave Mg^{2+} rejection of 42%, PWP of 17 l/m^2.h.bar and separation factor (Na^+/Mg^{2+}) of 1.8. Moreover, according to Ouyang *et al.*, PAH swells less as compared to PDADMAC (Ouyang, Malaisamy *et al.* 2008).

The number of deposited polyelectrolyte layers also has an effect on the nanofiltration properties of polyelectrolyte multilayer membranes. The more polyelectrolyte pairs are deposited, the thicker the skin is. As a consequence, PWP decreased and ion rejection increased. $[PAA/PAH]_3PAA$ films has a thickness of 29.4 nm, PWP of 1 l/m^2.h.bar and SO_4^{2-} rejection of 54%, while $[PAA/PAH]_4PAA$ films has a thickness of 51.7 nm, PWP of 0.95 l/m^2.h.bar and SO_4^{2-} rejection of 84% (Hong, Malaisamy *et al.* 2006).

Addition of salts into the deposition solution would change the ionic strength of the deposition solution, which would reduce the electrostatic repulsion of the polymer chains. Therefore, polymer chains would present a coil conformation rather than flat conformation. Consequently, the thickness of the individual layer increased and hence, the flux decreased while the rejection increased (Krasemann and Tieke 2000).

As indicated by Choi and Rubner, the degree of ionization of the weak polyelectrolytes in a solution and in a multilayer film was influenced by pH adjustment. The right pH will give the highest charge. Therefore, it can give the strongest interaction. PAH, for instance, is a weak polycation (carry positive charges). At a higher pH, PAH will be deprotonated. Because it has less charges, the amount of PAH required to neutralize

the polyanion will be increased and hence, the thickness of multilayer polyelectrolyte will increase. A strong polyelectrolyte, on the other hand, will not be affected by pH difference (Choi and Rubner 2005).

At a high pH, polyanions will be highly ionized and at a low pH, polycations will be highly protonated (Krasemann, Toutianoush *et al.* 2001). To achieve a high cross-linking density, both the cationic and anionic polyelectrolytes need to be adsorbed in a highly charged state. The optimum pH for the preparation of a multilayer polyelectrolyte membrane, pH_{opt}, can be expressed as the mean pK_a value of the cationic and anionic groups of the polyelectrolyte (Krasemann, Toutianoush *et al.* 2001).

Charge density of a weak electrolyte, such as poly(acrylic acid) (PAA) and poly(allylamine hydrochloride) (PAH), is pH dependent. A strong electrolyte, on the other hand, is less pH dependent (Choi and Rubner 2005). For example, both PAA/PAH are weak PE. For the same number of bilayers, the deposition solution with a pH of 7.0 gives a higher flux of 1.48 $l/m^2.h.bar$ and higher SO_4^{2-} rejection of 93.2% as compared to pH 4.5 (flux of 0.95 $l/m^2.h.bar$, SO_4^{2-} rejection of 84.2%) (Hong, Malaisamy *et al.* 2006). PSS and PDADMAC, on the other hand, are strong electrolytes. The changes in flux (from 19.1 to 20.8 $l/m^2.h.bar$) and SO_4^{2-} rejection (from 94.1% to 92.3%) for the deposition solutions with pH of 5.5 and 7.0 are insignificant.

- *Chemical cross-linking*

This method utilizes the unique feature in molecular structure of membrane material. A cross-linking reagent can be used to link one polymer chain to another. Therefore, many researchers have considered this method to physically and chemically modify membrane surface. As a result of modification, the surface pore of the membrane can be reduced and pore size distribution can be adjusted. Furthermore, using a certain cross-linking reagent is able to impart additional charges on membrane surface.

Qiao *et al.* modified P84 copolyimide (BTDA- TDI/MDI, copolyimide of 3,3',4,4'-benzophenone tetracarboxylic dianhydride abd 80% methylpenylene-diamine + 20% methylene diamine) flat sheet membrane by utilizing *p*-xylylene diamine and

ethylenediamine (EDA) as cross-linkers since amine is able to have a reaction with polyimide backbone. The reaction had been confirmed by fourier transform infra red (FTIR) and X-ray photoelectron spectroscopy (XPS) that the imide groups gradually disappear, forming amide groups & establishing intermolecular bonds. Based on experimental results, EDA, which is a smaller molecules compared to p-xylylene, was found to be more effective in reaction with imide groups (Qiao and Chung 2006).

Furthermore, Ba *et al.* functionalized the surface of P84 copolyimide (BTDA-TDI/MDI) flat sheet membrane with amine and/or ammonium groups from branched polyethyleneimine (PEI) material to prepare positively charged NF membranes. Fourier transform infra red spectroscopy had been used to confirm the cross-linking reaction. The results showed that the imide groups' spectra disappeared and amide peak became visible. The imide groups in P84 copolyimide can undergo cross-linking reaction with amines resulting in the opening of imide groups to form ortho diamine functionalities. Salt rejection sequence of $CaCl_2$ > NaCl > Na_2SO_4 showed that the resultant membranes carried positive charges (Ba, Langer *et al.* 2009). Similarly, Wang and co-workers developed NF membrane from polybenzimidazole (PBI) and employed p-xylylene dichloride to fine tune pore size distribution and effective mean pore size. The –NH– functional group in the heterocyclic imidazole ring of PBI can be cross-linked by p-xylylene dichloride (Wang, Yang *et al.* 2009).

Wang *et al.* made use of nitrile groups in polyacrylonitrile (PAN) to fabricate positively charged and negatively charged membranes. Positively charged membranes were prepared by a reaction between PAN and 3-(dimethylamino) propylamine followed by $ZnCl_2$ saturation and soaking in a concentrated HCl solution. The FTIR spectra showed a reduction of nitrile and presence of amide groups after reaction. The positive charges were confirmed by various salts filtration that showed the rejection sequence of $CaCl_2$ > NaCl > Na_2SO_4. The negatively charged membranes, on the other hand, were synthesized by hydrolysis of PAN in a NaOH solution, saturated with $ZnCl_2$ and treated with a dilute NaOH solution. The nitrile groups (–C≡N) was disappeared from FTIR spectra while –C=O and –COONa functional groups turned up after reaction. This membrane has rejection in the order of Na_2SO_4 > NaCl > $CaCl_2$ (Wang, Yue *et al.* 2008).

Cheng *et al.* produced a positively charged flat sheet NF membrane by combining polyelectrolyte deposition and chemical cross-linking. The negatively charged substrates were made from polyetherimide/sulfonated polyether ether ketone blend membranes. It is then followed by polyethylenimine deposition via electrostatic interactions to get the positive charges. Subsequently, the membranes were cross-linked with butanedioldiglycidylether to improve the stability of the modified membranes (Cheng, Oatley *et al.* 2011).

- *Dual layer*

Dual layer hollow fiber membranes, prepared by a single-step simultaneous extrusion of two different polymer dope solutions using the non-solvent induced phase inversion method, have become increasingly attractive in recent years. Emerging applications of dual layer hollow fiber membranes involve forward osmosis membranes consisting of a dense selective layer supported by a porous polymer matrix (Wang, Shi *et al.* 2010), direct contact membrane distillation (DCMD), which requires a combination of a thin hydrophobic layer to prevent wetting supported by a hydrophilic layer to enhance water flux (Bonyadi and Chung 2007), gas separation (Pereira, Nobrega *et al.* 2003; Ding, Cao *et al.* 2008), nanofiltration (Sun, Wang *et al.* 2010a), ion exchange membranes (He, Mulder *et al.* 2002) and pervaporation (Liu, Qiao *et al.* 2007). In addition to the structural benefits, dual layer hollow fiber membranes offer advantages from the economic point of view due to the flexibility of material preference. It can reduce the material cost of high performance polymers or utilize materials having weak mechanical strength but exceptional selectivity and/or permeability by combining them with inexpensive and robust polymers as a second layer.

It is important to obtain dual layer hollow fibers with good lamination between the two layers as well as regular cross-section morphology. However, the fabrication of dual layer hollow fiber membranes is a complex process as many parameters have to be considered from the chemistry of two polymer dope solutions to the operating conditions of the spinning process. The composition of the polymer solution plays a critical role as it directly affects the thermodynamic property and phase inversion kinetics. It includes polymer concentration, solvents and non-solvent additives in most cases. He *et al.* studied the critical polymer concentration used for making dual layer

hollow fiber membranes. The membranes were made from sulfonated polyethersulfone (SPES) as the outer layer and polysulfone (PSf) as the inner layer. The results showed that when the concentration of SPES increased, the non-solvent diffusion from the outer layer to the interface decreased accordingly. Thus, less water was accumulated on the interface, leading to an improved lamination of both layers (He, Mulder *et al.* 2002).

Barzin and Sadatnia varied the solvent used in a dope solution for the purpose of studying the mutual affinity of the solvent with the non-solvent in the coagulation bath. It was found that a higher affinity between the solvent and the non-solvent caused a more sponge-like structure for the resultant membrane when the vitrification boundary was located in a lower polymer concentration (Barzin and Sadatnia 2008).

The addition of organic or inorganic components to a polymer dope solution has been extensively used to tailor the membrane structure and morphology (Shi, Wang *et al.* 2007; Shi, Wang *et al.* 2008; Sun, Wang *et al.* 2010a; Loh, Wang *et al.* 2011; Wongchitphimon, Wang *et al.* 2011). Shi *et al.* investigated the effect of various additives (e.g. LiCl, glycerol and polyvinylpyrrolidone) on the membrane morphology of single layer poly(vinylidene fluoride-co-hexafluropropylene) (PVDF-HFP) hollow fiber membranes. It was found that the addition of a certain additive might reduce the thermodynamic stability of the dope solution, resulting in a lower non-solvent tolerance. The addition of LiCl was able to suppress the large macrovoid formation significantly (Shi, Wang *et al.* 2008). Furthermore, Loh *et al.* used an amphiphilic additive of pluronic F127 for making single layer PES hollow fiber membrane. As the additive concentration increased, the finger-like macrovoids became narrower and more sponge-like structures were found (Loh, Wang *et al.* 2011). Sun *et al.* utilized alcohols as the additive to improve the adhesion of poly(amide-imide) (PAI)-cellulose acetate (CA) dual layer hollow fiber membranes. The addition of the non-solvent additive in the outer polymer dope solution enhanced the viscosity so as to slow down the water diffusion across the outer layer of the membrane (Sun, Wang *et al.* 2010a).

Alternatively, the membrane structure and morphology can be tailored by varying the spinning conditions as discussed in many literatures (Pereira, Nobrega *et al.* 2003; Jiang, Chung *et al.* 2004; Li, Chung *et al.* 2004; Bonyadi, Chung *et al.* 2007; Shi,

Wang *et al.* 2007; Widjojo, Chung *et al.* 2007; Wongchitphimon, Wang *et al.* 2011). Pereira *et al.* reported that a longer air gap distance can prolong the contact time for the interpenetration of the outer and inner dope solutions at the interfacial region (Pereira, Nobrega *et al.* 2003). Bonyadi *et al.* also observed the effect of the air gap during the fabrication of single layer polyacrylonitrile (PAN) membranes (Bonyadi, Chung *et al.* 2007). It was found that increasing the air gap can enhance the solvent exchange between the bore fluid and the dope solution and reduce the cross-section area of the membrane, consequently, decrease the precipitated shell radius in the inner contour. These factors are responsible for the improvement of inner contour regularity.

The outer and inner surface morphologies of hollow fiber membranes can also be easily tailored by adjusting the compositions of the internal (bore fluid) and external coagulants. The addition of solvent into the bore fluid can slow down the precipitation rate in the lumen side, allowing a certain extent of macromolecular relaxation and re-arrangement to eliminate the deformation of the inner contour (Bonyadi, Chung *et al.* 2007; Shi, Wang *et al.* 2007). Widjojo *et al.* studied the effects of the external and internal coagulants on the fabrication of polyetherimide (PEI)/polyimide (P84) dual layer hollow fiber membranes. A more open-cell structure with macrovoids can be observed in the outer and inner layers when the coagulants having a larger solubility parameter difference with the polymer were used (Widjojo, Chung *et al.* 2007).

In addition, the temperatures of the external coagulation bath and the spinneret affect the mass transfer of the polymer, solvent and non-solvent during the phase inversion process, thus alter the membrane morphology (Jiang, Chung *et al.* 2004; Wongchitphimon, Wang *et al.* 2011). Experiments revealed that the outer skin might become denser and there were more and bigger macrovoids at a low external coagulation bath temperature, while a high spinneret temperature favors the interpenetration of the outer and inner dope solutions due to decreased dope viscosities and increased molecular diffusion rates. Moreover, Widjojo *et al.* modified the dual layer spinneret with an indented premixing feature to allow the outer and inner dopes to contact each other before they are extruded from the spinneret. The results showed that the premixing feature is able to improve the adhesion of the outer and inner layers (Widjojo, Chung *et al.* 2007).

CHAPTER 3

Fabrication of Novel PAI FO Hollow Fiber Membranes with a Positively Charged NF-like Selective Layer

3.1. Introduction

Forward osmosis (FO) process is a natural phenomenon, which can be defined as the net movement of water molecules across a semi-permeable membrane from a less concentrated solution to a more concentrated solution. FO process utilizes an osmotic pressure gradient instead of hydraulic pressure or temperature as a driving force, thus it has the potential to produce water with less energy consumption (Cath, Childress *et al.* 2006). However, the main drawback of FO system is permeate flux decline due to internal concentration polarization in the dense substrate when conventional RO membranes were used (Cath, Childress *et al.* 2006). As an alternative option, nanofiltration (NF) membranes have been explored for use in FO process due to their properties of 'loose' RO and high rejections to multivalent salts. Wang *et al.* reported that polybenzimidazole (PBI) NF hollow fiber membranes with a desirable mean pore size can be used for FO process. Under FO tests using 1M $MgCl_2$ as the draw solution, these membranes showed water flux of 4 and 6 $l/m^2.h$ for the configurations of active layer facing feed water (AL-FW) and active layer facing draw solution (AL-DS), respectively (Wang, Chung *et al.* 2007; Wang, Yang *et al.* 2009). PBI, however, has poor mechanical strength for fabrication of self-standing membranes (Chung 1997). Su *et al.* fabricated cellulose acetate NF hollow fiber membrane and explored its FO application. The membrane exhibited water flux in the range of 2.7-7.3 $l/m^2.h$ with 0.5-2.0 M $MgCl_2$ draw solutions for the AL-DS orientation and 1.8-5.0 $l/m^2.h$ with the same draw solutions for the AL-FW orientation (Su, Yang *et al.* 2010). Hydrophilic polymers such as cellulose and its derivatives exhibit good properties as membrane materials in desalination applications. However, these polymers are very sensitive to thermal, chemical and biological degradation (Mulder 1996). Hydrolysis to this type of

material occurs very rapidly in alkaline conditions. The separation process using cellulose-based membranes must be carried out at an optimum pH of 4 to 6.5 at ambient temperature (Mulder 1996).

This study aims to fabricate poly(amide-imide) (PAI) hollow fiber membranes suitable for FO applications. PAI, known commercially as Torlon®, has an excellent mechanical property and high thermal stability (Robertson, Guiver *et al.* 2004). It also presents a good chemical stability at a wide pH range and a high resistance to many organic solvents because of its ability to form intra- and inter-chain hydrogen bonding (Robertson, Guiver *et al.* 2004; Kosuri and Koros 2008). In addition, PAI can be utilized in hollow fiber membrane fabrication using non-solvent induced phase separation (NIPS) technique (Higuchi, Yoshikawa *et al.* 2005; Kosuri and Koros 2008). However, different from prior studies, the present work explores a simple method to make hollow fiber membranes with a NF-like selective layer by utilizing the unique feature of PAI. That is, the imide group in PAI can react with an amine-functionalized polyelectrolyte (i.e., PEI) to form a positive charged diamine on the membrane surface, which has been confirmed in the present work. To the best of our knowledge, this is the first time to report the fabrication of PAI hollow fiber membranes with a positively charged NF-like selective layer using a simple chemical post-treatment. The performance of modified PAI hollow fiber membranes have been tested for FO application.

3.2. Experimental

3.2.1. Materials

Torlon® 4000T (copolymer of amide and imide) (PAI, Solvay Advanced Polymers, Alpharetta GA) was used to make porous hollow fiber substrates. N-Methyl-2-pyrrolidone (NMP, > 99.5%, CAS#872-50-4, Merck Chemicals, Singapore) and Lithium chloride (LiCl, anhydrous, CAS#7447-41-8, MP Biomed) were used as a solvent and additive, respectively. Purified water by a Milli-Q system (18MΩcm) was used as the internal coagulant. Dextrans with different molecular weights (from 6,000 to 500,000 Da, $(C_6H_{10}O_5)_n$, CAS#9004-54-0, Sigma) were used to characterize the molecular weight cut off (MWCO) of hollow fiber membranes. Polyethyleneimine

(PEI) ethylenediamine end-capped (molecular weight (M_w) ~800, Sigma Aldrich) was used to perform chemical post-treatment of the hollow fiber substrate. For filtration experiments, sodium chloride (NaCl, ≥ 99%), magnesium chloride ($MgCl_2$, hexahydrate), sodium sulfate (Na_2SO_4, anhydrous), magnesium sulfate ($MgSO_4$, heptahydrate) were purchased from Merck. All the reagents were used as received.

3.2.2. Preparation of polymer dope solutions

PAI and LiCl were dried in a 50°C vacuum oven for 24 h to remove moisture prior to the dope preparation. Desired amounts of the dry polymer, additive, and solvent were mixed in a jacket flask equipped with an overhead stirrer and connected to a circulator bath at a controlled temperature of 70°C. The detailed compositions of the polymer dope solution are shown in Table 3.1. After the polymer mixture became a homogeneous solution, the solution was cooled down to room temperature, filtered by using a 15 μm stainless steel filter, transferred to a dope tank, and subsequently degassed under vacuum at ambient temperature over night prior to spinning.

3.2.3. Fabrication of poly(amide-imide) hollow fiber substrates and post-treatments

PAI hollow fiber substrates, designated as ST#1, ST#2 and ST#3, were made based on the same polymer material but different spinning conditions and different additive concentrations. The spinning conditions are listed in Table 3.1. PAI hollow fiber substrates were fabricated by a dry jet-wet spinning technique. The dope solution, connected to a high pressure nitrogen gas cylinder, was extruded through the outer channel of the spinneret (see Figure 3.1) at a specific flow rate using a Zenith gear pump. The bore fluid was extruded using a high precision syringe pump (Isco) through the inner channel of the spinneret. The nascent fibers went through a certain air gap before immersing into an external coagulation bath at a controlled temperature, and then collected by a roller at a free fall take-up speed. The resultant hollow fiber membranes were stored in a water bath for approximately 2 days at ambient temperature to ensure that the residual solvent has been removed completely. A post-treatment was performed in order to minimize the membrane shrinkage during drying process for storage purpose. The membranes were immersed in a glycerol/water

mixture (1:1 by volume) for 24h. This process allowed the glycerol to stay inside the membrane pores as pore supporter to alleviate the pore collapse during membrane drying process. Removing the glycerol can be done by immersing the membranes in DI water for 24h prior to use.

Table 3.1. Spinning conditions and parameters.

Parameters	ST#1	ST#2	ST#3
Dope composition (PAI/LiCl/NMP) (wt.%)	20/0/80	15/2/83	15/3/82
Dope flow rate (g min^{-1})	6.0	6.0	6.0
Bore fluid (NMP/H_2O) (vol.%)	0/100	25/75	25/75
Bore fluid flow rate (mL min^{-1})	4.0	8.0	8.0
Air gap (cm)	5.0	5.0	5.0
Take up speed	free fall	free fall	free fall
External coagulant	tap water	tap water	tap water
Spinning temperature (°C)	23	23	23
Spinneret diameter (mm)	1.50	1.50	1.50
ID of bore fluid needle (mm)	0.70	0.70	0.70

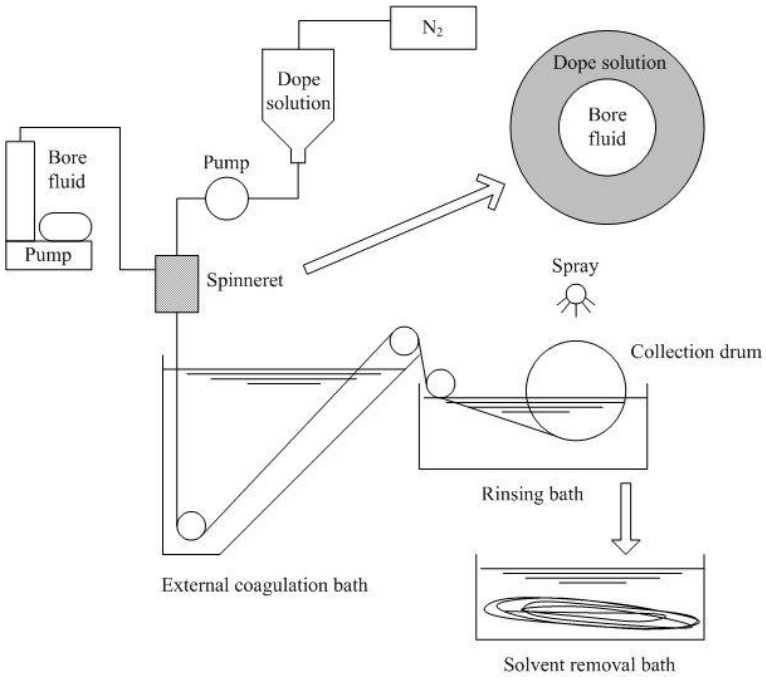

Figure 3.1. Single layer hollow fiber spinning setup.

3.2.4. Development of NF-like selective layer by PEI cross linking

NF-like selective layer was developed on the outer side of PAI hollow fiber substrates by PEI cross-linking. The reaction was conducted by immersing the hollow fiber substrates into a 500 mL of PEI aqueous solution at temperature of 60-80°C. The reaction time varied from 0 to 120 min and the PEI concentration varied from 0.5% to 2% (wt/wt). Next, the membranes were rinsed using purified water and stored for characterization.

3.2.5. Characterization of PAI hollow fiber substrates

The dimension of the hollow fiber membranes was measured by a Keyence VHX 500F Digital Microscope. Four different fibers were taken and a mean value was calculated for each sample measurement. The morphology of the cross-section and the membrane surface were examined by a Zeiss EVO 50 scanning electron microscope (SEM). Dry membrane samples were frozen and cracked in liquid nitrogen and subsequently mounted on the SEM stubs and dried overnight in a 50°C vacuum oven prior to sputter coating. An Emitech SC7620 gold sputter coater was used to deposit a layer of gold under argon environment.

The average overall porosity of the membrane was determined by gravimetric method which measures the weight of isopropyl alcohol as the wetting solvent contained in membrane pores. Tensile strength test of the hollow fiber membranes was performed using a Zwick 0.5kN Universal Testing Machine at room temperature.

Four pieces of PAI hollow fibers were potted into a module and sealed to prepare a lab-scale module with an effective length of 21 cm. PWP experiments were performed by using two to three modules from the same batch of the membrane spinning process. Milli-Q ultra pure water was circulated through the shell side of the membrane module under a pressure of 1 bar for 90 minutes to compact the membrane prior to PWP measurement (Persson, Gekas *et al.* 1995). The PWP of the membranes ($l/m^2.h.bar$) was calculated by:

$$PWP = \frac{V}{t\,A\,\Delta P} \tag{3.1}$$

where V is the volume of permeate taken (l) per determined time, t (h); A is the filtration area of the hollow fiber membrane (m^2); and ΔP represents the pressure difference between the feed side and the permeation side of the membrane (bar).

MWCO and pore size distribution of PAI hollow fiber substrate were assessed by using a 2000 ppm dextran aqueous solution containing a mixture of several different molecular weights from 6,000 Da to 500,000 Da. The dextran solution was circulated through the shell side of the hollow fiber module and the permeate was collected for analysis by gel permeation chromatography (GPC) on a Polymer Laboratories-GPC 50 plus system (double PL aquagel-OHMixed-M 8μ columns). The details of the pore size distribution calculation can be found elsewhere (Ren, Wang *et al.* 2006). The molecular weight of dextran that gave 90% rejection was recorded as the MWCO.

3.2.6. Measurements of chemically modified PAI hollow fibers

Membrane surface charge (zeta potential) was observed based on the streaming potential measurement by using a SurPASS electrokinetic analyzer (Anton Paar GmbH, Austria). An electrolyte solution of 10 mM potassium chloride (KCl, Merck, Singapore) solution was circulated through a cylindrical measuring cell containing the membrane sample. The streaming potential was detected by Ag/AgCl electrodes located at both ends of the sample. Automatic titration was performed using a 0.1 M hydrochloric acid (HCl, Qrec) solution and a 0.1 M sodium hydroxide (NaOH, Merck, Singapore) solution to investigate the effect of pH on membrane surface charge. The Fairbrother-Mastin approach was used to determine the zeta potential of the membrane (Anton-Paar 2009).

The chemical reaction occurred in the post-treatment was confirmed by a fourier transformed infrared spectrometer (FTIR, Perkin Elmer, Spectrum 2000) using the attenuated total reflection (ATR) with ZnSe crystal method. The hollow fiber membranes were dried in a vacuum oven overnight before the analysis.

The salt rejection of chemically modified PAI hollow fibers was conducted in a bench scale cross-flow filtration unit. The hydraulic pressure of 1 bar was applied on the shell side of the hollow fiber membrane module. The salt rejection experiment was carried

out using a 500 ppm $MgCl_2$ solution (~5.3mM $MgCl_2$ solution) based on conductivity measurement (Mettler Toledo) of permeate and feed solutions.

The schematic diagram of a lab-scale cross-flow FO unit used in this study is illustrated in Figure 3.2. The same modules used for PWP and salt rejection measurements were used for FO experiment. One variable-speed gear pump was used to supply the draw solution and two variable speed peristaltic pumps were used to supply the feed and dosing solution, respectively. The volumetric flow rates of the Shell side and lumen side were 1250 ml/min and 500 ml/min, respectively, to ensure a similar Reynolds number (around 2600) of the liquid flowing both in the module shell and fiber lumen. FO experiments were performed in two configurations: (1) draw solution flowed in shell side or active layer facing draw solution (AL-DS), or known as PRO mode, and (2) draw solution flowed in lumen side or active layer facing feed water (AL-FW), or known as FO mode. The volumetric water flux, J_v, was determined at a certain time interval by measuring the weight changes of the feed tank with a digital mass balance connected to a data logging system.

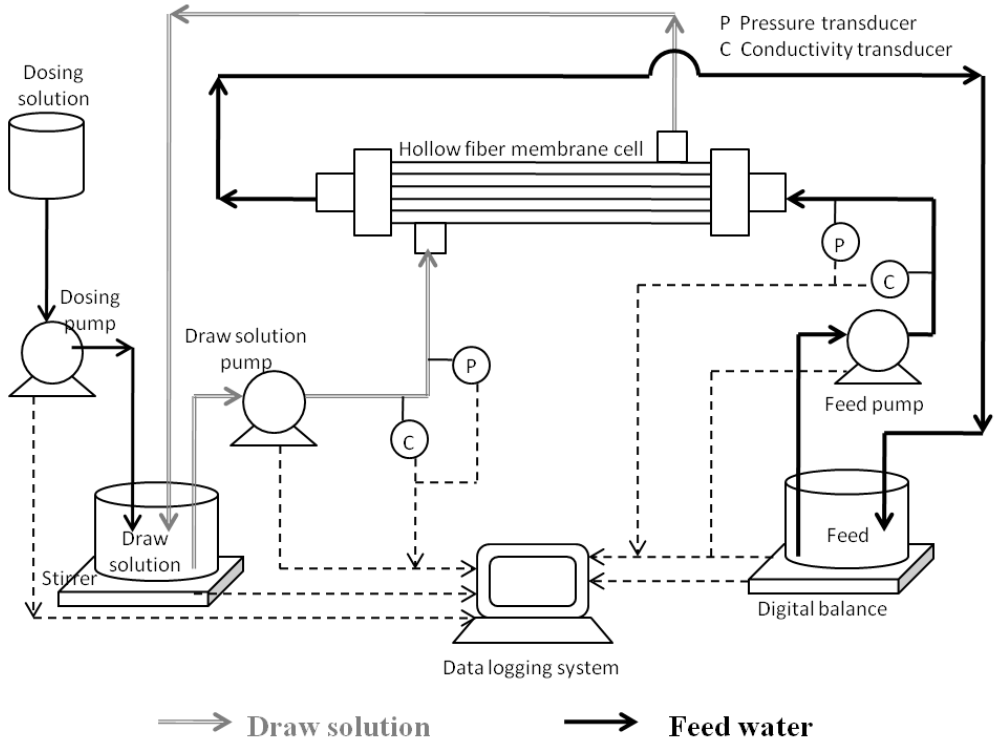

Figure 3.2. The schematic diagram of a lab-scale cross-flow FO unit.

3.3. Results and discussion

3.3.1. Morphology and property of PAI hollow fiber substrates

Figure 3.3 shows the cross-section morphologies of SEM for three PAI hollow fiber substrates prepared by a variation of dope composition and spinning parameter, as indicated in Table 3.1. It can be seen that these substrates exhibited similar cross-section morphologies in which the finger-like structures were developed simultaneously beneath the inner and outer surfaces without forming large macro-voids. However, the ST#1 hollow fiber substrate presented the thickest sponge-like structure in the middle of the cross-section, followed by the ST#2 and ST#3 hollow fiber substrates, as shown in Figure 3.3 a2, b2 and c2. Moreover, the difference in wall thickness of the fibers can be easily observed. The thinner walls for the ST#2 and ST#3 substrates are mainly attributed to the higher flow rate of the bore fluid used (for ST#2 and ST#3) during membrane fabrication. A thinner substrate and less sponge-like structure are favorable to the FO process, which will be discussed in Section 3.3.4.

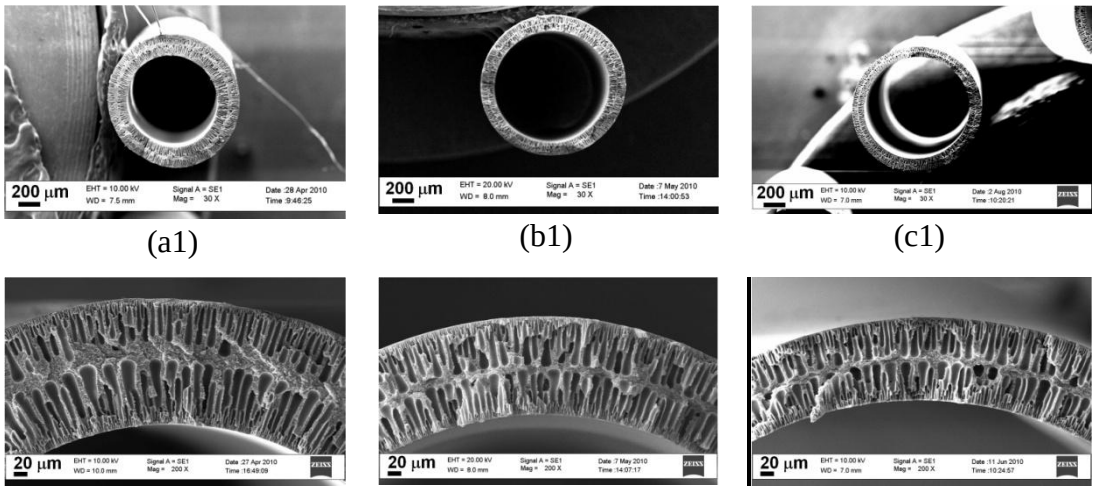

(a1) (b1) (c1)

(a2) (b2) (c2)

Figure 3.3. Cross section morphology of PAI hollow fiber substrates: (a1) ST#1 at 30X; (a2) ST#1 enlarged at 200X; (b1) ST#2 at 30X; (b2) ST#2 enlarged at 200X; (c1) ST#3 at 30X; (c2) ST#3 enlarged at 200X.

The properties of PAI hollow fiber substrates in terms of dimension, PWP, MWCO and porosity are listed in Table 3.2. The ST#2 and ST #3 hollow fiber substrates possessed quite large dimensions (ID/OD around 1.2/1.5 mm/mm) in comparison with

conventional NF hollow fibers. A larger fiber lumen is favorable to the fluid flow inside the lumen with less resistance based on the Hagen-Poiseuille's law. The NF membranes applied for FO process reported in literature, however, had much smaller fiber dimensions. For instance, the ID/OD of the PBI NF membrane was 0.14/0.27 mm (Wang, Chung *et al.* 2007).

Table 3.2. Properties of PAI hollow fiber substrates.

Properties	ST#1	ST#2	ST#3
Fiber ID/OD (mm/mm)	0.87/1.27	1.19/1.50	1.17/1.45
Fiber wall thickness (μm)	200	155	140
PWP (l/m^2.h.bar)	27	122	134
Outer skin MWCO (KDa)*	20	23	< 6
Inner skin MWCO (KDa)$^+$	37	44	24
Porosity (%)	51	70	85

From Table 3.2 it can also be seen that the ST#1 has the lowest PWP compared to ST#2 and ST#3 substrates as the polymer concentration in the original dope composition decreased from 20% to 15%, leading to increased membrane porosity. It seems the ST#3 hollow fiber substrate possessed an excellent pore structure, which is indicated by the low MWCO (<6 KDa, dextran filtration was performed from the shell side), high pure water flux (134 l/m^2.h.bar) and high porosity (85%). The MWCO experiment was repeated to confirm the correctness of the measurement. The possible reason responsible for the low MWCO may be linked to the dope composition of ST#3 substrate (PAI/LiCl/NMP: 15/3/82). Since the concentration of the additive is high (higher than ST#2), the thermodynamic stability of the initial dope composition was reduced, so instantaneous demixing might take place in the phase inversion process, resulting in a denser surface but more porous support (Shi, Wang *et al.* 2008). These properties are believed to be relevant to the subsequent chemical post-treatment and FO application.

Table 3.3 shows the mechanical properties (tensile modulus, tensile stress at break and tensile strain) of the PAI hollow fiber substrates along with the counterparts of

polyethersulfone (PES) hollow fiber membranes reported in literature (Qin and Chung 1999; Chung, Qin *et al.* 2000; Wang, Shi *et al.* 2010). The PAI hollow fibers possessed tensile modulus of 151–239 MPa, which is much higher than that of PES hollow fibers (57.5–138.9 MPa). A high tensile modulus suggests a high rigidity of the membrane. While the tensile stress and strain at break measured for the PAI hollow fibers can reach as high as 6.4–12.2 MPa and 26–50%, respectively, the combination of high tensile stress and strain at break makes the membrane to have a high toughness.

Table 3.3. Mechanical properties of PAI hollow fiber substrate.

Sample	Tensile Modulus (MPa)	Stress at break (MPa)	Strain at break (%)
ST#1	239 ± 16	9.8 ± 0.5	42 ± 4
ST#2	224 ± 7	12.2 ± 1.1	50 ± 7
ST#3	151 ± 4	6.4 ± 0.2	26 ± 4
PES (Wang, Shi *et al.* 2010)	81.9 – 88.4	4.1 – 5.4	34.0 – 58.6
PES (Chung, Qin *et al.* 2000)	57.5 – 104.0	0.9 – 1.7	9.9 – 16.9
PES (Qin and Chung 1999)	107.0 – 138.9	2.8 – 3.4	29.5 – 43.8
PES (Sukitpaneenit and Chung 2012)	196 – 273	5.8 – 6.9	48 – 51

3.3.2. Optimal conditions for chemical post-treatment

The optimal post-treatment temperature was determined by varying the temperature from 60 to 80°C using the ST#1 hollow fiber as the model substrate while the PEI concentration was fixed at 1% and the post treatment time was controlled at 2h. The temperature effect on the PWP and salt rejections of the modified membrane can be observed from Table 3.4. Before the post treatment, the original membrane had the PWP of 26.7 l/m^2.h.bar and the rejection of 11.9% to $MgCl_2$. As the temperature of post-treatment increased, the PWP decreased to l/m^2.h.bar while the salt rejection to $MgCl_2$ increased to 94% at 70°C due to more surface pores being sealed as a result of cross-linking reaction between the PAI and PEI. The chemical reaction has been confirmed by ATR-FTIR experiments and will be discussed in Section 3.3.3. The mechanical strength of the membranes modified at 60 and 70°C remained almost

unchanged. However, when the post-treatment temperature increased to 80°C, the reaction might be too severe, resulting in a membrane with a very poor mechanical strength. Hence, the post-treatment temperature of 70°C was selected as an optimal condition applied for the treatment of other hollow fiber substrates.

Table 3.4. Effect of post treatment temperature on membrane properties*.

Post treatment Temperature (°C)	Tensile strength (MPa)	PWP ($l/m^2.h.bar$)	Salt rejection (%)	
			NaCl	$MgCl_2$
Original-ST#1	9.8 ± 0.5	26.7 ± 1.5	5.1 ± 0.7	11.9 ± 1.5
60	9.9 ± 0.2	14.6 ± 0.1	7.9 ± 0.7	46.3 ± 8.8
70	9.7 ± 0.2	1.8 ± 0.03	49.4 ± 3.0	94.4 ± 0.4

*Post treatment condition: 1 wt.% PEI solution for 2h.

In order to determine the optimal PEI concentration, three PEI aqueous solutions of 0.5 wt%, 1 wt% and 2 wt% were prepared. As observed in Figure 3.4, the ST#1 hollow fiber membranes modified with a 0.5 wt% PEI solution gave the lowest salt rejection to $MgCl_2$ and the highest PWP as compared to those modified with 1 wt% and 2 wt% PEI solutions. When 1 wt% and 2 wt% PEI solutions were used, there was no significant difference in the PWP of the modified membranes, but the membrane treated in a 1 wt% PEI solution presented the highest rejection of NaCl. Thus, the PEI solution with 1 wt% concentration was used for the post-treatment.

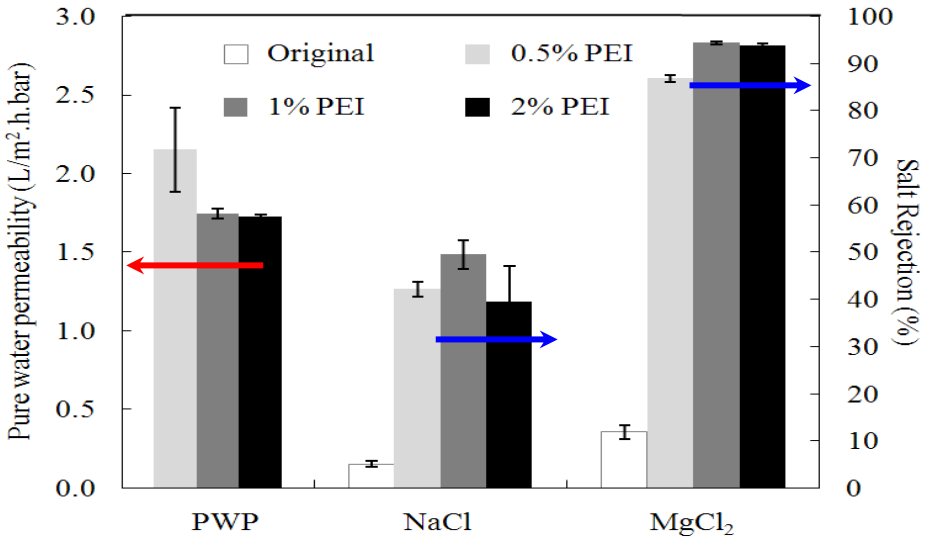

Figure 3.4. Salt rejections of ST#1 membranes immersed in various concentrations of PEI solution at 70°C for 120 min.

Figure 3.5 shows the effect of post-treatment time on the filtration performance of modified ST#1 membrane using a 1 wt% PEI solution at 70°C. Obviously, a longer post-treatment time allowed more PEI molecules to crosslink with PAI, leading to an increase in the thickness of dense outer layer. Consequently, the PWP decreased and the salt rejection (R_s) increased. The membranes immersed in the PEI solution for 60 min showed $MgCl_2$ rejection of 47% and the PWP of 12 l/m^2.h.bar. Increasing the immersion time to 120 min enhanced the $MgCl_2$ rejection significantly to 94% and dropped the PWP to 1.74 l/m^2.h.bar.

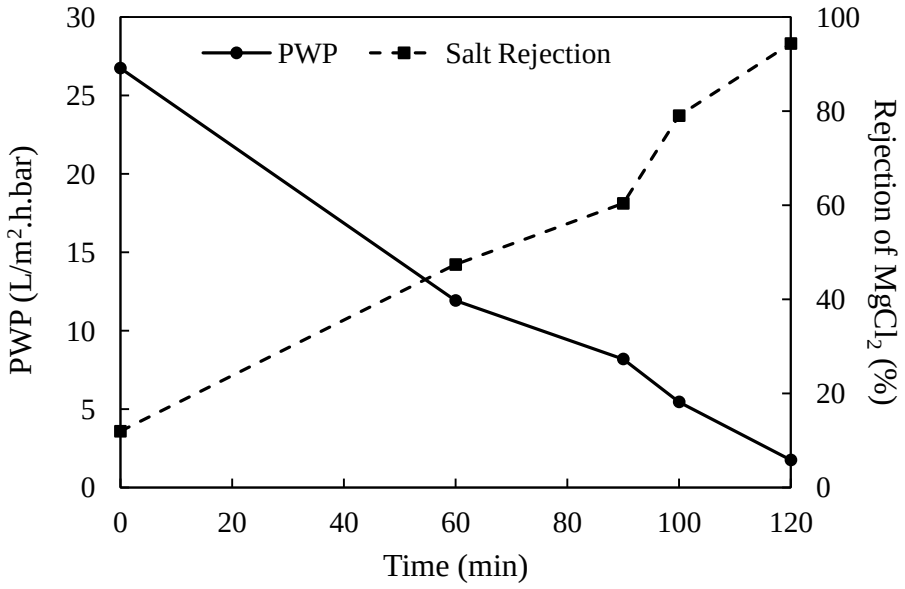

Figure 3.5. Effect of post-treatment time on filtration performance of treated ST#1 membrane (test conditions: 1.0 bar, room temperature and 500ppm salt aqueous solution; post-treatment conditions: 70°C and 1 wt% PEI solution).

3.3.3. Characteristics of modified PAI hollow fiber membranes

Figure 3.6 a-c show the cross section and outer surface morphology of ST#1 modified PAI hollow fiber. It can be seen that there is no visible difference on the cross section morphology as compared to the original ST#1 hollow fiber substrate depicted in Figure 3.3 a1 and a2. However, the difference in the outer surface morphology for modified and unmodified membranes can be noticed as shown in Figure 3.6 c and d. The outer surface became denser after the post treatment.

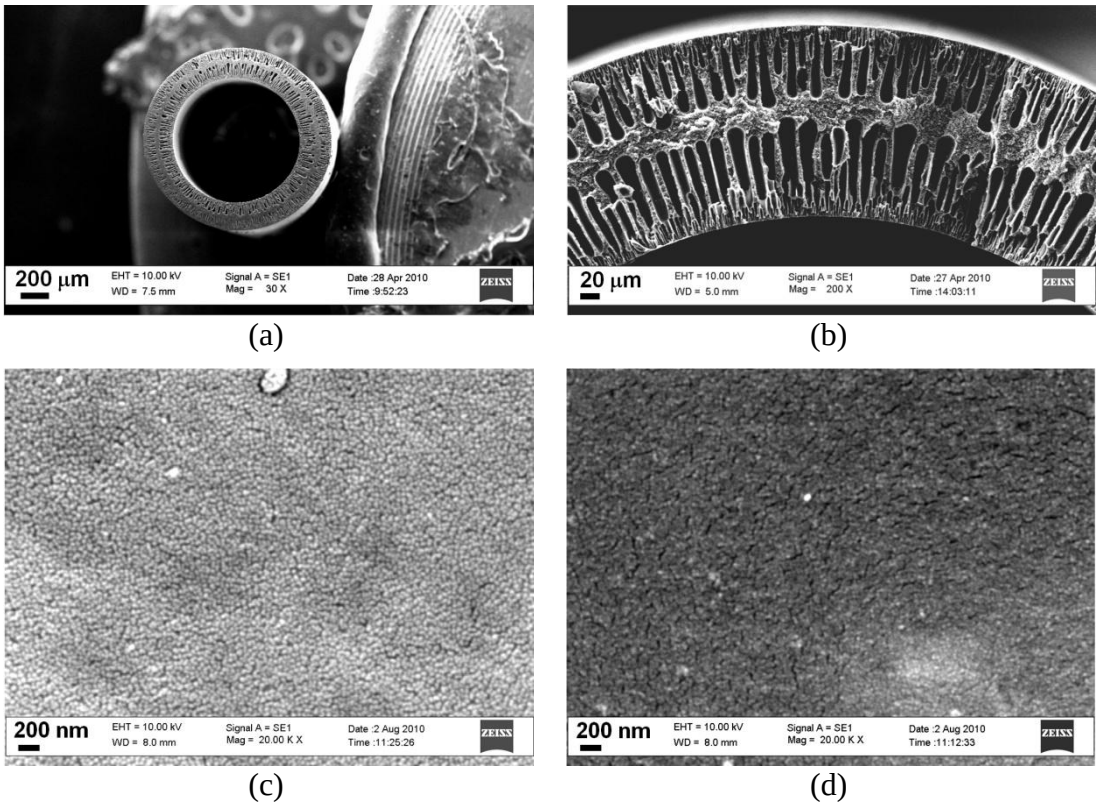

Figure 3.6. Cross section morphology of ST-1 PAI hollow fiber after post treatment: (a) enlarged at 30X; (b) enlarged at 200X. Outer surface morphology of ST#1 PAI hollow fiber: (c) after post treatment, enlarged at 20KX (post treatment condition: 1 wt% PEI solution at 70°C for 2h); (d) before post treatment, enlarged at 20KX.

The chemical reaction between the PAI and PEI was verified by ATR-FTIR measurements as shown in Figure 3.7. The typical imide bands can be detected at 1778 and 1717 cm^{-1} (symmetric and asymmetric C=O stretching, respectively), 1379 cm^{-1} (C-N-C stretching), 1109 and 725 cm^{-1} (imide ring) for the ST#1 PAI hollow fiber substrate. It can be seen clearly that after the post-treatment, the imide peaks disappearred while amide peaks became stronger (C=O at 1641 cm^{-1} and C-N at 1532 cm^{-1}). This confirms that the cross-linking has effectively taken place as depicted in Figure 3.8 where the imide rings were opened and a bond between the amine functional group in PEI and the imide rings in PAI has been formed.

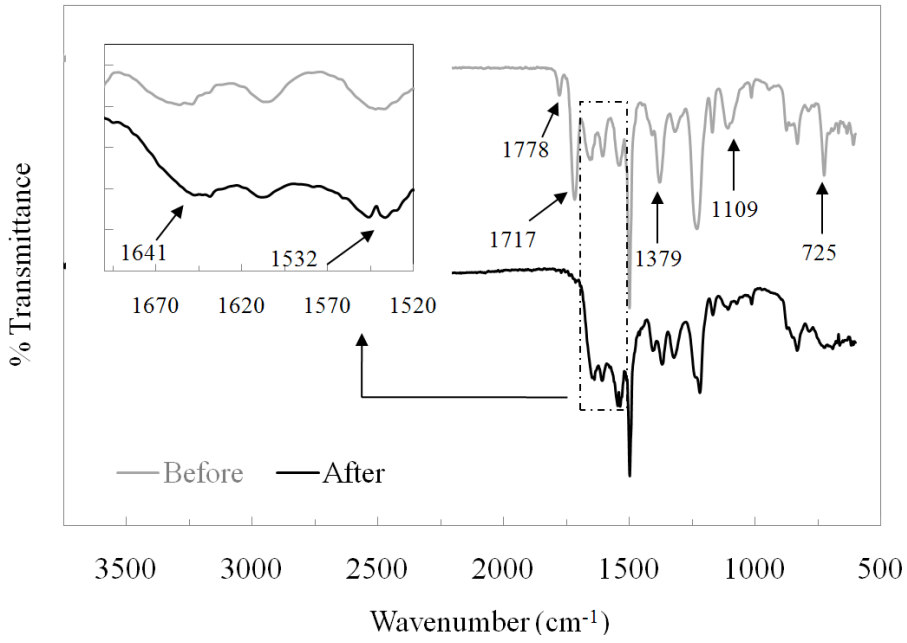

Figure 3.7. ATR-FTIR spectra of the ST#1 substrate before post-treatment (top) and after post treatment (bottom). The inset is the spectra in the wave number region of 1520-1670 cm^{-1}. (Post-treatment conditions: 1 wt% PEI solution at 70°C for 2h).

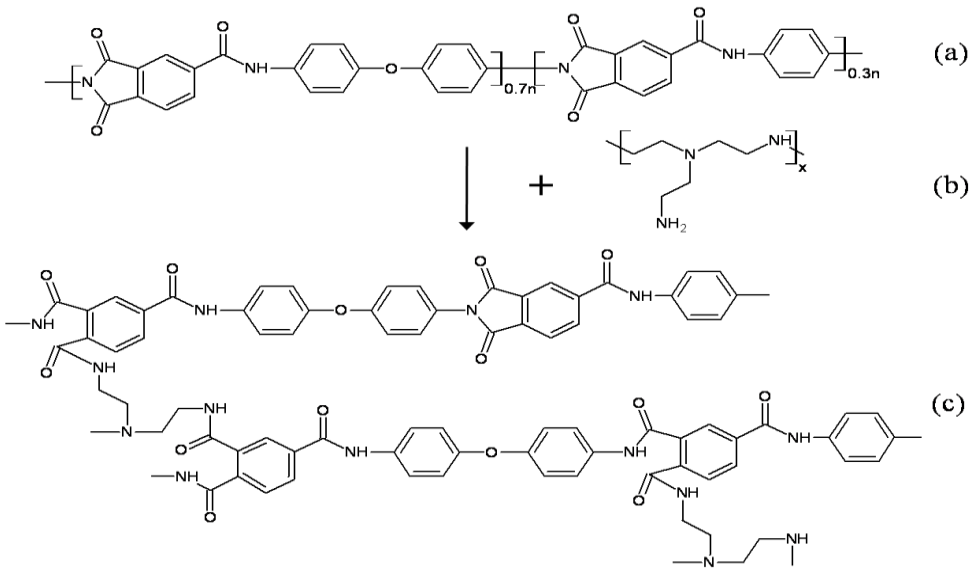

Figure 3.8. Reaction scheme between (a) PAI (adapted from (Robertson, Guiver *et al.* 2004)) and (b) PEI; (c) cross-linked PAI.

The charge characteristics of the ST#1 hollow fiber membrane before and after the post-treatment were determined in terms of zeta potential. It can be seen in Figure 3.9 that the original PAI membrane had an isoelectric point of 4.4. At a pH below the

isoelectric point, the membrane were positive charged due to amine protonation, while at a pH above the isoelectric point the membrane was negative charged because of the deprotonation of carboxyl group (Childress and Elimelech 2000). Similar results were reported in literature (Sun, Wang *et al.* 2010b). However, it was noticed that after the post-treatment the isoelectric point was shifted to 10.4 due to more amine groups attached to the surface. This means the membrane presented positive charges in a wide pH range, which could be beneficial to some applications.

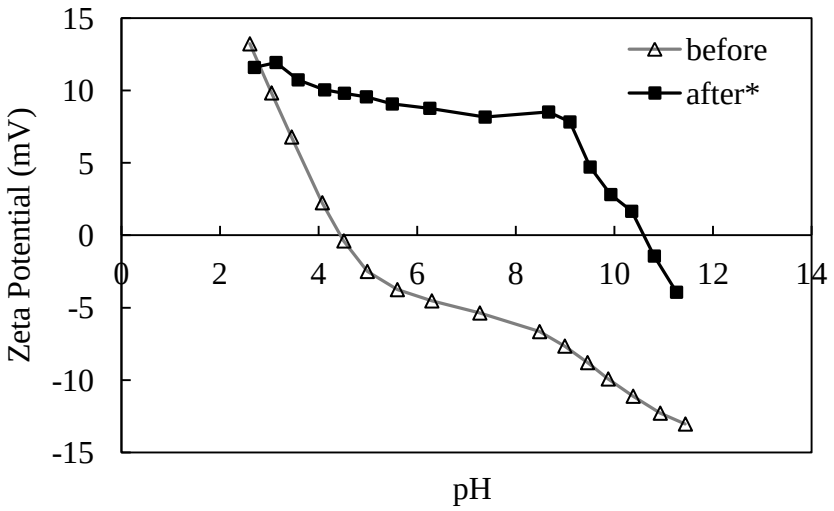

Figure 3.9. Zeta potential of ST#1 hollow fiber membrane before and after post-treatment (*post-treatment conditions: 1 wt% PEI solution at 70°C for 2h).

The rejection behaviors of the modified ST#1 membrane to various salts are depicted in Figure 3.10. The chemical reaction between the PAI and PEI resulted in a positive charged membrane due to amine groups attaching on the membrane surface. Thus, a high rejection of $MgCl_2$ is expected. It was also observed that the membrane presented a higher rejection to divalent cations than monovalent cations. The $MgCl_2$ rejection was the highest at all post-treatment time while Na_2SO_4 had the lowest rejection though the diffusion coefficients for those salts are comparable ($MgCl_2$: 1.25 10^{-9} m^2/s; Na_2SO_4: 1.23 .25 10^{-9} m^2/s (Schaep, Van Der Bruggen *et al.* 1998)). These results may be attributed to the combination of several factors: (1) the valency of the co-ion and counter-ion, (2) the electric charge on the membrane, and (3) the hydrated radius of the ions. Especially, when a charged membrane was placed in an electrolyte solution, the concentration of the co-ion near the membrane surface was lower than

that in the bulk solution, while the counter-ion concentration was higher near the membrane surface than in the bulk solution (Peeters, Boom *et al.* 1998). Since the counter-ion valency of SO_4^{2-} is higher than that of co-ion (Na^+) in the Na_2SO_4 solution, the positive charges of the membrane may be shielded. Therefore, the contribution from the electric interaction to the selective rejection behavior (Donnan repulsion effect) of the membrane was weakened, leading to a lower rejection to Na_2SO_4. Similar results were reported in literature (Peeters, Boom *et al.* 1998).

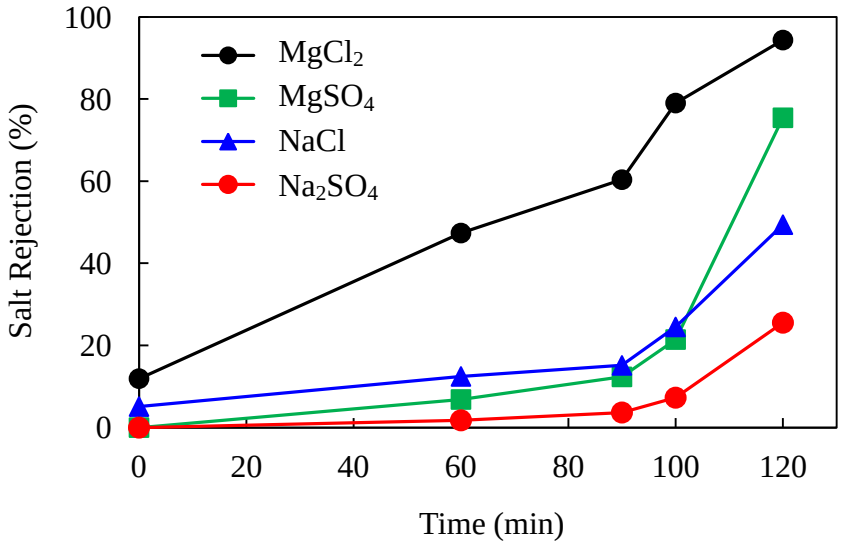

Figure 3.10. Rejection behaviors of treated ST#1 membrane to various salts (test conditions: 1.0 bar, room temperature and 500ppm salt aqueous solution; post-treatment conditions: 1 wt% PEI solution at 70°C).

3.3.4. PAI hollow fiber membranes with a positively charged NF-like selective layer for FO application

The intrinsic properties of PAI hollow fiber membranes with a positively charged NF-like selective layer (hereafter denoted as PAI FO hollow fibers) such as water permeability *A*, salt permeability *B*, and $MgCl_2$ rejection measured in an RO cross-flow filtration setup are tabulated in Table 3.5. It can be seen that the PAI FO hollow fibers presented a water permeability ranging from 1.74 to 2.25 l/m^2.h.bar which is higher than commercial HTI's FO flat sheet membranes (HTI's FO membrane: *A* value of 0.8 – 1.13 l/m^2.h.bar) (Gray, McCutcheon *et al.* 2006; Tang, She *et al.* 2010). The three PAI FO hollow fibers also exhibited a high $MgCl_2$ rejection over 91.1% at 1 bar pressure.

Table 3.5. Intrinsic properties of PAI FO hollow fiber membranes.

Sample	Water permeability, A (l/m^2.h.bar)	Salt permeability* B (l/m^2.h)	$MgCl_2$ Rejection @ 1 bar, R_{salt} (%)
ST#1	1.74	0.065	94.4
ST#2	2.25	0.113	92.7
ST#3	2.19	0.138	91.1

*Salt permeability, B, is determined based on 500ppm $MgCl_2$ solution.

The performance of three different PAI FO hollow fiber membranes in FO process was determined using a 1.5 M $MgCl_2$ solution as the draw solution and de-ionized water as the feed water at 23°C, and the results are listed in Table 3.6. It was found that in the configuration of the AL-DS, the ST#1, ST#2, and ST#3 PAI FO hollow fibers showed a water flux of 6.34, 17.28, and 17.15 l/m^2.h, respectively. The ST#2 and ST#3 PAI FO membranes presented almost three-time higher water flux as compared to the ST#1. Since the water flux in the FO process is determined by both the skin layer and the substrate structure (Chou, Shi *et al.* 2010), and the water permeability (A) of the ST#2 and ST#3 membranes is only ~1.3 times of the ST#1 membrane, the three-time higher water flux presented by the ST#2 and ST#3 membranes is believed to be mainly attributed to their much thinner and more porous substrate structure, as shown in Figure 3.3 and Table 3.2.

Table 3.6. Performance of PAI FO membranes applied in FO process*.

Sample	AL-DS		AL-FW	
	J_v (l/m^2.h)	J_s/J_v (g/l)	J_v (l/m^2.h)	J_s/J_v (g/l)
ST#1	6.34	0.48	4.15	0.46
ST#2	17.3	0.96	11.7	0.33
ST#3	17.2	2.19	12.9	0.37

*Draw solution:1.5M $MgCl_2$ solution.

The experimental FO water flux and the ratio of salt flux over water flux (J_s/J_v) as a function of draw solute concentration are shown in Figure 3.11 for the ST#2 and ST#3 PAI FO hollow fiber membranes. General speaking, water flux (J_v) and salt flux (J_s) increase as the concentration of draw solution increases which is also consistent with

those reported in literature (Hancock and Cath 2009; Phillip, Yong *et al.* 2010). It was found that the two membranes exhibited similar water flux profiles. The water flux increased steadily as the concentration of the draw solution increased. For both the AL-DS and AL-FW configurations, the ST#2 and ST#3 PAI FO membranes presented similar performance. This result is rather surprising, as the UF substrates of the ST#2 and ST#3 had different MWCOs and porosities (ε) though the fiber wall thickness (l) of the two membranes is similar. Perhaps, the difference in the pore size of the outer surface was mitigated by the chemical crosslink reaction. In the substrate, porosity, fiber wall thickness and tortuosity (τ) are the main parameters to affect the FO flux. Since the ST#2 substrate had bigger pores, it might have better pore interconnections, i.e., a smaller value of tortuosity as compared with the ST#3 substrate. Though the ST#2 substrate has a lower porosity than the ST#3 substrate, the structural parameters $S = \tau l / \varepsilon$ of these two substrates might be similar.

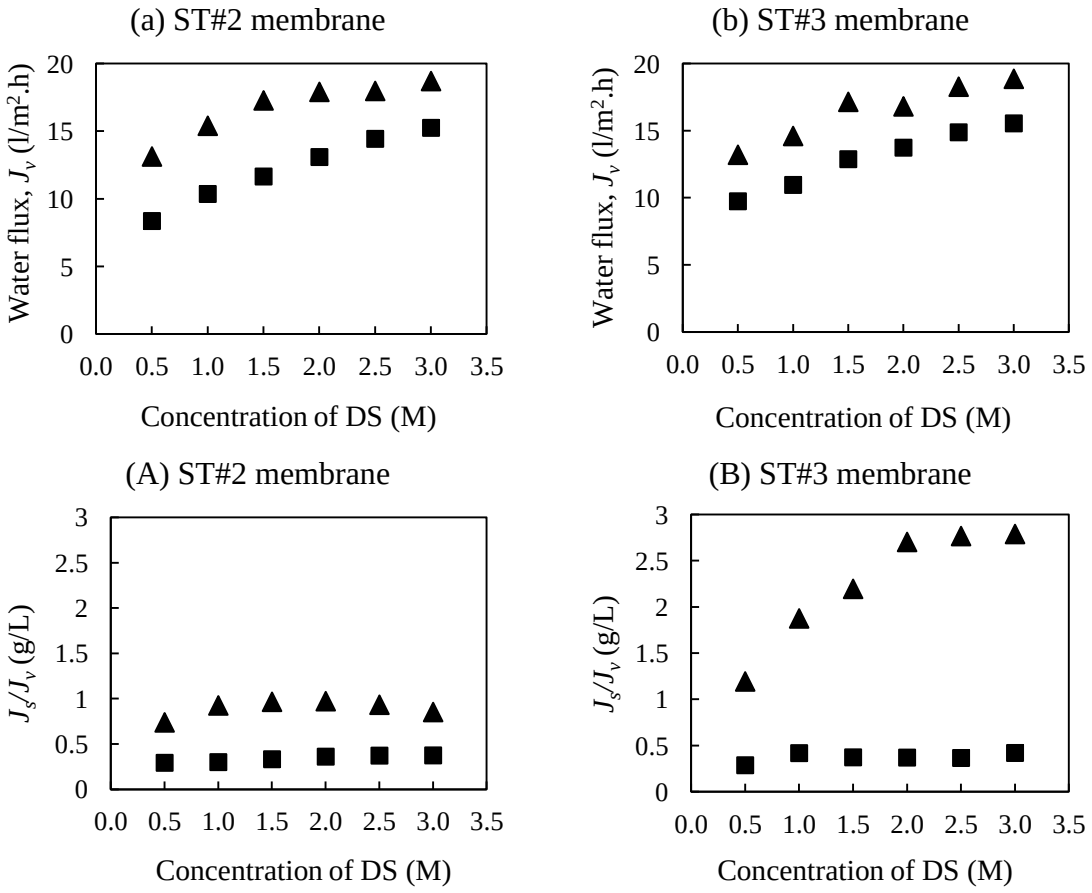

Figure 3.11. FO experimental results of water flux and J_s/J_v in two configurations (▲ AL-DS; ■ AL-FW).

The J_s/J_v profiles as a function of the draw solute concentration for the ST#2 and ST#3 PAI FO hollow fiber membranes are illustrated in Figure 3.11 (A) and (B). Overall, in the configuration of the AL-FW, the ST#2 and ST#3 membranes show similar J_s/J_v profiles. The J_s/J_v of the two membranes is smaller than 0.4 g/l, which is lower than in the AL-DS configuration for both membranes. This value is also lower than the data for HTI's FO membrane which is 0.85 g/l (Tang, She *et al.* 2010). Surprisingly, when the orientation changed, a significant difference in the J_s/J_v profile occurred between the two membranes. The J_s/J_v of the ST#2 PAI FO hollow fiber membrane increased slightly as the draw solute concentration increased to 2.0 M and then it maintained almost unchanged. In contrast, the J_s/J_v of the ST#3 membrane was much higher than the ST#2 PAI FO hollow fiber membrane, and it raised sharply with an increase in draw solute concentration.

To understand this behavior, schematic concentration profiles in a positively charged membrane are depicted in Figure 3.12 to illustrate the salt transportation in the FO process. The PAI FO hollow fiber membrane consists of two parts: (1) a dense active skin layer (shaded) which contains most of the charge; and (2) a porous substrate (white) which may contain less charge, as the membrane substrate was immersed in a PEI solution after both fiber ends were sealed. It should be noted that different from a neutral membrane, the mass transfer in the charged substrate is also affected by the electric repulsion in addition to the structural parameter. In the AL-FW configuration (Figure 3.12-a), the C_1 and C_4 are the salt concentrations of the bulk feed and the draw solution, and the C_2 and C_3 are the salt concentrations at the interfaces between the feed and the membrane surface, and between the active layer and the porous substrate, respectively. The difference between the C_3 and C_4 was caused by water permeation (dilution effect) for a neutral membrane, which is so-called internal concentration polarization effect (Cath, Childress *et al.* 2006). However, the C_3 in a positively charged membrane substrate may be smaller than in a neutral membrane substrate due to the Donnan exclusion that tended to expel the $MgCl_2$ back to the draw solution. In addition, the charges in the dense-active surface also imposed a repulsive force to the salt penetration through the membrane (salt flux and salt repulsion are in opposite directions). Thus there were double electrical repulsions to the salt transfer in a positively charged FO membrane under the configuration of AL-FW.

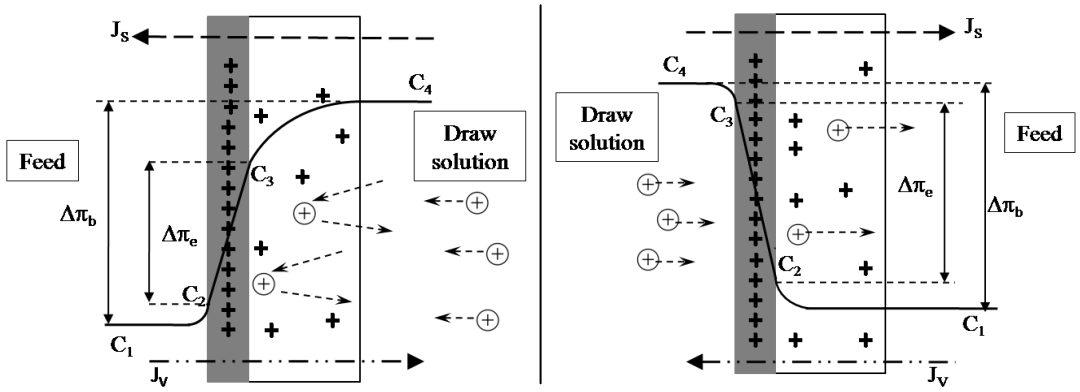

Figure 3.12. Illustration of effective osmotic pressure difference in a positively charged FO membrane (a) AL-FW; (b) AL-DS.

However, in the AL-DS configuration (Figure 3.12-b), when some of the salt penetrated through the dense-active layer into the porous substrate, a salt concentration of C_2 at the interface of the active layer with the porous substrate was built up. The positive charges in the support layer tended to expel the ions to the feed side because of a less mass transfer resistance in the substrate. Thus the salt transportation through a positively charged FO membrane was facilitated in the configuration of AL-DS (salt flux and salt repulsion are in the same direction). That is why the J_s/J_v in the AL-FW is lower than in the AL-DS for both membranes.

Comparing the ST#2 PAI FO hollow fiber membrane with the ST#3 PAI FO hollow fiber membrane, the main difference lies in the substrate porosity (70% for ST#2 vs. 85% for the ST#3). In the AL-DS configuration, a highly porous substrate would significantly reduce the hindrance of mass transfer, making the facilitated ion transportation imposed by the positive charges in the substrate easily realized. Thus, the J_s/J_v of the ST#3 PAI FO membrane was much higher than the ST#2 PAI FO membrane, and it increased sharply with an increase in draw solute concentration.

Table 3.7 lists the water flux of various membranes with a NF-like selective layer used for FO process. It seems the performance of the ST#2 and ST#3 PAI FO hollow fiber membranes in the configuration of AL-FW are better than most of other NF membranes reported in literature. In addition, the ST#2 and ST#3 PAI FO hollow fiber membranes exhibited the largest fiber lumen, which is a desirable feature for liquid processes. However, it should be noted that a positively charged membrane has

a limit with respect to fouling propensity by negatively charged foulants. The possible applications of this positively charged FO membrane include the treatment of industrial waste water containing heavy metals, or the feed steams with less organic foulants, etc.

Table 3.7. Comparison of various membranes used in FO process.

Sample	ID/OD (mm)	PWP ($l/m^2.h.bar$)	R_S $MgCl_2$ (%)	FO water flux ($l/m^2.h$)	DS: $MgCl_2$ (M)	Orientation	Ref
ST#2	1.24/1.58	2.25	92.7	13.1	0.5	AL-DS	present work
				15.4	1.0		
ST#2	1.24/1.58	2.25	92.7	8.36	0.5	AL-FW	
				10.4	1.0		
ST#3	1.24/1.54	2.19	91.1	13.2	0.5	AL-DS	
				14.6	1.0		
ST#3	1.24/1.54	2.19	91.1	9.74	0.5	AL-FW	
				11.0	1.0		
PBI	0.14/0.27	0.50	86.0	9.02	2.0	AL-DS	(Wang, Chung *et al.* 2007)
PBI	0.14/0.27	0.50	86.0	5.20	2.0	AL-FW	
4m-PBI*	0.21/0.29	1.34	92.0	11.0	1.0	AL-DS	(Wang, Yang *et al.* 2009)
4m-PBI*	0.21/0.29	1.34	92.0	5.00	1.0	AL-FW	
9m-PBI*	0.21/0.29	1.25	96.0	5.00	1.0	AL-DS	(Wang, Yang *et al.* 2009)
9m-PBI*	0.21/0.29	1.25	96.0	1.70	1.0	AL-FW	
DL-PBI[#]	0.54/0.95	1.74	87.0	15.7	1.0	AL-DS	(Yang, Wang *et al.* 2009a)
DL-PBI[#]	0.54/0.95	1.74	87.0	7.50	1.0	AL-FW	
CA	0.35/0.55	0.47	97.0	2.70	0.5	AL-DS	(Su, Yang *et al.* 2010)
CA	0.35/0.55	0.47	97.0	1.80	0.5	AL-FW	

*Chemically modified PBI; [#]Dual-layer PBI.

3.4. Conclusions

Novel FO hollow fiber membranes with a positively charged NF-like selective layer have been successfully fabricated for the first time by the phase inversion method making PAI UF hollow fibers as the substrate followed by a simple chemical post-treatment using a PEI solution to develop a positively charged dense selective layer. The advantages of this approach include simple fabrication process, tailorable

membrane structure and promising membrane performance in the AL-FW configuration for FO applications.

The PAI FO hollow fibers possess the following important features:

- PAI FO hollow fiber membranes have a large lumen with an inner diameter > 1 mm and a wall thickness of 0.15-0.17 mm.
- The substrate has a high porosity (70-85%)
- PAI FO hollow fiber membranes possess a high pure water permeability of 2.19-2.25 l/m^2.h.bar and reasonable rejections of 49% and 94% at 1 bar pressure for NaCl and $MgCl_2$, respectively.
- In the FO process, when using a 0.5 M $MgCl_2$ as a draw solution and DI water as the feed in the AL-FW configuration at 23°C, the water fluxes of the ST#2 and ST#3 PAI FO hollow fiber membranes are 8.36 and 9.74 l/m^2.h, respectively, and the J_s/J_v of the two membranes is smaller than 0.4 g/l, which is lower than the data of 0.85 g/l for HTI's FO membrane.
- Different from a neutral membrane, the positively charged FO membrane provides double electric repulsions to the salt transfer through the membrane in the AL-FW configuration, leading to a reduction of salt penetration, while in the AL-DS configuration, the positive charges facilitate salt transportation.

The PAI FO hollow fiber membranes with a NF-like skin showed a good performance for multivalent heavy metal removal. Therefore, this type of membrane has good potential to be applied for water softening, or for the treatment of industrial waste water containing heavy metals using FO process.

CHAPTER 4

Fabrication and Characterization of FO Hollow Fiber Membranes with Antifouling NF-like Selective Layer

4.1. Introduction

As described in Chapter 3, PAI composite FO membranes with a positively charged NF-like selective layer has been developed using UF hollow fiber as a porous substrate. In the FO process, the resultant membranes possess reasonable water flux of 13 l/m^2.h and 9.7 l/m^2.h in the configurations of active layer facing draw solution (AL-DS) and active layer facing feed water (AL-FW), respectively, when using 0.5 M $MgCl_2$ as the draw solution and DI water as the feed at ambient temperature of 23°C.

NF membranes are commonly used for removing natural organic matter (NOM) which generally presents in fresh water (Alborzfar, Jonsson *et al.* 1998; Zularisam, Ismail *et al.* 2006). Fresh water contains 1-50 mg/l dissolved organic carbon (DOC) and 60-90% of DOC is NOM. This number usually varies with climate, geology and topography (Evans, Monteith *et al.* 2005; Zularisam, Ismail *et al.* 2006). NOM comprises of aromatic and aliphatic compounds (such as carboxylic, methoxyl carbonyls and phenolic structures) which reduce the water quality. These compounds carry negative charge in neutral pH. Hence, the positively charged selective layer may induce membrane fouling due to the electrostatic interaction (Al-Amoudi 2010).

Therefore, in the present study, an attempt was made to develop FO hollow fiber membranes with a less positively charged NF-like selective layer for fouling mitigation. Basically, the fabrication involves a step of PAI UF hollow fiber spinning via phase inversion, followed by simple polyelectrolyte post-treatments using positively charged polyethyleneimine (PEI) for cross-linking and negatively charged polystyrene sulfonate sodium salt (PSS) for deposition. The resultant membranes were subjected to a series of characterizations using standard protocols and performance

evaluation in the FO process, where the feed solution used was de-ionized water, or water containing 2000 ppm Na_2SO_4, or water containing organic foulants such as 1000 ppm bovine serum albumin (BSA).

4.2. Experimental

4.2.1. Materials

Negatively charged polyelectrolyte deposition was performed by using polystyrene sulfonate sodium salt (PSS) with molecular weights of 70K and 500K purchased from Sigma Aldrich and Alfa Aesar, respectively. Glutaraldehyde (50% in solution, Sigma Aldrich) was used to improve the stability of the polyelectrolyte deposition. Hydrochloric acid (HCl, 37%, Schedelco) was used for pH adjustment. Bovine serum albumin (BSA, Sinopharm) was used as a model foulant in FO experiments. All the reagents were used as received. Other materials have been described in Chapter 3 Section 3.2.1.

4.2.2. Poly(amide-imide) hollow fiber substrates

A dope composition of PAI/LiCl/NMP 14/3.5/82.5 was employed to fabricate PAI UF hollow fiber substrates. Dope preparations and membrane spinning process can be found in Chapter 3 Section 3.2.2 and 3.2.3.

The structure and morphology of resultant membranes were examined by a Zeiss EVO 50 SEM. The filtration experiments for measuring PWP and MWCO were conducted using a bench scale cross-flow setup. The standard protocol of substrate characterizations has been described clearly in Chapter 3 Section 3.2.5.

4.2.3. Modification of PAI hollow fiber substrates

The cross-linking reaction between PAI substrate and PEI was conducted by immersing the hollow fiber membranes into a 500 ml of 1% (wt/wt) PEI aqueous solution at temperature of 70 °C. The reaction time varied from 30 to 75 min. Next, the membranes were rinsed three times using purified water to remove the remaining PEI

solution on the membrane surface. The cross-linked fibers were, then, split into two groups. One was to store in purified water for further modification and characterization in terms of surface charge, salt rejection and pure water permeability. The other was dried over night in a vacuum oven at 50°C for subsequent characterization of SEM.

Prior to the deposition of PSS layer onto the outer surface of the PAI-PEI-cross-linked hollow fiber membranes, four of the cross-linked fibers were put together for each module. A PSS solution was prepared by dissolving 1 g PSS into 1 l 0.5 M NaCl solution followed by the addition of concentrated hydrochloric acid to pH 2.0. The deposition of PSS layer onto the outer surface of the hollow fiber substrate was carried out at ambient temperature of 20 °C by circulating the PSS solution in the shell side of a hollow fiber module at a flow rate of 450 ml/min for 30 min (Qiu, Qi *et al.* 2011). The module was then rinsed thoroughly by de-ionized water for approximately 5 min. A glutaraldehyde solution (1 wt%) was, subsequently, circulated through the membrane module at the same flow rate for 30 min in order to stabilize the deposition of PSS (Qiu, Qi *et al.* 2011). Lastly, the modified membranes were cleaned with de-ionized water and stored for further use. The membranes modified with different conditions were designated as ST#1-ST#5 membranes, and the details of NF-like skin formation were summarized in Table 4.1.

Table 4.1. Conditions used for NF-like skin formation.

Code	Duration of PEI post-treatment (min)	Molecular weight of PSS (kDa)
ST#1	0	70
ST#2	30	70
ST#3	60	70
ST#4	60	500
ST#5	75	-

4.2.4. Characterizations and analysis

The procedures for PWP measurement and morphology observation by SEM have been described in Chapter 3 Section 3.2.5.

The membrane surface chemistry before and after modification was analyzed by fourier transform infrared spectrometer (FTIR, Shimadzu IR Prestige-21) using the attenuated total reflection (ATR) equipped with ZnSe crystal method. The characterization was performed on PAI flat sheet membrane prepared with the same concentration and modification condition as used for hollow fiber. The PAI flat sheet membranes were prepared by casting the polymer solution on a glass plate with a 150 μm gap casting knife followed by PEI cross-linking and PSS deposition as described previously. PAI flat sheet membranes were used in order to get a full coverage on the ATR sample holder. The flat sheet membrane samples were dried in a 50 °C vacuum oven overnight prior to analysis. A total of 45 scans were performed at a resolution of 4 cm^{-1} at ambient temperature.

The original and modified membrane surface charge (zeta potential) was observed based on the streaming potential measurement by using a SurPASS electrokinetic analyzer (AntonPaarGmbH, Austria) on the PAI flat sheet membranes. The measurements were performed by circulating a potassium chloride (KCl, Merck, Singapore) electrolyte solution (10^{-2} and 10^{-3} M, 500 mL) through an adjustable gap cell containing membrane samples with a pressure ramp from 0 to 300 mbar. The measurement pH was based on the original pH of the electrolyte solution of 5.8 and was then increased stepwise (0.5-1 units) by titration with a 0.1 M sodium hydroxide (NaOH) solution until pH 11 was reached. The zeta potential of membrane surface was calculated based on Helmholz-Smoluchowski equation (Anton-Paar 2009).

The details of FO performance evaluation have been described in Chapter 3 Section 3.2.6. FO experiments were performed in two configurations: (1) the draw solution flowed in shell side of the membrane module where the selective layer were placed (AL-DS) and (2) the feed flowed in shell side (AL-FW). FO experiments with foulants were performed in the configuration of AL-FW only for 3 h. A 5 L feed solution was

prepared in order to eliminate the concentration of the feed solution due to the high retention of the solutes.

4.3. Results and discussion

In the following sections, a systematic analysis of unmodified and modified membranes in terms of morphology, physical and chemical properties will be discussed. The change in membrane surface chemistry will be correlated to the FO performance.

4.3.1. Characterization of PAI membranes

- *SEM morphologies*

The SEM morphologies of the membrane cross-sections before and after modification are presented in Figure 4.1. It can be seen from Figure 4.1-a that the PAI substrate comprised finger-like structures which were developed simultaneously from the inner and outer surfaces without forming large macrovoids. The substrate had a thin skin layer (~ 2-3 μm in thickness) on top of the finger-like pores and a thin sponge-like structure (~ 4-5 μm in thickness). As compared to the previous chapter (Chapter 3), the hollow fiber membrane matrix used in this chapter was better defined with a thinner sponge-like structure in the middle and a thinner fiber wall thickness, which are preferred for lowering internal concentration polarization in a porous substrate during FO process (Chou, Shi *et al.* 2010; Wang, Shi *et al.* 2010).

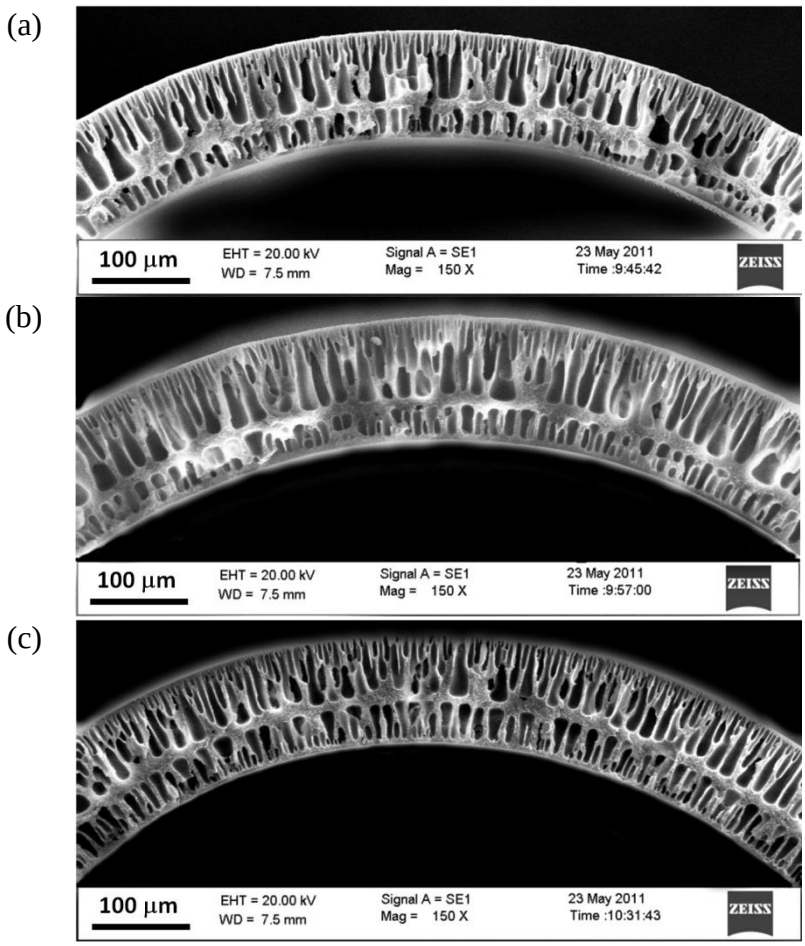

Figure 4.1. Cross-sectional SEM morphology of (a) PAI UF membrane substrate; (b) PAI membrane with 60 min PEI cross-linking; (c) PEI cross-linked PAI membrane with PSS deposition.

PEI post-treatment and PSS deposition were performed on the outer surface of the hollow fiber membranes. It was clear from Figure 4.1 b and c that the modification did not change the morphology of the membrane cross-section. As the modification took place, the outer surface became rougher as shown in Figure 4.2. It might be due to the PSS molecules adsorbed as a coil than in a flat conformation because of high ionic strength in the polyelectrolyte solution which may reduce the mutual electrostatic repulsion of PSS chains (Jin, Toutianoush *et al.* 2003).

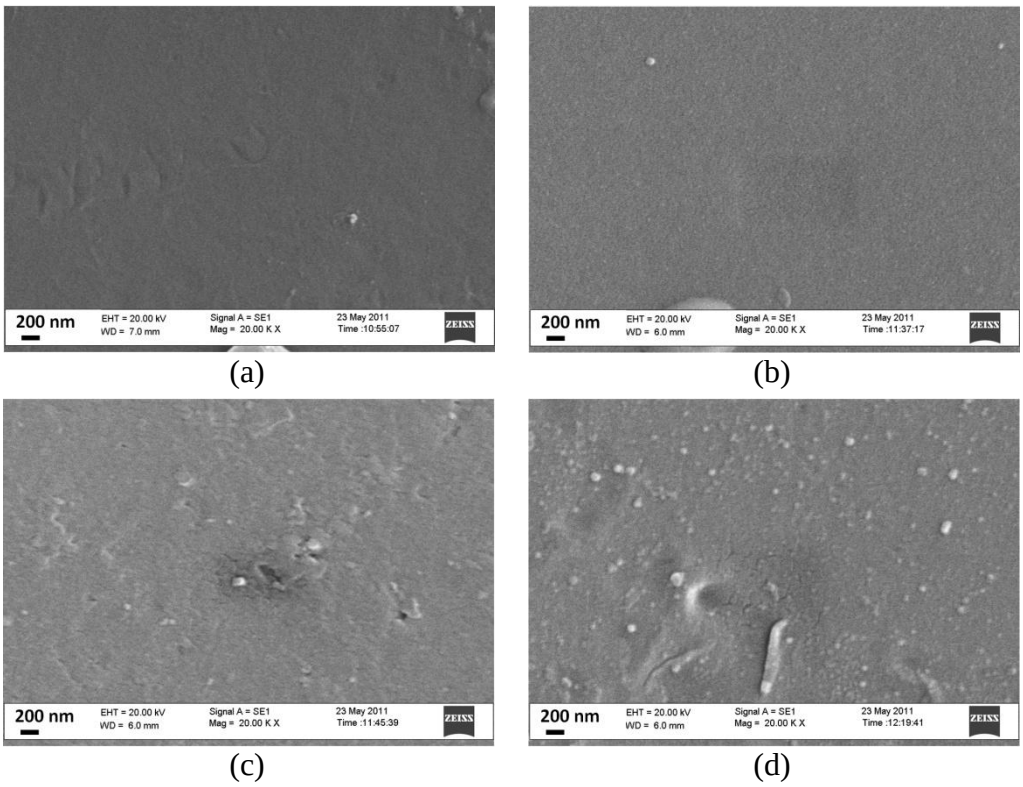

Figure 4.2. Outer surface morphology of (a) PAI UF hollow fiber substrate; (b) PAI UF hollow fiber substrate with 60 min PEI cross-linking; (c) PEI cross-linked PAI membrane with deposition of PSS 70K (ST#3); (d) PEI cross-linked PAI membrane with deposition of PSS 500K (ST#4).

- *FTIR analysis*

The PEI post-treatment by the cross-linking method as well as PSS deposition were confirmed by the ATR-FTIR measurements. The change of the outer surface chemistry that occurred through the modification can be seen in Figure 4.3. The details of chemical reaction between the PAI and PEI have been described in Chapter 3 Section 3.3.3. It is clearly observed from Figure 4.3 that as the cross-linking reaction between PAI and PEI took place (PAI-PEI30 and PAI-PEI60), the imide peaks gradually decreased while the amide peaks became stronger (C=O at 1641 cm^{-1} and C-N at 1532 cm^{-1}). After deposition of PSS on to the outer surface, a new peak emerged at wave length of 1035 cm^{-1} due to the characteristic stretching vibration of the $–SO_3$ group in PSS (Temmel, Kern *et al.* 2006; Qiu, Qi *et al.* 2011).

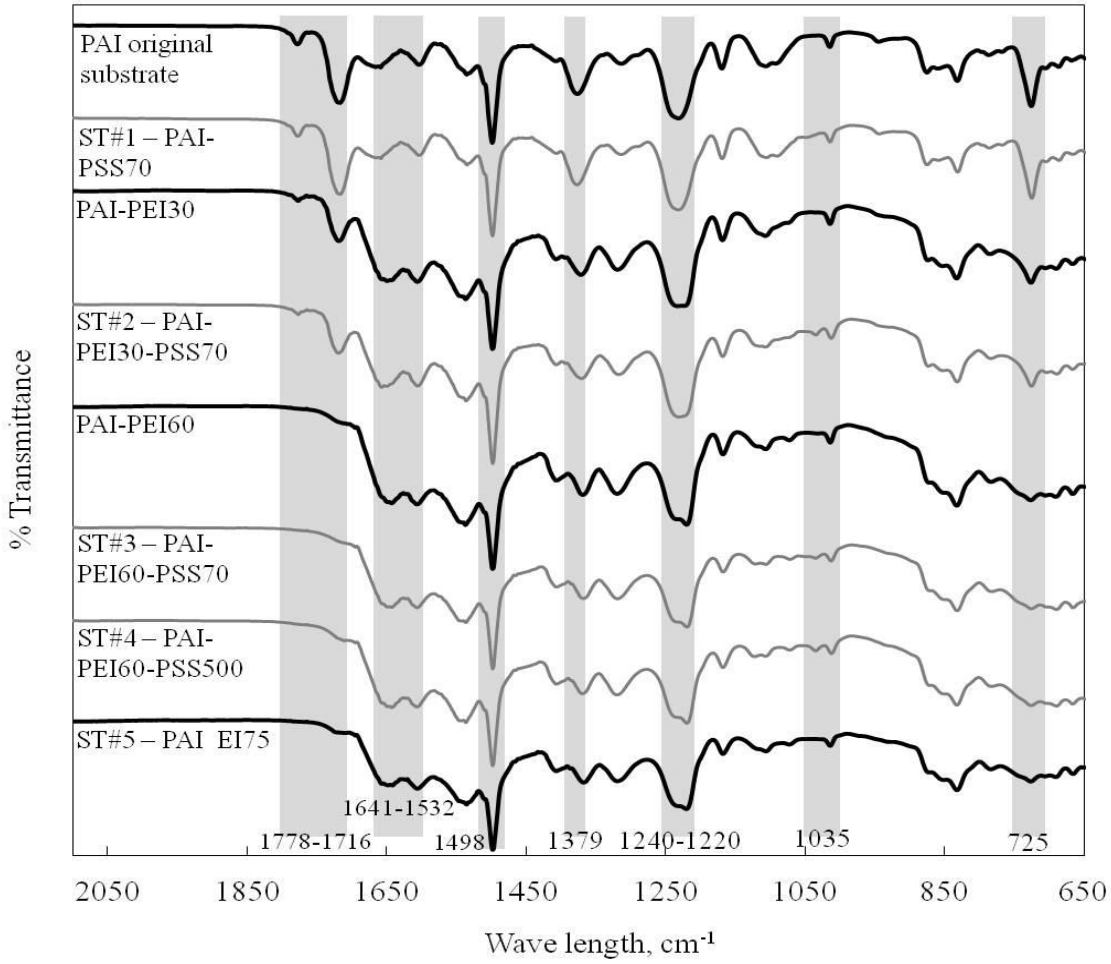

Figure 4.3. ATR-FTIR spectra of PAI FO membranes. Note: PAI-PEI30/60/75 is PAI membrane cross-linked with PEI for 30/60/75 min; PSS70/500 is PSS used for deposition having molecular weight of 70K/500 kDa.

- *Zeta potential*

The charge characteristics of unmodified and modified PAI hollow fiber membranes were determined in terms of zeta potential. Based on electro-kinetic analysis, Figure 4.4 exhibits the zeta potential versus pH curves of original and modified PAI membranes. The discrepancy of all zeta potential measurements shown here is less than 10%. The observed value of zeta potential is affected by ionic strength of the electrolyte solution as shown in Figure 4.4-a. A decrease in the zeta potential with increasing the concentration of the electrolyte solution can be attributed to the compression of the double layer (stern and diffuse layer). However, the isoelectric point (IEP, pH where the zeta potential is zero) is independent of ionic strength on the condition that the surface property is the same (Chiu and James 2007; Lin, Yu *et al.*

2009). Therefore, the electrolyte solution of 1 mM KCl would be employed to characterize the PSS-modified membranes.

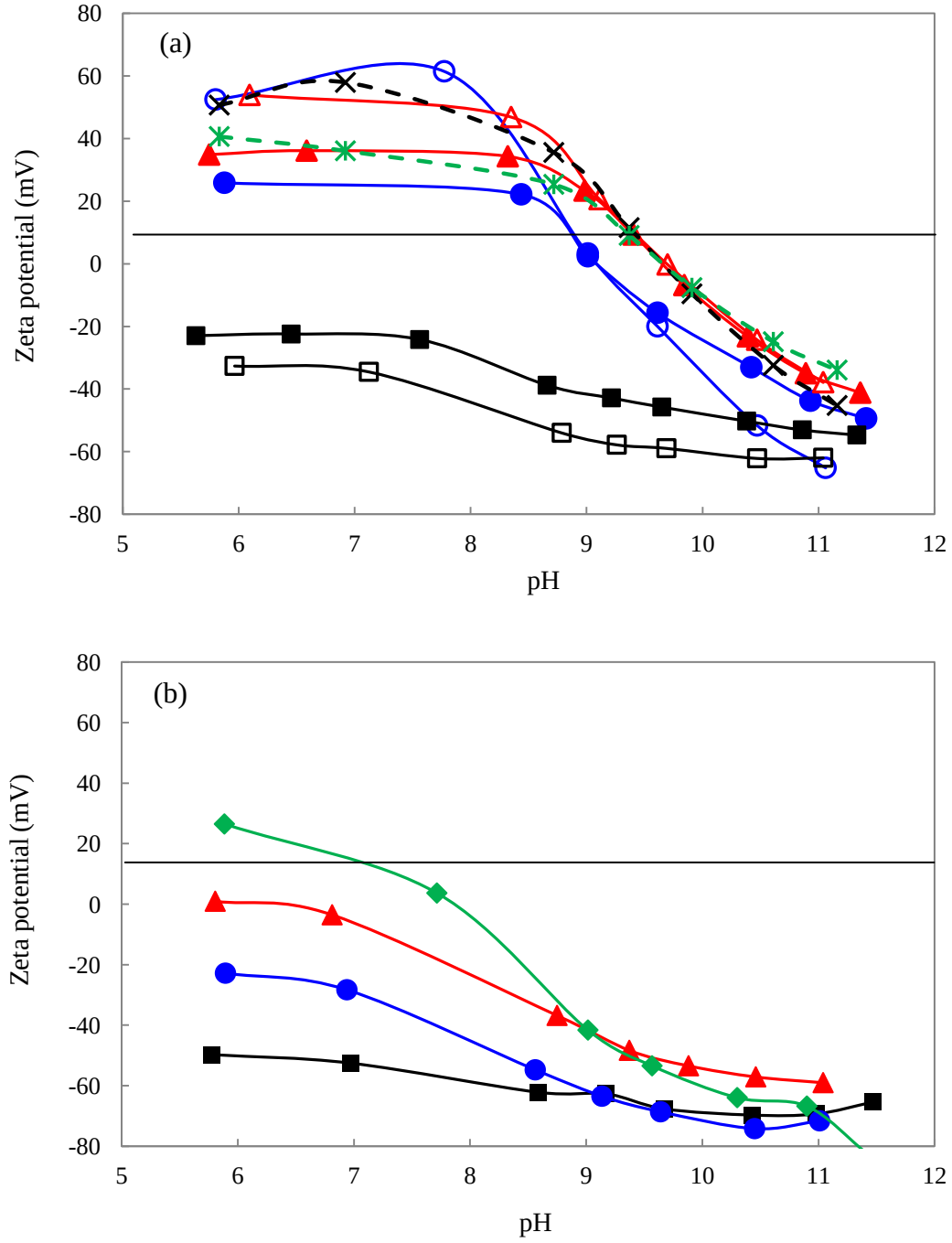

Figure 4.4. Plot of zeta potential vs pH of (a) PAI-PEI cross-linked at different concentration of electrolyte solution: 1 mM KCl (□ 0 min; ○ 30 min; △ 60 min; –×– 75 min) and 10 mM KCl (■ 0 min; ● 30 min; ▲ 60 min; –✳– 75 min); (b) PAI-PEI cross-linked after PSS deposition (■ ST#1; ● ST#2; ▲ ST#3; ◆ ST#4) measured by using an electrolyte solution of 1 mM KCl.

As shown in Figure 4.4, PAI original membrane has negative zeta potential at the pH range of 6-11. As mention in Chapter 3, the original PAI membrane had an IEP of 4.4. After cross-linking reaction with PEI, the zeta potential of the cross-linked membrane increased to the positive region and the IEP was shifted to a higher pH. It can be seen that for 30 min cross-linking time, the cross-linked PAI membrane has IEP of 9.1. It is because during the cross-linking reaction, the amines from PEI reacted with the imide group from PAI original membrane and imparted the positive charges to the membrane surface resulting in a rising of zeta potential. When the cross-linking time increased to 60 and 75 min, no significant change in zeta potential can be observed as well as the change in IEP (from 9.1 to 9.8) due to the readily formed hydrogen bonds between neighboring amine groups which suppresses the protonation of amine groups (Kuo, Chang *et al.* 2011).

All the PSS deposition experiments were conducted at pH 2.0 as the substrate possessed positive charges at this pH condition. It was recognized that the zeta potential for all PSS-modified membranes (ST#1 – ST#4) decreased after PSS deposition. ST#1 membrane had the lowest zeta potential as it did not undergo a PEI cross-linking. ST#2 and ST#3 membranes were cross-linked with PEI for 30 and 60 min, respectively, and followed by deposition of PSS having a molecular weight of 70 kDa. As the result, the zeta potential of ST#2 membrane after PSS deposition was lower than ST#3 membrane. Interestingly, ST#4 membrane, modified with 60 min PEI cross-linking and deposition of a higher molecular weight PSS (Mw 500 kDa), had a more positive zeta potential as compared to ST#3 membrane which had the same PEI cross-linking. Theoretically, for the polyelectrolyte with a larger molecular weight, the charge density on the modified surface should be higher. However, this may not always be the case as the polyelectrolyte chain might be too long to undergo appropriate conformational changes for maximal surface exposure (Greene and Tannenbaum 2004).

- *Intrinsic properties*

The detailed characteristic properties of PAI UF hollow fiber substrate (before modification) are summarized in Table 4.2. The hollow fiber substrate exhibits a large dimension (ID/OD around 1.2/1.5 mm), high PWP (151 l/m^2.h.bar), and high porosity

(86%). The PWP and salt rejections of modified PAI membranes are shown in Table 4.3. It can be seen that there is a PWP decline after PEI cross-linking and further decline can be expected after PSS deposition. With an increasing cross-linking time of PEI-PAI, the PWP decreased from 52 to 7.8 l/m^2.h.bar while rejection of $MgCl_2$ increased from 22% to 85%. This increase can be attributed to the more pores tighten on the selective layer. PSS depositions were performed on original PAI substrate (ST#1) and on PEI cross-linked substrates (ST#2–ST#4). One layer of PSS deposition was able to significantly decrease the PWP from 151 to 19.5 l/m^2.h.bar. However, it might be unable to completely seal the big pores leading to the quite poor rejection towards Na_2SO_4. When PSS deposition was performed on the surface of PEI cross-linked membranes, much better $MgCl_2$ and Na_2SO_4 rejections can be achieved. However, it can be distinguished from Table 4.3, that ST#2 membrane rejection to Na_2SO_4 is lower than the rejection to $MgCl_2$ even though the membrane had negative charge surface as shown in Figure 4.4. This discrepancy can be attributed to the sieving effect of the membrane pore radii and the size of ions as the hydrated ionic radius of magnesium ion (0.43 nm) is bigger than that of sulfate ion (0.38 nm) (Nightingale 1959; Schaep, Van Der Bruggen *et al.* 1998).

Table 4.2. Properties of PAI UF hollow fiber substrate.

Property	Value*
MWCO shell (kDa)	17 (±3)
MWCO lumen (kDa)	58 (±16)
PWP (l/m^2.h.bar)	151 (±15)
OD (μm)	1508 (±0.7)
ID (μm)	1248 (±1.4)
Porosity (%)	86 (±1.2)
Tensile strength (MPa)	6.2 (±0.1)

*Average value of four replicates (number inside bracket is standard deviation).

Table 4.3. PWP and salt rejection of modified membranes.

Code	After PEI cross-linking			After PSS deposition		
	PWP ($l/m^2.h.bar$)	Rej. $MgCl_2$ (%)	Rej. Na_2SO_4 (%)	PWP ($l/m^2.h.bar$)	Rej. $MgCl_2$ (%)	Rej. Na_2SO_4 (%)
ST#1		-		19.5±3.1	2 ± 0.5	11 ± 1.4
ST#2	52 ± 1.2	22 ± 1.6	4 ± 1.8	3.7 ± 0.4	81 ± 6.2	74 ± 1.5
ST#3	33 ± 2.8	47 ± 8.7	4 ± 0.8	4.1 ± 0.7	80 ±12	85 ± 3.6
ST#4				4.3 ± 0.6	81 ± 9.4	69 ± 3.2
ST#5	7.8 ± 0.1	85 ± 0.6	-	-	-	-

Since ST#3 and ST#4 membranes had the same PEI cross-linking, the amount of positive charge on the surface were similar. However, the molecular weight of PSS used was different. ST#4 was modified with 500 kDa PSS which was higher than that for ST#3, the PSS molecule, formed as coil in salt solution, might have difficulties to be absorbed by membrane surface. This is also supported by the membrane surface morphology observed by using SEM (section 4.3.1.1). As a result, the zeta potential was more positive (section 3.1.3) and it was difficult to completely cover the surface leading to lower rejection towards Na_2SO_4.

4.3.2. Effect of PEI post-treatment and PSS molecular weight on FO performances of resultant membranes

The performances of modified membranes (the ST#1 – ST#4) in FO process were determined using a 0.5 M Na_2SO_4 solution as the draw solution and de-ionized water/2000 ppm Na_2SO_4 solution as the feed at ambient temperature of 23°C, and the results are listed in Table 4.4. It can be seen that the ST#1 membrane presented the lowest water flux (9.0 $l/m^2.h$) and the highest salt flux (J_s/J_v 15 g/l) in the configuration of AL-DS. This result is not surprising, as the PEI-untreated outer surface of the ST#1 membrane cannot retain many PSS molecules as discussed in section 4.3.1.4, resulting in a very low Na_2SO_4 rejection (see Table 4.3). The significant reverse salt diffusion into the feed solution reduced the osmosis driving force across the membrane, thus the

water flux was very low. In the configuration of the AL-FW, on the other hand, the ST#1 membrane can achieve water flux as high as 17 l/m^2.h, and ratio of salt flux to water flux is 2.2 g/l which is much lower than the AL-DS configuration. This phenomenon can be explained as follows. ST#1 PAI membrane consists of a negative charge rejection layer supported by a porous substrate which is also negatively charged at pH > 4.4. In the AL-FW configuration, the draw solution is in the support layer side. The salt concentration at the interface between the active layer and the porous substrate may be smaller than in a neutral membrane substrate due to the Donnan exclusion that tended to expel the Na_2SO_4 back to the draw solution. In addition, the charges in the dense-active surface also imposed a repulsive force to the salt penetration through the membrane. Therefore, there were double electrical repulsions to the salt transfer in the configuration of AL-FW. However, in the AL-DS configuration, when the salts passed through the selective layer to the porous substrate, the salt concentration at the interface between the selective layer and the support layer was built up. The negative charges in the support layer tended to expel the coming salts to the feed side because of a less mass transfer resistance in the porous support layer. Therefore, the membrane facilitates the salts transport in the configuration of AL-DS. As a result, a lower J_s/J_v in the configuration of AL-FW was observed. It was also recognized that when AL-FW was used, the ST#1 membrane had the highest FO water flux as compared to other membranes. Given the fact that the ST#1 membrane was not treated by the PEI cross-linking, the relatively more porous substrate of the ST#1 membrane may be attributed to this result.

Table 4.4. FO performances for modified membranes.

Code	Feed: DI water*				Feed: 2000 ppm Na_2SO_4*			
	AL-DS		AL-FW		AL-DS		AL-FW	
	J_v (l/m^2.h)	J_s/J_v (g/l)	J_v (l/m^2.h)	J_s/J_v (g/l)	J_v (l/m^2.h)	J_s/J_v (g/l)	J_v (l/m^2.h)	J_s/J_v (g/l)
ST#1	9 ± 0.7	15 ± 1.3	17 ± 3	2.2 ± 0.9	N/A			
ST#2	23 ± 0.5	0.8 ± 0.1	13 ± 0.3	0.4 ± 0.1	16 ± 0.6	0.8 ± 0.1	11 ± 0.5	1.1 ± 0.1
ST#3	29 ± 0.5	0.3 ± 0.1	13 ± 0.3	0.2 ± 0.0	17 ± 0.4	0.4 ± 0.1	12 ± 0.3	0.2 ± 0.0
ST#4	26 ± 3.1	0.7 ± 0.3	14 ± 0.3	0.3 ± 0.0	17 ± 0.3	0.6 ± 0.1	12 ± 0.3	0.4 ± 0.0

*DS: 0.5 M Na_2SO_4.

By comparing ST#1, ST#2 and ST#3, the effect of PEI cross-linking can be clearly seen as the water flux increased and the salt flux decreased (Table 4.4). 30 min PEI cross-linking was able to decrease J_s/J_v from 15 g/l to 0.8 g/l and further decrease to 0.3 g/l when 60 min PEI cross-linking was used. This is due to the denser selective layer after PEI cross-linking which is supported by the increasing of $MgCl_2$ rejection in the RO mode (Table 4.3). In comparison of the ST#2 and ST#3 membranes, the salt flux of the ST#2 membrane is higher while the water flux is comparable though the zeta potential of the ST#2 membrane is less positive than the ST#3 membrane. The ST#2 membrane had undergone PEI post-treatment for 30 min while the ST#3 and ST#4 membranes were treated for 60 min. A higher salt flux might be due to the less dense selective layer of the ST#2 membrane, and this was also reflected by the lower Na_2SO_4 rejection than the ST#3 membrane in the RO mode of measurements (74% vs. 85% for ST#2 and ST#3, respectively, in Table 4.3).

As summarized in Table 4.4, the ST#3 membrane exhibited the best FO performance. It can achieve water flux of 29 l/m^2.h and 13 l/m^2.h in the configurations of AL-DS and AL-FW, respectively, when using de-ionized water as the feed and 0.5 M Na_2SO_4 as the draw solution. When the feed solution contained 2000 ppm Na_2SO_4, the flux decreased to 17 l/m^2.h and 12 l/m^2.h for two configurations accordingly. The flux reduction for the AL-DS configuration is higher than that for AL-FW due to more severe internal concentration polarization occurred in the membrane substrate if the feed contained salts and faced the membrane substrate (McCutcheon and Elimelech 2006).

The effect of the PSS molecular weight on the FO performances has also been investigated by examining the behaviors of the ST#3 and ST#4 membranes. The ST#3 was modified using PSS with a molecular weight of 70K while the ST#4 was treated by PSS with a molecular weight of 500K. Both the ST#3 and ST#4 membranes had similar water flux, but the ST#4 membrane had a higher back salt diffusion in the AL-DS configuration as compared to ST#3 membrane. A higher reverse salt diffusion in ST#4 membrane is related to the salt rejection as measured in RO mode where ST#3 membrane had a higher rejection towards Na_2SO_4 as compared to ST#4 membrane.

4.3.3. Effect of membrane surface charges on protein filtration

In order to investigate the benefit brought by altering the membrane surface chemistry, i.e., from a very positively charged surface to a less positively charged surface, two types of membranes have been tested: one is the ST#3 and ST#4 membrane modified by PEI and PSS and the other is the ST#5 modified by PEI only. BSA was used as a model foulant for FO test, as the BSA has an iso-electric point at pH of 4.7, meaning it carries negative charges at neutral pH (Tang, Chong *et al.* 2011).

The FO performances of the two membranes were evaluated in the following conditions: (a) for the ST#3 and ST#4 membrane - a 1000 ppm BSA solution was used as the feed and 0.5M Na_2SO_4 was used as the draw solution; (b) for the ST#5 membrane - a 1000 ppm BSA solution was used as the feed and 0.25 M $MgCl_2$ was used as the draw solution. The reason why $MgCl_2$ was used for the ST#5 membrane was because the membrane was positively charged. The concentration of draw solution was 0.25 M to ensure the three membranes had the same initial flux.

FO water flux for both DI water and BSA solution as feed are illustrated in Figure 4.5. The average water flux during the experiment with BSA was approximately 13 $l/m^2.h$ for ST#3, 14 $l/m^2.h$ for ST#4 and 11.8 $l/m^2.h$ for ST#5 membrane. It can be seen that there was a flux decline for the ST#5 membrane during the FO test while the flux of the ST#3-ST#4 membranes were remained the same as pure water flux for the first 4 h of the FO filtration. The likely cause of flux decline might be due to the increasing of hydraulic resistance caused by the attachment and/or adsorption of BSA onto the membrane surface and pores (Achilli, Cath *et al.* 2009b). These results demonstrate that the less positively charged membrane surface is favorable to the situations where the feed solution contains negatively charged foulants such as proteins.

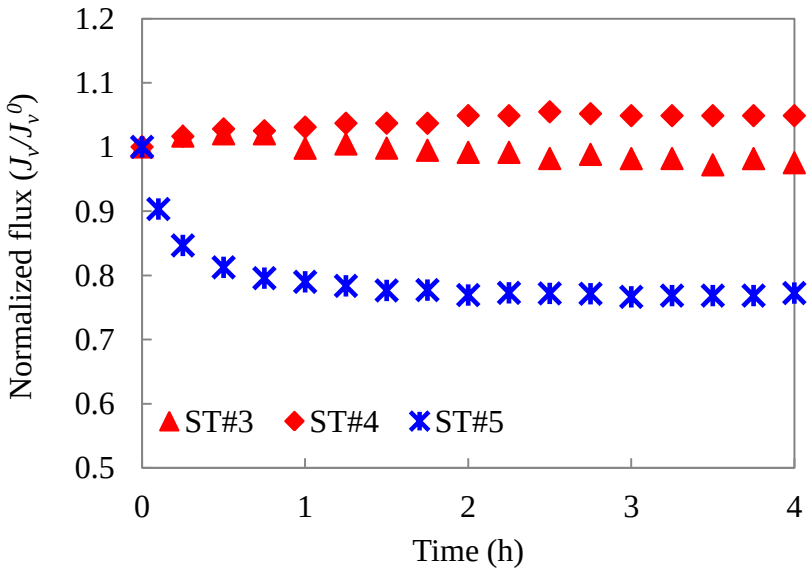

Figure 4.5. Plot of FO normalized water flux for 4 h filtration of 1000 ppm BSA solution (orientation: AL-FW; ST#3 and ST#4: 1000 ppm BSA solution was used as the feed and 0.5M Na_2SO_4 was used as the draw solution; ST#5 membrane: 1000 ppm BSA solution was used as the feed and 0.25 M $MgCl_2$ was used as the draw solution).

A comparison of resultant membranes presented in this study with other membranes published in literature is summarized in Table 4.5. It can be seen that an improvement has been made compared to the positively charged PAI membranes (Chapter 3), as the performance of the less positively charged ST#3 and ST#4 membranes are better. Cornelissen *et al.* tested the commercial FO membranes which had a very low J_s/J_v (0.04 g/l) (Cornelissen, Harmsen *et al.* 2008). However, the membrane possessed lower flux as compared to the ST#3/ST#4 membranes. Another commercial FO membrane (Achilli, Cath *et al.* 2010) showed similar J_s/J_v (0.33-0.58 g/l) with the this work, but the water flux was lower. The cellulose acetate NF hollow fiber membranes presented 5.0 l/m^2.h water flux using DI water as the feed and 2.0 M $MgCl_2$ as the draw solution in the AL-FW configuration (Su, Yang *et al.* 2010), while the ST#3/ST#4 membranes showed a reasonable water flux using 1000 ppm BSA in 2000 ppm Na_2SO_4 aqueous solution as the feed and 0.5 M Na_2SO_4 as the draw solution in the same configuration. In summary, the ST#3 and ST#4 membranes had fairly higher water flux as compared to others.

Table 4.5. Comparison of various membranes used in FO process.

Membrane	ID/OD (mm/mm)	PWP ($l/m^2.h.bar$)	FO performance			Testing conditions			Ref.
			J_v ($l/m^2.h$)	J_s/J_v (g/l)	Orientation	Feed solution	Draw solution	Temp.(°C)	
ST#3 hollow fiber	1.25/1.51	4.1 ± 0.7	17 ± 0.4	0.4 ± 0.1	AL-DS	2000ppm Na_2SO_4	0.5M Na_2SO_4	23	This work
			12 ± 0.3	0.2 ± 0.0	AL-FW	2000ppm Na_2SO_4	0.5M Na_2SO_4	23	
			11.2	0.2	AL-FW	1000ppm BSA + 2000ppm Na_2SO_4	0.5M Na_2SO_4	23	
ST#4 hollow fiber	1.25/1.51	4.3 ± 0.6	17 ± 0.3	0.6 ± 0.1	AL-DS	2000ppm Na_2SO_4	0.5M Na_2SO_4	23	This work
			12 ± 0.3	0.4 ± 0.0	AL-FW	2000ppm Na_2SO_4	0.5M Na_2SO_4	23	
			11.6	0.4	AL-FW	1000ppm BSA + 2000ppm Na_2SO_4	0.5M Na_2SO_4	23	
Positively charged FO hollow fiber	1.24/1.58	2.25	13.13	0.7	AL-DS	DI water	0.5M $MgCl_2$	23	(Setiawan, Wang *et al.* 2011)
			8.36	0.3	AL-FW	DI water	0.5M $MgCl_2$	23	
Positively charged FO hollow fiber	1.24/1.54	2.19	13.20	1.2	AL-DS	DI water	0.5M $MgCl_2$	23	
			9.74	0.3	AL-FW	DI water	0.5M $MgCl_2$	23	
Commercial FO flat sheet (thickness 40μm)	-		5.4	0.04	AL-FW	DI water	1.5M $MgSO_4$	20±2	(Cornelissen, Harmsen *et al.* 2008)
Cellulose acetate flat sheet composite (thickness 70-80μm)	-	-	6.5	-	AL-DS	3.5 wt.% NaCl	1.25M $MgSO_4$	20	(Sairam, Sereewatthanawut *et al.* 2011)
Cellulose acetate flat sheet with double-selective layer (thickness 36μm)	-	0.78	48.2	0.13	bottom layer-DS	DI-water	5.0M $MgCl_2$	22±0.5	(Wang, Ong *et al.* 2010)
	-	0.78	27.4	0.14	top layer-DS	DI-water	5.0M $MgCl_2$	22±0.5	
Double dense layer flat sheet (thickness 35μm)	-	0.17 ± 0.01	17.3 ± 0.4	0.07	AL-DS	DI-water	2.0M $MgCl_2$	22±0.5	(Zhang, Wang *et al.* 2010)
			10.3 ± 0.3	0.08	AL-FW	DI-water	2.0M $MgCl_2$	22±0.5	
Single dense layer flat sheet (thickness 34μm)	-	0.13 ± 0.02	14.7 ± 1.0	0.15	AL-DS	DI-water	2.0M $MgCl_2$	22±0.5	
			9.8 ± 0.7	0.12	AL-FW	DI-water	2.0M $MgCl_2$	22±0.5	
Cellulose acetate NF hollow fiber	0.35/0.55	0.47	7.3	-	AL-DS	DI-water	2.0M $MgCl_2$	22±0.5	(Su, Yang *et al.* 2010)
			5.0	-	AL-FW	DI-water	2.0M $MgCl_2$	22±0.5	
Commercial FO flat sheet (thickness 40μm)			9.2	0.33	AL-FW	DI-water	0.9M Na_2SO_4	25	(Achilli, Cath *et al.* 2010)
			9.7	0.58	AL-FW	DI-water	0.5M $MgCl_2$	25	

4.4. Conclusions

Novel FO hollow fiber membranes with an antifouling NF-like selective layer have been successfully developed. The fabrication involves a step of PAI UF hollow fiber spinning via phase inversion, followed by simple polyelectrolyte post-treatments using positively charged PEI for cross-linking and negatively charged PSS for deposition. The surface chemistry and the permeabilities of water and salt of resultant membranes have been characterized. The membrane performance in the FO process has also been evaluated.

The newly developed PAI FO hollow fibers possess the following important features:

- The PAI FO hollow fiber membranes have a large lumen with an inner diameter > 1 mm and a wall thickness of 0.13 mm. The substrate has a high porosity of 85%.
- The PAI FO hollow fiber membranes possess a high pure water permeability of 3.7-4.3 l/m^2.h.bar and reasonable Na_2SO_4 rejections up to 85% at 1 bar.
- In the FO process, when using 2000 ppm Na_2SO_4 as the feed and 0.5 M Na_2SO_4 as the draw solution at 23 °C, the PAI FO hollow fiber membranes can achieve water flux of 17 l/m^2.h and 12 l/m^2.h for the configurations of AL-DS and AL-FW, respectively.
- Different from highly positively charged membranes, the PSS deposited membranes can maintain a steady water flux of 11 l/m^2.h when the feed contained 1000 ppm BSA and 2000 ppm Na_2SO_4, and 0.5 M Na_2SO_4 was used as the draw solution at ambient temperature of 23 °C.

The approach of making FO membranes developed in the present study offers the advantages of simple fabrication process, tailorable selective layer and promising membrane performance for protein contained wastewater treatment by FO process.

CHAPTER 5

Explorations of Delamination and Irregular Structure in PAI-PES Dual Layer Hollow Fiber Membranes

5.1. Introduction

Despite the fact that the membranes developed by means of simple post-chemical treatments exhibited a high water flux and high salt rejection in the FO process, the chemical cross-linking through entire PAI substrate still resulted in a dense structure which adversely affected the water flux. To overcome the drawback of cross-linking modification on entire PAI membrane, we intend to fabricate a dual-layer hollow fiber with PAI polymer as the outer layer, supported by an inner layer made of other material inert to PEI polyelectrolyte.

However, obtaining a good lamination between the two layers as well as a regular morphology is critical to making a usable dual layer hollow fiber membrane. In spite of many prior studies of the dual-layer hollow fiber membrane fabrication, the mechanisms of lamination/delamination and regular/irregular morphology of dual layer hollow fiber membranes are still debated. Delamination occurs when the inter-diffusion of the polymer chains in the outer and inner dope solutions is interrupted by the penetration of the non-solvent from the coagulation bath (He, Mulder *et al.* 2002). Similarly, Sun *et al.* reported that delamination happens if there is accumulation of water at the interface (Sun, Wang *et al.* 2010a). In addition, the additive from the inner dope solution may move across the outer dope solution due to a concentration gradient, thus promoting phase separation in the interfacial region and subsequent separation of the two layers (Pereira, Nobrega *et al.* 2003). Furthermore, the experimental observation of Li *et al.* revealed that the lamination/delamination and regular/irregular morphology occurring in dual layer hollow fiber membrane are attributed to the shrinkage difference of both layers (Li, Chung *et al.* 2004). This problem can be

overcome by decreasing the ratio of the outer and inner dope flow rates. As a result, the outer layer, which has a higher shrinkage percentage, can tighten the inner layer.

In this chapter, a systematic investigation of the lamination/delamination and regular/irregular morphology of PAI-PES dual layer hollow fiber membranes intended for FO applications is reported. In particular, it examines the effect of LiCl additive on the thermodynamic stability and phase inversion kinetics of the polymer solution by using the ternary phase diagram, viscosity measurements and optical microscopy observations. The results are then used to support the explanation and understanding of various morphologies and structures of dual layer membranes spun from different spinning conditions. The following spinning conditions were specially selected in order to study the underlying mechanisms of the lamination/delamination and regular/irregular structure of dual layer hollow fiber membranes: (1) varying the composition of the outer and inner polymer solutions since they directly affect the thermodynamic stability and phase inversion kinetics; (2) altering the bore fluid and air gap since they contribute to the interpenetration of the polymer solutions; (3) varying the ratio of the outer and inner dope flow rates; and (4) changing the temperature of the external coagulation bath.

5.2. Experimental

5.2.1. Materials

Torlon® 4000T-MV (copolymer of amide and imide) (PAI, Solvay Advanced Polymers, Alpharetta GA) was used as the outer layer material because of its excellent mechanical properties, and thermal and chemical stability (Setiawan, Wang *et al.* 2011). Gafone™ polyethersulfone (PES, Solvay Advanced Polymers, Gujarat) was used as the inner layer material since PES is compatible with PAI and possesses excellent properties for hollow fiber spinning (Chou, Shi *et al.* 2010; Wang, Shi *et al.* 2010; Chou, Wang *et al.* 2012; Shi, Chou *et al.* 2012). N-Methyl-2-pyrrolidone (NMP, > 99.5%, CAS#872-50-4, Merck Chemicals, Singapore) was used as solvent. Lithium chloride (LiCl, anhydrous, CAS#7447-41-8, Merck) was used as an additive in both the outer and inner dope solutions. Purified water by a Milli-Q system (18MΩcm) was used as the bore fluid and tap water was used as the external coagulant.

5.2.2. Preparation of polymer dope solutions and dope viscosity measurements

Preparation of polymer dope solutions prior to dual layer spinning is the same as single layer PAI which has been described in Chapter 3 Section 3.2.2. The detailed of the polymer dope compositions are shown in Table 5.1.

Table 5.1. Composition of polymer dopes.

Dope code*	Outer layer composition	Inner layer composition
DL-14-0	PAI/NMP 14/86	PES/NMP 16/84
DL-14-Li3	PAI/NMP 14/86	PES/LiCl/NMP 16/3/81
DL-14-Li6	PAI/NMP 14/86	PES/LiCl/NMP 16/6/78
DL-14^{+}-0	PAI/LiCl/NMP 14/3.8/82.2	PES/NMP 16/84
DL-14^{+}-Li3	PAI/LiCl/NMP 14/3.8/82.2	PES/LiCl/NMP 16/3/81
DL-14^{+}-Li6	PAI/LiCl/NMP 14/3.8/82.2	PES/LiCl/NMP 16/6/78
DL-14^{+}-Li7	PAI/LiCl/NMP 14/3.8/82.2	PES/LiCl/NMP 16/7/77
DL-18-Li6	PAI/NMP 18/82	PES/LiCl/NMP 16/6/78
DL-19-Li7	PAI/NMP 19/81	PES/LiCl/NMP 16/7/77

*DL-XX^{+}-YYY: XX stands for composition of outer layer (concentration of PAI) and '+' sign means that LiCl (3.8 %) as additive is added into the system (e.g., 14 means the concentration of PAI used is 14%). YYY stands for composition of LiCl additive added into the inner dope systems. Concentration of PES in the inner layer is fixed at 16%; for example, Li3 means PES/LiCl/NMP 16/3/81.

The dynamic viscosity of the polymer dope solutions and the NMP-additive dilute solution was measured by a Physica MCR 101 rheometer (Anton Paar). The measurements were performed using a 25 mm cone plate (CP25-1) for the high viscosity polymer solution and a 50 mm cone plate (CP50-1) for the low viscosity solution of the NMP-additive at a shear rate of 0.01 to 100 s^{-1} at 25°C. The viscosity was obtained at the shear rate of 10 s^{-1}.

5.2.3. Determination of cloud points and phase diagrams

The cloud points of PAI/NMP/water and PES/NMP/water systems with and without the additive (LiCl) were determined by a titrimetric method at room temperature of 23±1 °C. The homogeneous solution, consisting of a polymer and solvent with/without the additive, was prepared in a clear glass bottle. Water was subsequently added drop-by-drop into the homogeneous polymer solution with stirring until the solution turned cloudy. The amount of water needed for the phase separation of the homogeneous solution can be determined by weighing the bottle before the addition of water and after the solution turned cloudy.

5.2.4. Dual layer hollow fiber spinning by using a triple orifice spinneret

Dual layer hollow fibers were fabricated by the dry jet-wet spinning technique illustrated in Figure 5.1. Different pairs of the outer and inner dope solutions were used to make PAI-PES dual layer hollow fiber membranes as described in Table 5.1.

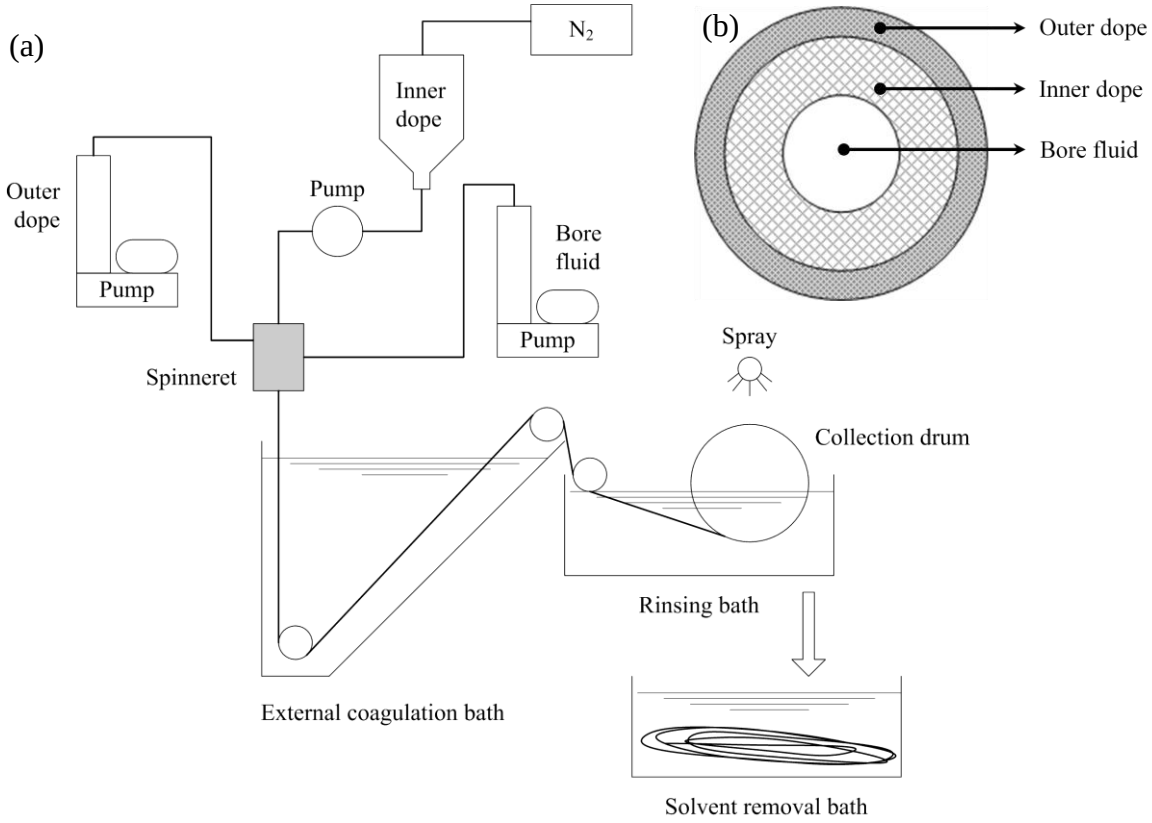

Figure 5.1. (a) Schematic diagram of dual layer spinning; (b) Cross-section of dual layer spinneret.

The inner dope solution, connected to a high pressure nitrogen gas cylinder, was extruded through channel B of the spinneret (see Figure 5.1-b) at a specific flow rate using a Zenith gear pump. The outer dope solution and the bore fluid were extruded using two high precision syringe pumps (Isco) through channels A and C, respectively. The nascent fibers went through a predetermined air gap before immersing into an external coagulation bath at a controlled temperature, and then were collected by a roller at a free fall take-up speed. The resultant hollow fiber membranes were stored in a water bath for approximately 2 days at ambient temperature to ensure that the residual solvent has been removed completely. The spinning conditions of PAI-PES dual layer hollow fiber membranes are summarized in Table 5.2.

Table 5.2. Spinning conditions of PAI-PES dual layer hollow fiber membranes.

Outer dope flow rate (g/min)	1.7, 2.2, 3.3, 4.4
Inner dope flow rate (g/min)	4.6
Bore fluid composition (NMP/water, wt%)	0/100, 25/75, 50/50, 80/20
Bore fluid flow rate (g/min)	6
Air gap (cm)	1, 5, 10
Take up speed	Free fall
External coagulant	Tap water
External coagulant bath temperature (°C)	10, 25

5.2.5. Observations of membrane morphology by scanning electron microscopy (SEM) and phase separation by optical microscope

The procedures for membrane morphology observation by SEM and digital microscope have been described in Chapter 3 Section 3.2.5. An optical microscope (Axiolab, Carl Zeiss) equipped with a colour video camera (TK-C921BEG, JVC) was used to investigate the phase separation rate of individual polymer solution. A drop of a homogeneous polymer solution was sandwiched in between two clean cover slips. Water was dropped and the growing macrovoid fingers within the solution were recorded.

5.3. Results and discussion

5.3.1. Thermodynamic properties of polymer dope solutions

The ternary phase diagrams of the PAI/NMP/water and PES/NMP/water systems with and without additives at 23°C are shown in Figure 5.2. The phase diagrams were developed from the cloud point experiments. As illustrated in Figure 5.2-a, there is no significant change in the binodal curve of the PAI system with and without the addition of LiCl. It was reported that the ion-dipole interaction of LiCl and PAI can cause the PAI/LiCl/NMP system to be more thermodynamically stable even though LiCl also has a strong interaction with NMP (Balasubramanian and Shaikh 1973). The interactions of imide with Li^+ (Choo, Rychnovsky *et al.* 1994) as well as amide with Li^+ (Balasubramanian and Shaikh 1973) have been studied in the literature.

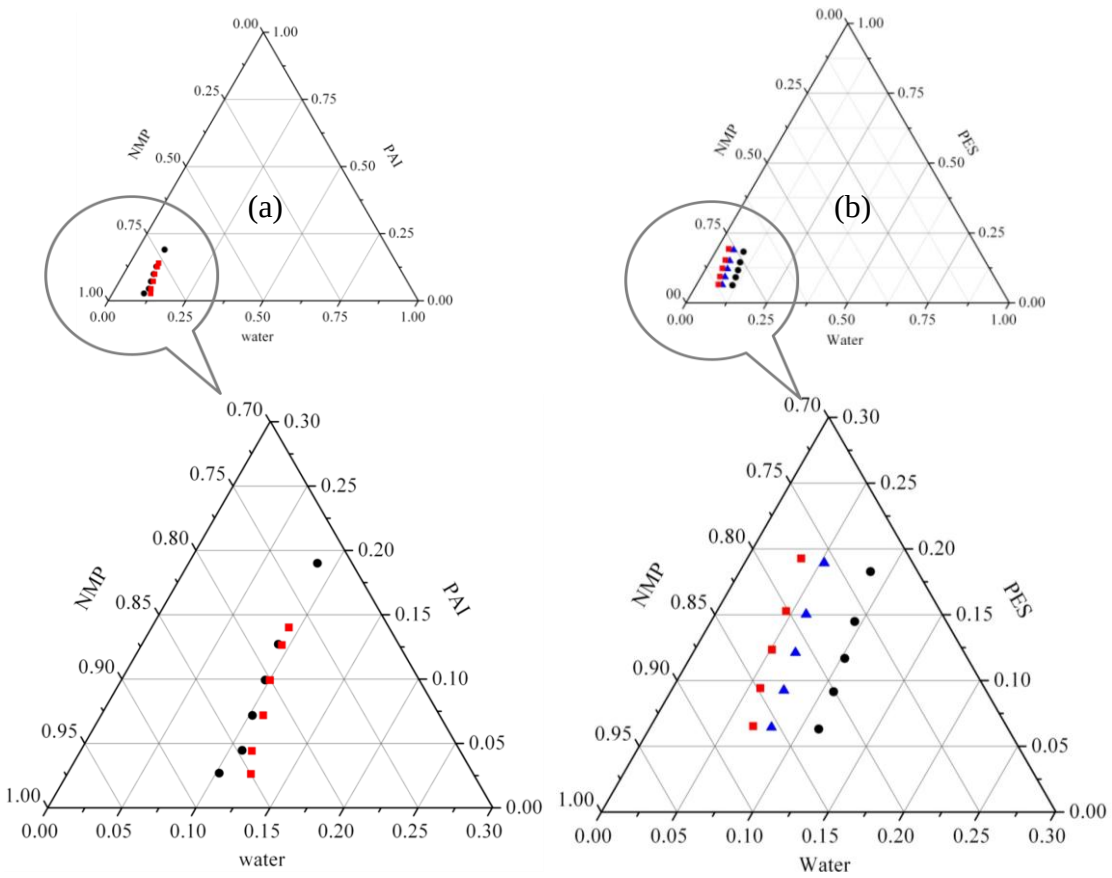

Figure 5.2. Ternary phase diagram of (a) PAI systems (● no additive; ■ 3.8% LiCl) and (b) PES systems (● no additive; ▲ 3% LiCl; ■ 6% LiCl).

In contrast to the PAI/NMP system, the PES/NMP system is more sensitive to the addition of LiCl as shown in Figure 5.2-b. It can be seen that the addition of LiCl shifted the binodal curve of the PES system toward the polymer-solvent axis. The addition of LiCl makes the system thermodynamically unstable due to its interaction with NMP; hence, the ability of the solvent to dissolve the polymer decreases. Therefore, less water is needed for the phase separation to occur in the PES/NMP system with LiCl as the additive as compared to the solution without LiCl. A similar phenomenon has been reported in literature for the PVDF/NMP/water system (Shi, Wang *et al.* 2008).

5.3.2. Kinetics of phase inversion

The kinetics of the phase separation during the membrane formation for the PAI and PES systems are illustrated by the optical micrographs shown in Figure 5.3 and Figure 5.4, respectively. These figures were taken for each polymer solution at different times, where the dark area represents the precipitated zone. As can be seen in Figure 5.3, the rate of water penetration slows down as the PAI concentration increases from 14% to 19%. The addition of 3.8% LiCl decreases the penetration rate considerably at the same PAI concentration of 14% (Figure 5.3 a and d). In contrast, as shown in Figure 5.4 a and b, the addition of 3% LiCl to the PES/NMP system increases the water penetration rate, but a further increase in additive concentration decreases the penetration rate.

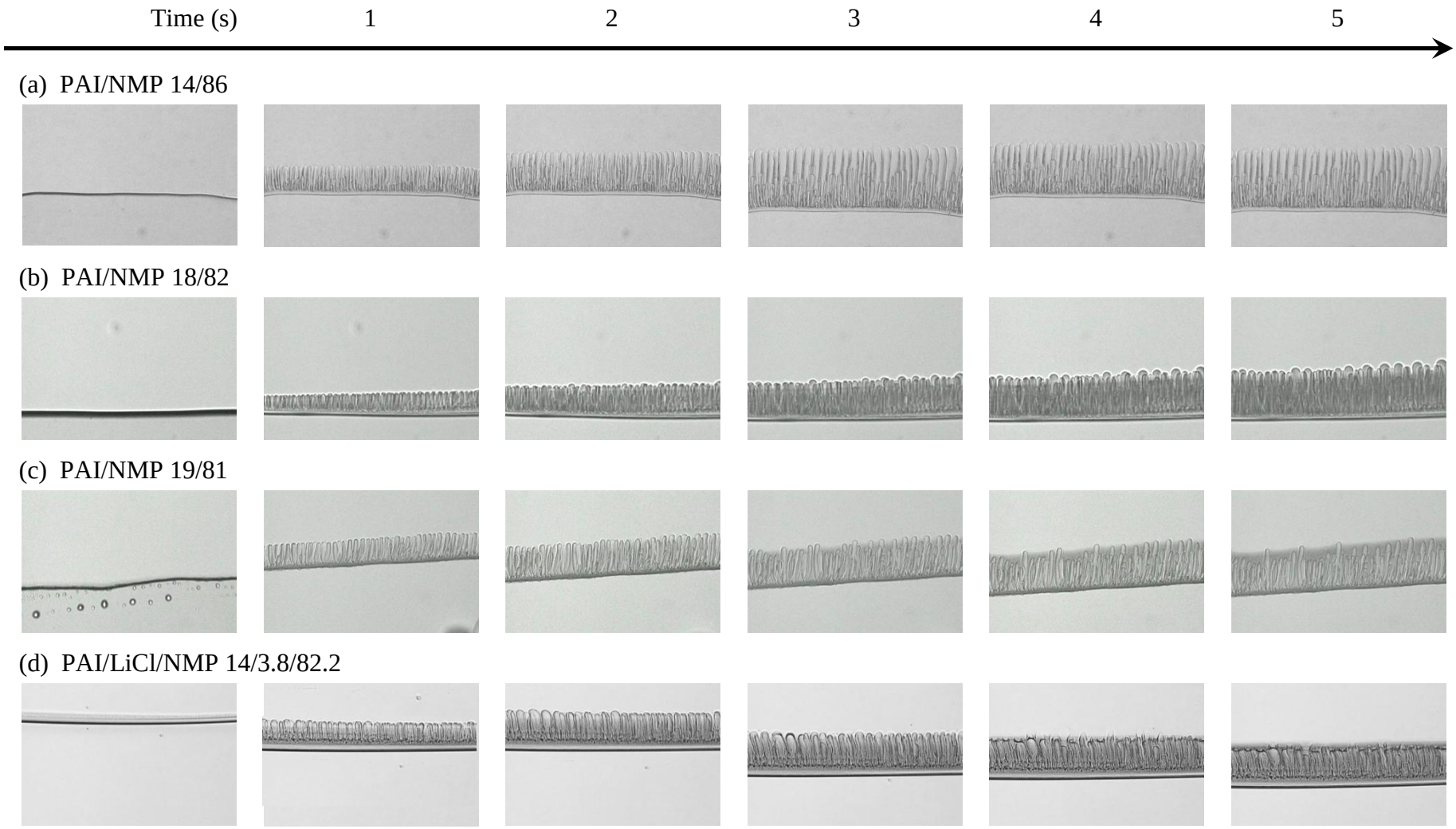

Figure 5.3. Optical micrographs for water penetration through PAI/NMP systems with and without LiCl.

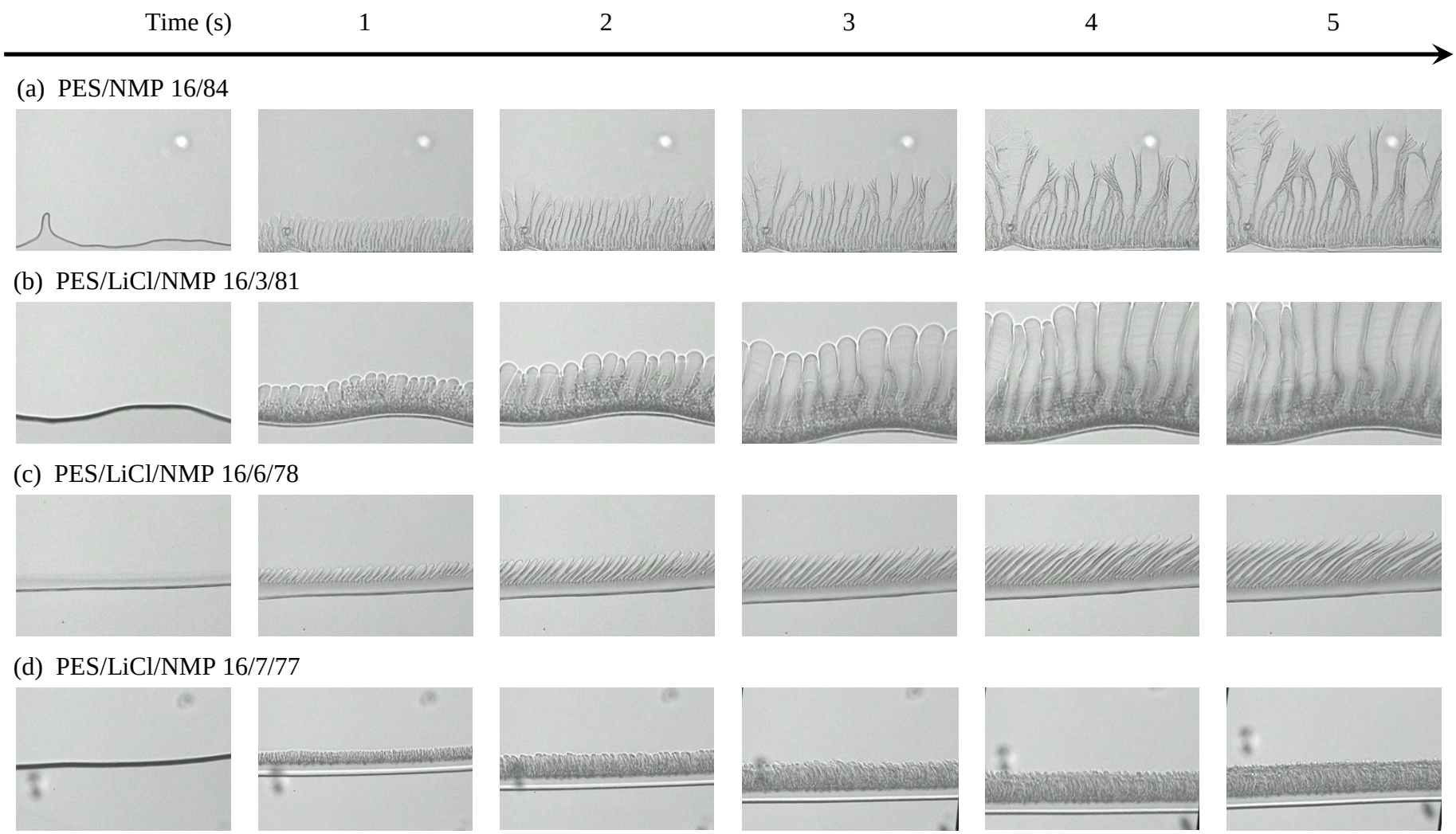

Figure 5.4. Optical micrographs for water penetration through PES/NMP systems with and without LiCl.

The viscosity of PAI and PES system is shown in Figure 5.5 and it is summarized in Table 5.3 for each polymer system. It can be seen that the addition of LiCl significantly increases the viscosity of the polymer solutions. This is because NMP is a polar aprotic solvent that has a lone pair of electrons. This electron pair is able to form an ion-dipole interaction with cations such as Li^+ (as shown in Figure 5.6-a) (Balasubramanian and Shaikh 1973) and thus, the viscosity of NMP increases with the increasing of LiCl concentration (Figure 5.6-b). As a result, the viscosity of PAI or PES dope solutions increases accordingly. The increased viscosity of the polymer solution normally tends to retard water penetration during the phase inversion process, as shown in Figure 5.3-d in comparison with Figure 5.3-a.

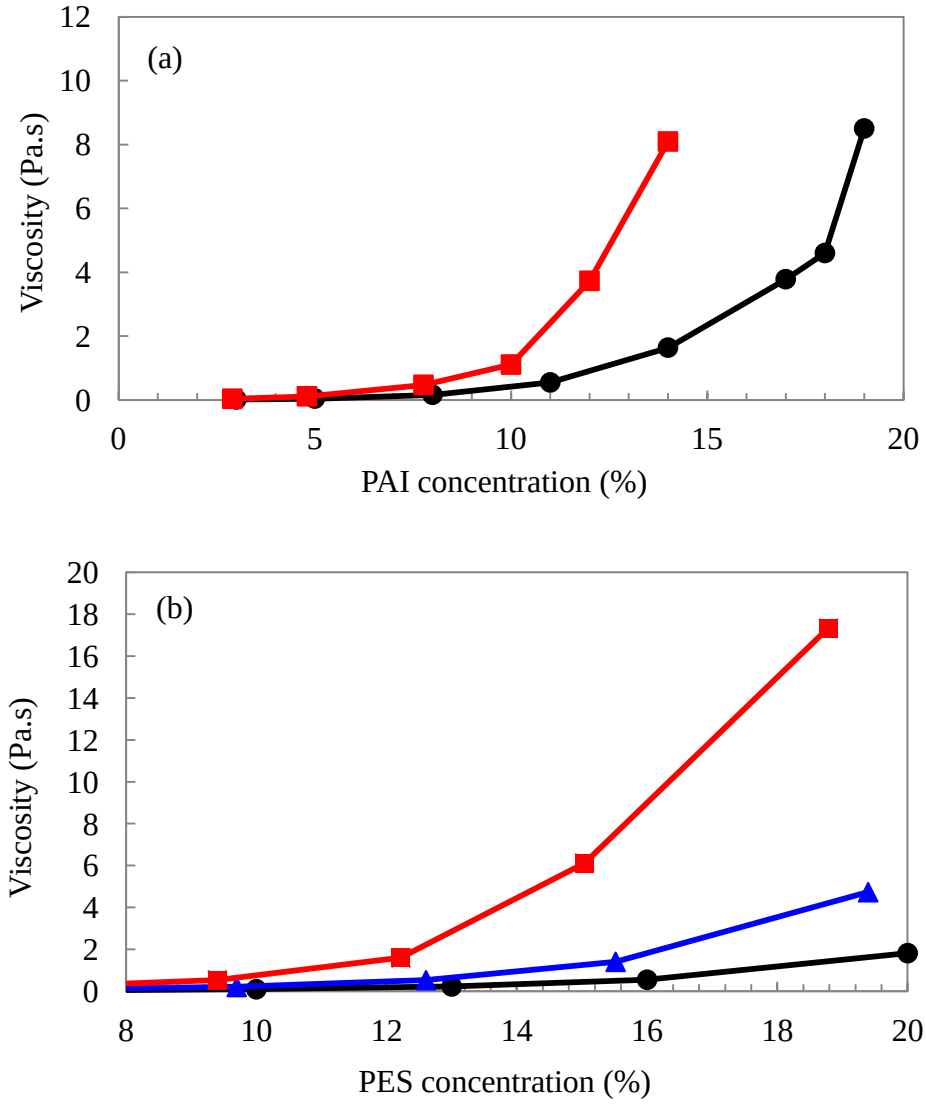

Figure 5.5. Plot of viscosity vs polymer concentration of (a) PAI systems (● no additive; ■ 3.8% LiCl) and (b) PES systems (● no additive; ▲ 3% LiCl; ■ 6% LiCl).

Table 5.3. Viscosity and solubility parameter differences.

Outer layer			Inner layer		
Composition	Visc. (Pa.s)	Δδ*	Composition	Visc. (Pa.s)	Δδ*
PAI/NMP 14/86	1.6	1.8	PES/NMP 16/84	0.5	1.08
PAI/NMP 18/82	4.6	1.8	PES/LiCl/NMP 16/3/81	1.4	6.76
PAI/NMP 19/81	8.5	1.8	PES/LiCl/NMP 16/6/78	6.9	11.9
PAI/LiCl/NMP 14/3.8/82.2	8.2	-	PES/LiCl/NMP 16/7/77	11.1	13.6

*$\Delta\delta = |\delta_{solvent\text{-}additive} - \delta_{polymer}|$, unit = $MPa^{1/2}$.

However, the addition of LiCl also reduces the thermodynamic stability of the PES/NMP system. Thus, the phase separation is mainly affected by whether the dominant factor is the thermodynamic properties or the phase inversion kinetics. It appears that the increased thermodynamic instability due to the LiCl addition in the PES/LiCl/NMP 16/3/81 system (Figure 5.4-b) plays a more important role than the increase in viscosity.

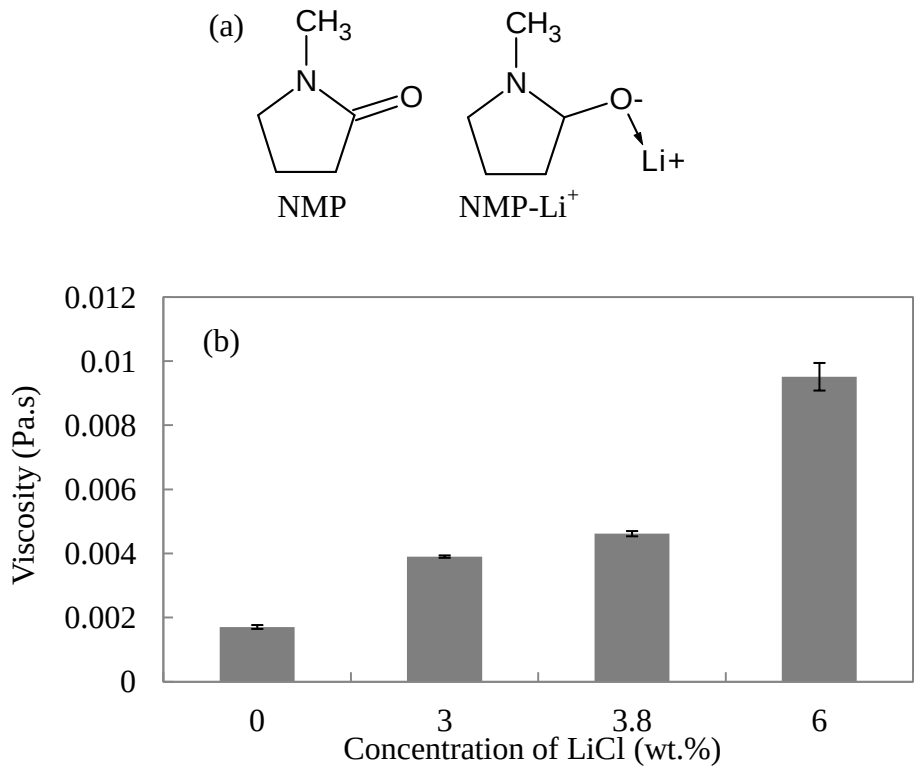

Figure 5.6. (a) Chemical structure of NMP and NMP-Li^+; (b) Plot of NMP viscosity without and with LiCl.

5.3.3. Effect of the ratio of inner dope to bore fluid flow rates

As shown in Table 5.2, the bore fluid flow rate used is higher than the inner dope flow rate because of following reasons. As shown in Figure 5.7 a and d, the two membranes have a deformation inner contour when the inner dope to the bore fluid flow rate ratio of 1:1 was used at 1 cm air gap. When the pressure inside the fiber lumen is low due to insufficient supply of the bore fluid, there will be a compression of the inner wall because of a rapid formation of the lumen skin when a strong bore fluid is used. Therefore, the irregularity of the inner contour can be prevented by increasing the bore fluid flow rate (Figure 5.7 c and f) (Santoso, Chung *et al.* 2006).

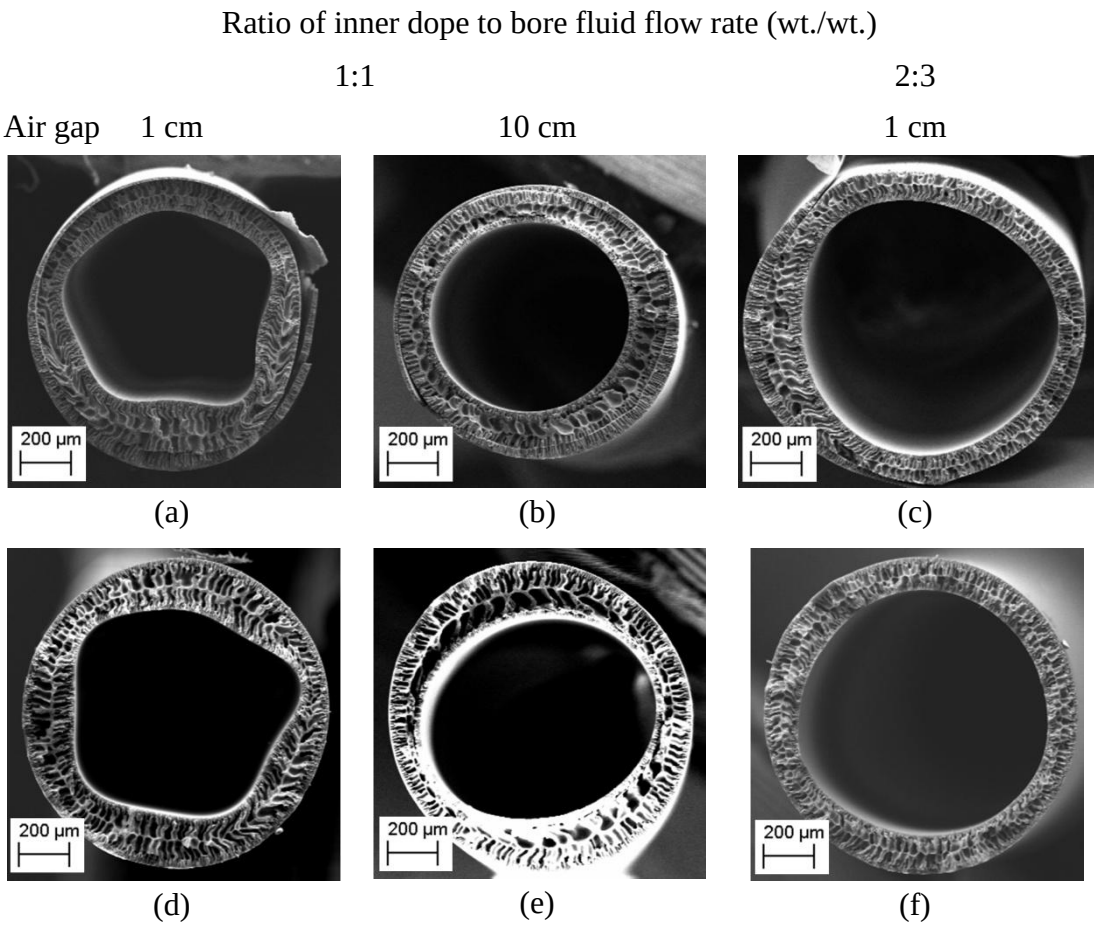

Figure 5.7. Effect of inner dope to bore fluid flow rate ratio on the cross section dual layer hollow fiber membrane: (a, b, c) DL-14-0 (delamination); (d, e, f) DL-14^{+}-0 (no delamination).

In addition, at a lower air gap, the polymer molecules have a shorter time to relax and release the stress after extruding out from spinneret. The instantaneous demixing and

solidification at the outer side of the fiber caused by a strong coagulant tended to freeze the polymer molecules. It forces the stress held by the macromolecules to release toward lumen radial direction (Shi, Wang *et al.* 2007). Hence, the increasing of air gap is able to eliminate the deformation but it generates big macrovoids. Therefore, here after, the inner dope to bore fluid flow rate ratio of 2:3 was applied (the inner dope flow rate of 4.6 g/min and the bore fluid flow rate of 6 g/min were used).

5.3.4. Effect of the compositions of inner and outer polymer dope solutions

Figure 5.8 shows the cross-sectional morphologies of six membranes at a magnification of 150X that were spun from different compositions of the outer and inner dope solutions. Their morphologies at a higher magnification of 500X and 1000X are shown in Figure 5.9 and Figure 5.10, respectively. It can be seen that the most severe delamination occurs in Figure 5.10-a (dope code: DL-14-0) followed by that shown in Figure 5.10-c (dope code: DL-14-Li6), while others have a good adhesion at the interface of two layers. Figure 5.9 (b, d-f) shows continuously developed finger-like structures from outer to inner layer for fibers with good lamination. In addition, the hollow fiber with the most severe delamination has the largest macrovoids in the outer layer (Figure 5.10-a).

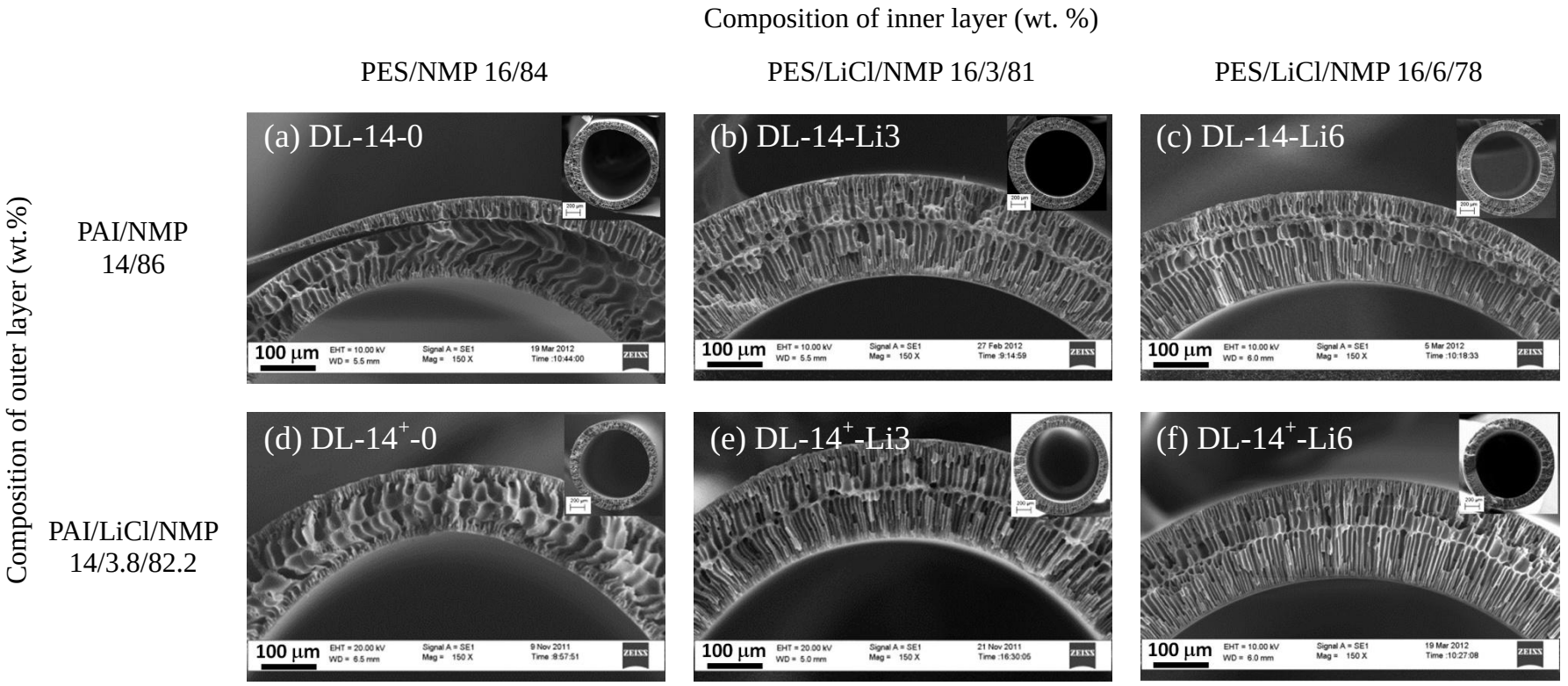

Figure 5.8. Cross-section morphology of dual layer hollow fiber membranes spun from different compositions of outer and inner layers at magnification of 150X. Spinning conditions: outer dope flow rate: 1.7 g/min; inner dope flow rate: 4.6 g/min; bore fluid flow rate: 6 g/min; air gap: 1 cm; coagulation bath temperature: 25°C; bore fluid: water.

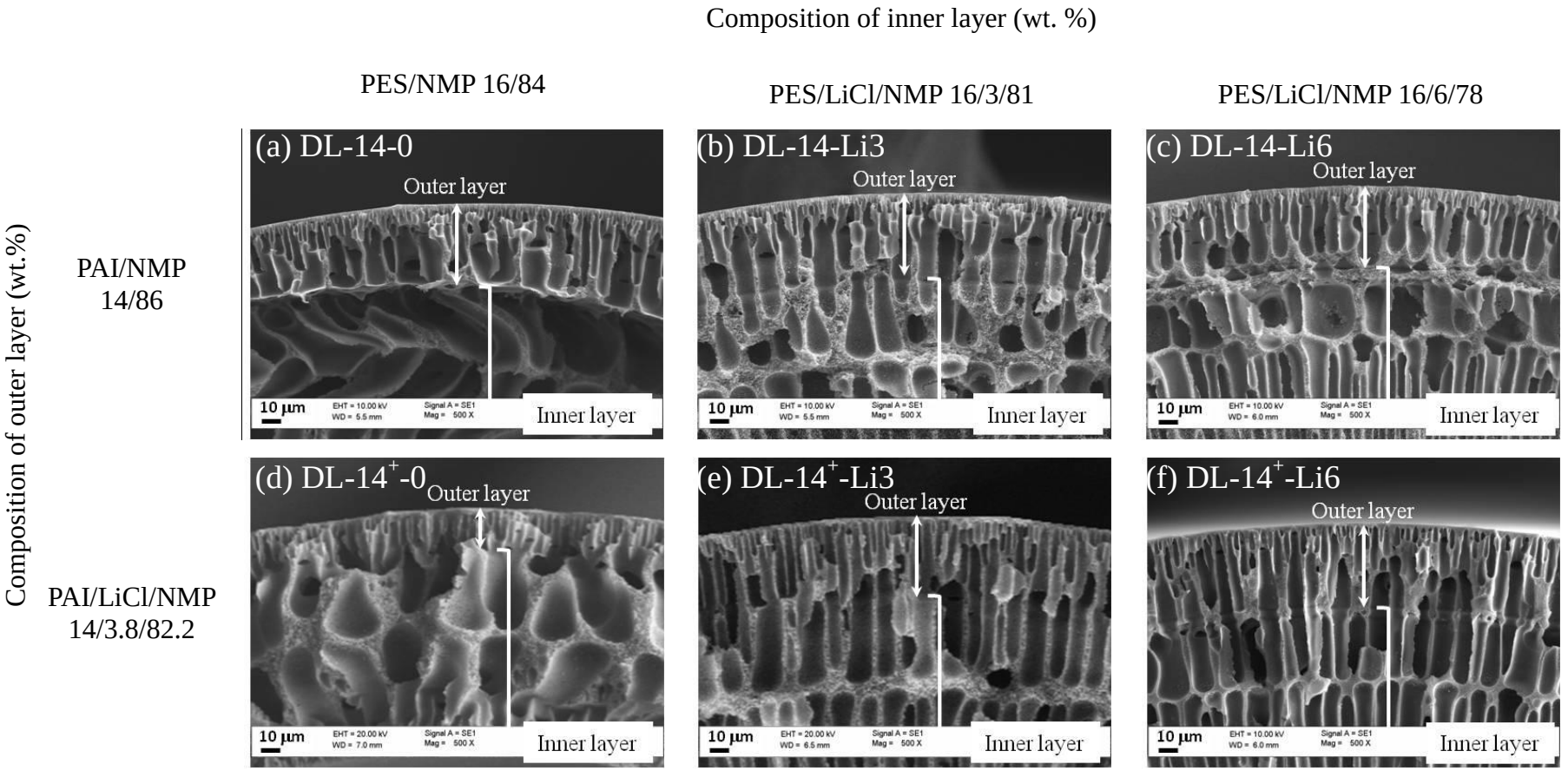

Figure 5.9. Cross-section morphology of dual layer hollow fiber membranes spun from different compositions of outer and inner layers at magnification of 500X. Vertical white arrows indicate the outer layer. Spinning conditions: outer dope flow rate: 1.7 g/min; inner dope flow rate: 4.6 g/min; bore fluid flow rate: 6 g/min; air gap: 1 cm; coagulation bath temperature: 25°C; bore fluid: water.

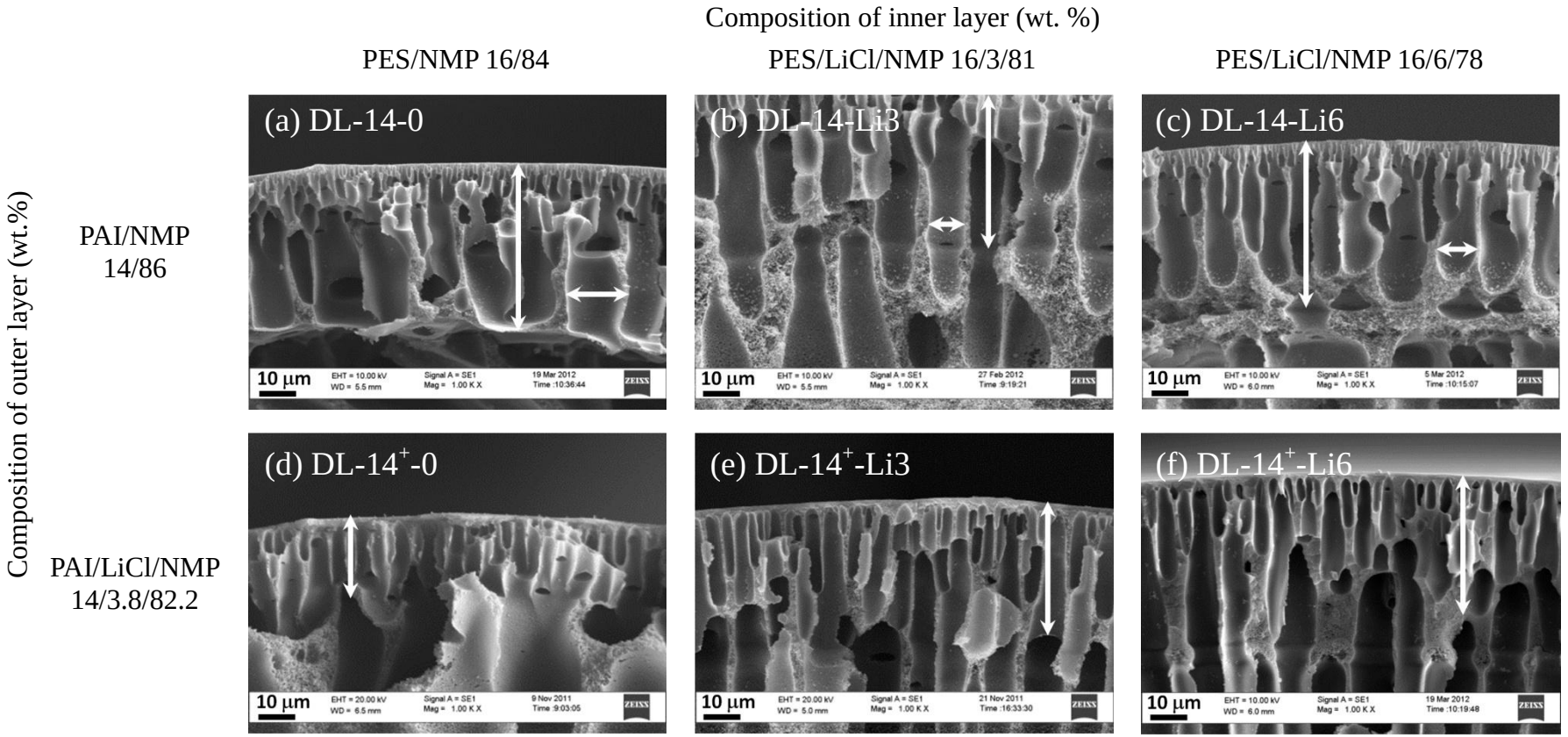

Figure 5.10. Cross-section morphology of dual layer hollow fiber membranes spun from different compositions of outer and inner layers at magnification of 1000X. Vertical white arrows indicate the outer layer. Spinning conditions: outer dope flow rate: 1.7 g/min; inner dope flow rate: 4.6 g/min; bore fluid flow rate: 6 g/min; air gap: 1 cm; coagulation bath temperature: 25°C; bore fluid: water.

It is important to understand the mechanisms of lamination/delamination at the interface of the outer and inner layers of dual layer membranes. In the present study, it is hypothesized that the delamination is mainly controlled by the rates of the non-solvent (water) diffusion through the outer ($J_{NS\text{-}outer}$) and inner ($J_{NS\text{-}inner}$) layers, which also have a direct impact on the growth of the macrovoids. There are two scenarios to be considered as illustrated in Figure 5.11 and Table 5.4 in which the "up" and "down" arrows denote an increase or decrease in the quantity, respectively:

(1) When the non-solvent (water from the external coagulant bath) has a higher diffusion rate in the outer layer as compared to that in the inner layer, the outer layer tends to expand to form large macrovoids and to hold more water at the interface. As a result, the accumulated water can impede the adhesion of the two layers, leading to a delamination.

(2) If water has a slower penetration rate through the outer layer dope than the inner layer dope, good adhesion of these two layers is expected. Under this scenario, since macrovoids can form in the inner layer leading to the expansion of the inner layer, they can become distorted and the inner contour can become irregular.

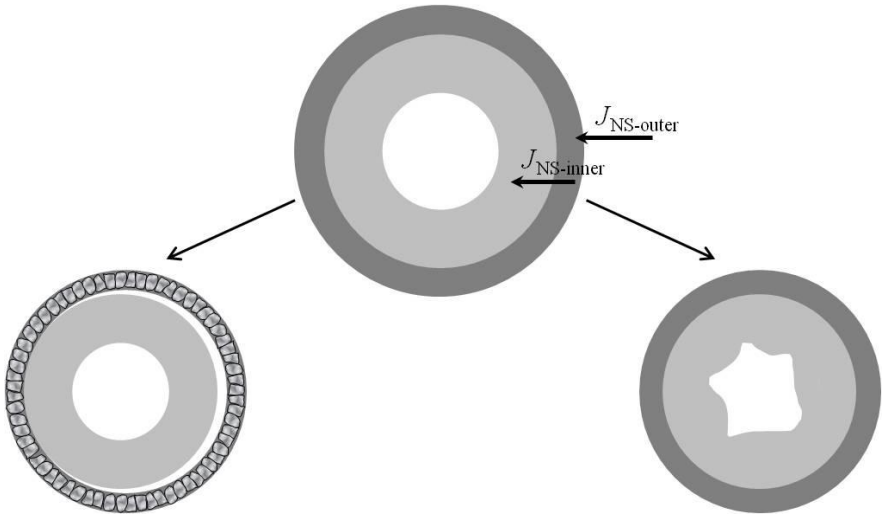

Scenario 1:
Delamination happens
if $J_{NS\text{-}outer} > J_{NS\text{-}inner}$
$J_{NS\text{-}inner}$ depends on thermodynamic instability and viscosity

Scenario 2:
No delamination happens
if $J_{NS\text{-}outer} < J_{NS\text{-}inner}$
The expansion of the inner layer results in the deformation of the inner contour.

Figure 5.11. Illustration of the mechanisms of lamination/delamination at the interface of the layers and regular/irregular morphology of dual layer membranes.

Table 5.4. List of parameters involved in PAI-PES dual layer hollow fiber fabrication.

Parameters	Effect	$J_{NS\text{-}inner}$	$J_{NS\text{-}outer}$
LiCl ↑	Viscosity ↑	↓	↓
LiCl ↑	Thermodynamic instability ↑[a]	↑	-
Air gap ↑	Inner layer expansion ↑	-	↓
Ratio of outer to inner dope flow rate ↓	regularity of fiber cross-section ↑	-	-
External coagulation bath temperature ↓	-	-	↓
NMP in bore fluid ↑	Inner layer expansion ↑[b]	-	-

[a] For PES system only
[b] Up to 50% NMP in bore fluid

The first hypothesis can be used to explain the results observed in Figure 5.8 to Figure 5.10. First, consider the cases shown in Figure 5.8 (and Figure 5.10) a, b, and c, in which the same outer dope composition of PAI/NMP 14/86 was used. It implies that the rate of non-solvent (water) penetration from the external coagulation bath into the outer polymer dope is the same. When water reaches the interface, for the case shown in Figure 5.8-a (and Figure 5.10-a), since the inner layer is very stable as indicated by the phase diagram in Figure 5.2-b (dope composition: PES/NMP 16/84, without LiCl additive), the penetration of water and NMP (from the outer dope) cannot cause the inner dope to phase separate rapidly. With the expansion of the PAI layer due to water penetration, water accumulates at the interface and delamination takes place.

It is interesting to see that the finger-like structure developed from the outer layer can penetrate continuously through the interface between the two layers in Figure 5.8-b (Figure 5.10-b), which may be attributed to the addition of an appropriate amount of LiCl in the inner dope solution (dope composition: PES/LiCl/NMP 16/3/81). It seems that the addition of 3% LiCl in the inner dope solution makes the inner system highly unstable. The solubility parameter difference can be used to confirm the compatibility of PES/NMP with LiCl. As shown in Table 5.3, PES/NMP without LiCl has a solubility parameter difference of 1.08 $(MPa)^{1/2}$. The addition of 3% LiCl increases the solubility parameter difference to 6.76 $(MPa)^{1/2}$. A lower the solubility parameter

difference implies better interaction between the polymer and solvent. The increase of the solubility parameter difference from 1.08 to 6.76 $(MPa)^{1/2}$ implies that the solubility of the polymer in the solvent decreases; hence, a small amount of water is sufficient to induce phase separation to occur. However, a further increase of LiCl concentration to 6% decreases the adhesion of both layers. Despite increasing the thermodynamic instability, the addition of 6% LiCl significantly increases the viscosity of the polymer solution (6.9 Pa.s vs. 1.4 Pa.s, in Table 5.3). A high viscosity solution could hinder water diffusion. Interestingly, the macrovoids observed in the outer layer are larger when the adhesion between the outer and inner layer is poor.

Second, consider the cases shown in Figure 5.10 a and d, in which the same inner dope composition of PES/NMP 16/84 was used. It is assumed that the water penetration rate through the inner polymer solution is the same. The fiber spun from the composition of DL-14^{+}-0 (Figure 5.10-d) has a perfect adhesion in contrast to that for DL-14-0 (Figure 5.10-a). The addition of 3.8% LiCl in the PAI dope has not resulted in a significant change in the thermodynamic stability as can be seen in Figure 5.2-a. However, it indeed increases the viscosity of the outer dope solution from 1.6 Pa.s to 8.2 Pa.s (Table 5.3). The decrease in water penetration rate through the outer layer has been observed using optical microscopy as described previously (Figure 5.3 a and d). Thus, the water penetration in the outer layer dope must match the rate of water diffusion in the inner layer dope, leading to a good adhesion of two layers. A similar approach has been reported to improve the adhesion by increasing the polymer concentration and thus the viscosity of the outer dope solution (He, Mulder *et al.* 2002).

Figure 5.12 shows the cross-section morphologies of two membranes having the same inner layer composition of PES/LiCl/NMP 16/7/77 and different outer layer compositions but with similar viscosity. The outer layer of the fiber in Figure 5.12-a (dope code: DL-19-Li7) has a viscosity of 8.5 Pa.s, while the fiber in Figure 5.12-b (dope code: DL-14^{+}-Li7) also has a similar viscosity of 8.2 Pa.s. It is observed that the finger-like structures are developed inward and outward simultaneously (shown by the arrows). The outer layer was solidified by the external coagulant only, while both the external coagulant and the bore fluid were involved in the solidification of the inner layer. However, the outer and inner layers of the membrane made of DL-19-Li7 have poor adhesion (Figure 5.12-a). At 500X and 1000X magnifications, it can be seen

clearly that the fiber has large macrovoids in the inner layer that was developed inward by the external water coagulant (shown by a rectangle in Figure 5.12-a2), as compared to that of DL-14^{+}-Li7 (Figure 5.12-b2).

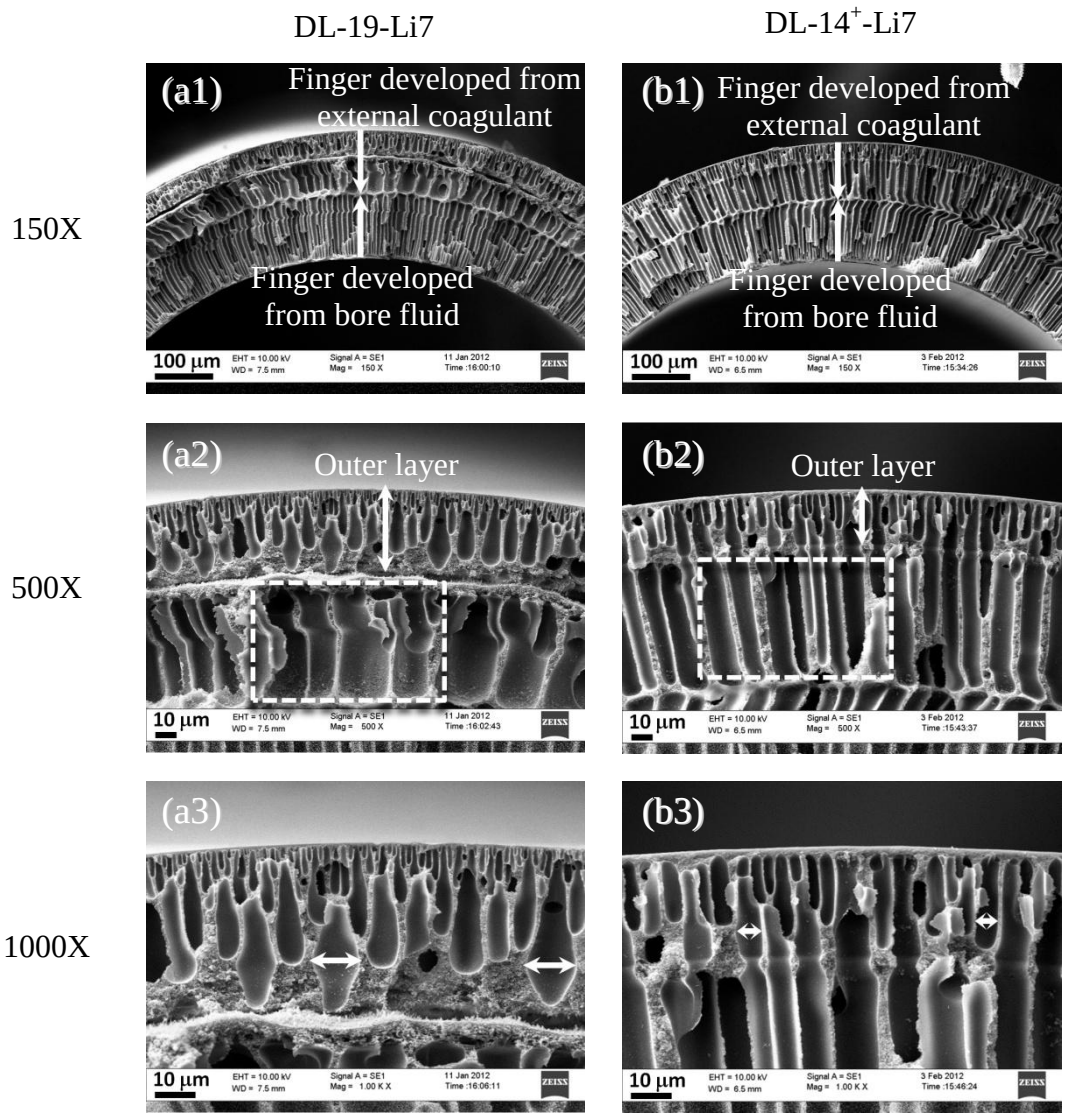

Figure 5.12. Cross-section morphology of dual layer hollow fiber membranes spun from the same inner layer composition of PES/LiCl/NMP 16/7/77 and different outer layer compositions with similar viscosity (PAI/NMP 19/81: 8.5 Pa.s and PAI/LiCl/NMP 14/3.8/82.2: 8.2 Pa.s). Spinning conditions: outer dope flow rate: 1.7 g/min; inner dope flow rate: 4.6 g/min; bore fluid flow rate: 6 g/min; air gap: 1 cm; coagulation bath temperature: 25°C; bore fluid: water.

The delamination that occurred on the fiber made from DL-19-Li7 composition can also be explained using the first hypothesis. Based on the phase diagram shown in Figure 5.2-a, the PAI/NMP/water system without LiCl is more unstable, which may

lead to a faster phase separation than that with LiCl. Thus, despite the similar viscosities, the PAI/NMP 19/81 and PAI/LiCl/NMP 14/3.8/82.2 dopes have different precipitation rates as shown in Figure 5.3 c and d due to the difference in their associated thermodynamic stability. It may be deduced that more water from the external coagulation bath can diffuse into the outer layer of the membrane made of DL-19-Li7 than that made of DL-14^{+}-Li7. More water penetration results in larger macrovoids in the outer layer. Subsequently, the macrovoids in the inner layer, which were developed from the outer side, are also larger.

It is interesting to examine the surfaces of outer and inner layers at the interface when delamination takes place. The DL-14-0 and DL-19-Li7 fibers, which were spun from different compositions of the outer and inner dope solutions, suffer a severe delamination. The inner surface of the outer layer and the outer surface of the inner layer were, then, observed by using SEM as shown in Figure 5.13 and Figure 5.14 for the DL-14-0 and DL-19-Li7 fibers, respectively. Large pores can be seen on the inner surface of the outer layer for both fibers which were formed during the penetration of the non-solvent (water) in the external coagulant bath. However, the texture of the surface between the large pores differs for the two fibers. The DL-14-0 fibers have a 'skin' or a dense surface while the DL-19-Li7 has 'no skin' or a sponge-like surface. The difference in the surface texture is due to the difference in the phase inversion kinetics. The outer layer of DL-14-0 hollow fiber was composed of 14% PAI which has viscosity of 1.6 Pa.s, while DL-19-Li7 hollow fiber consists of 19% PAI with viscosity of 8.5 Pa.s. As described previously, a high viscosity solution could hinder water diffusion leading to delayed demixing.

Furthermore, the observation of the outer surface of the inner layer also gives a clear picture on the degree of the phase inversion. A very porous structure on the outer surface of the inner layer can be seen in Figure 5.13 for the DL-14-0 fibers. In contrast, there are no pores on the outer surface of the DL-19-Li7 inner layer as shown in Figure 5.14. The inner layer of the DL-14-0 fiber was made from 16% PES without any additive whereas DL-19-Li7 consisted of 16% PES and 7% LiCl as the additive. The viscosity of 16% PES without additive is measured to be 0.5 Pa.s and the total solubility parameter difference is 1.08 $(MPa)^{1/2}$. The addition of 7% LiCl significantly increased both viscosity and total solubility parameter difference to 11 Pa.s and 13.6

$(MPa)^{1/2}$, respectively. The viscosity and the total solubility parameter difference are shown in Table 5.3. As mentioned earlier, the total solubility parameter difference of a polymer/solvent system presents the interaction between the polymer and the solvent. The interaction is better at a lower solubility parameter difference favoring higher thermodynamic stability. The interaction between PES and NMP in DL-14-0 is much lower than that in DL-19-Li7. Therefore, delayed demixing occurs on the outer surface of DL-14-0 inner layer resulting in a 'no-skin' polymer matrix. The DL-19-Li7, on the other hand, has a poor affinity of polymer and solvent resulting in a dense outer skin due to a rapid demixing. It should be noted that the outer surface of DL-19-Li7 inner layer is quite rough which can be attributed to the polymer mesh from the outer layer (PAI). The dense outer skin of DL-19-Li7 inner layer is located underneath the polymer mesh.

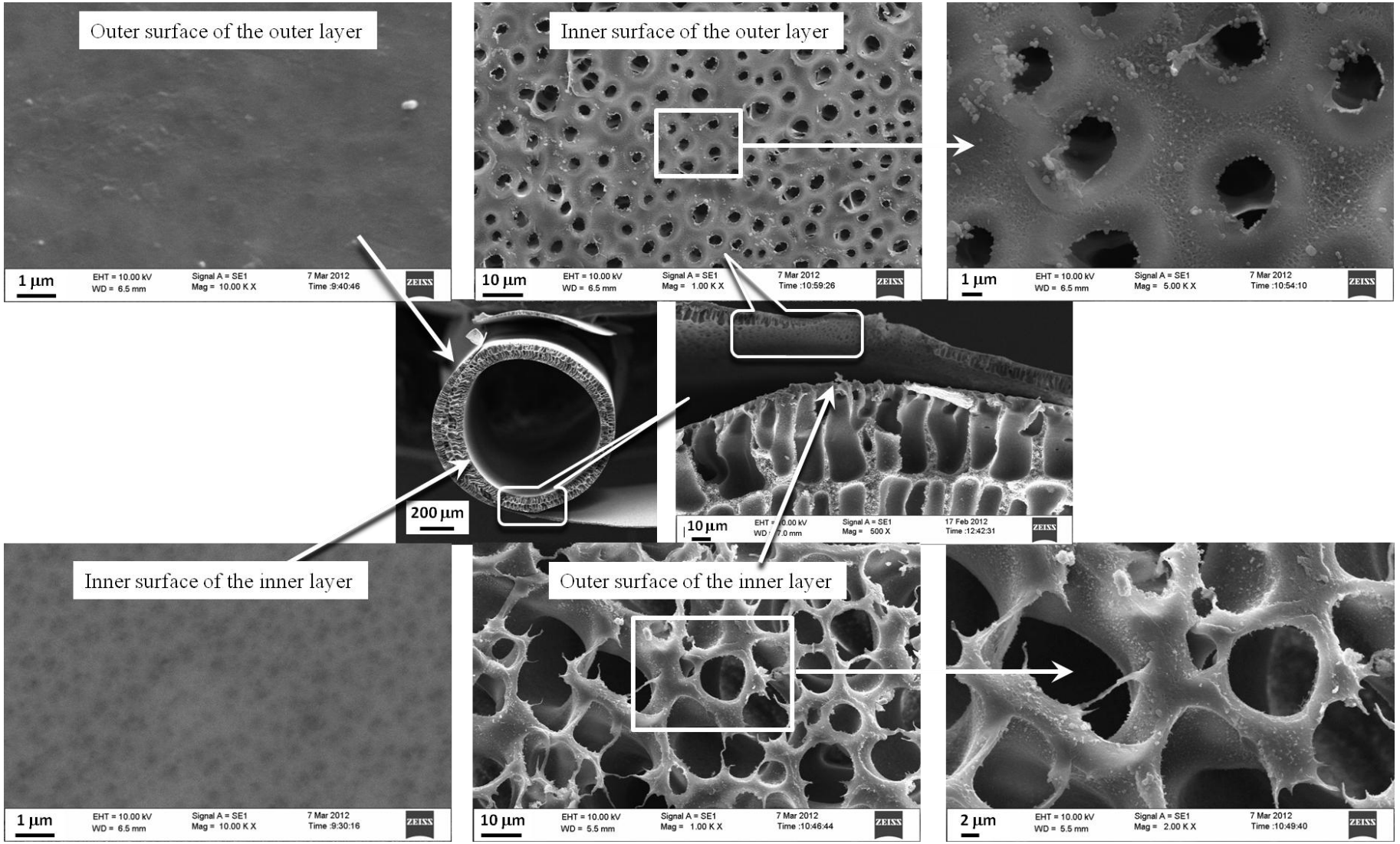

Figure 5.13. Surface morphology of the dual layer hollow fiber membrane made from DL-14-0 composition.

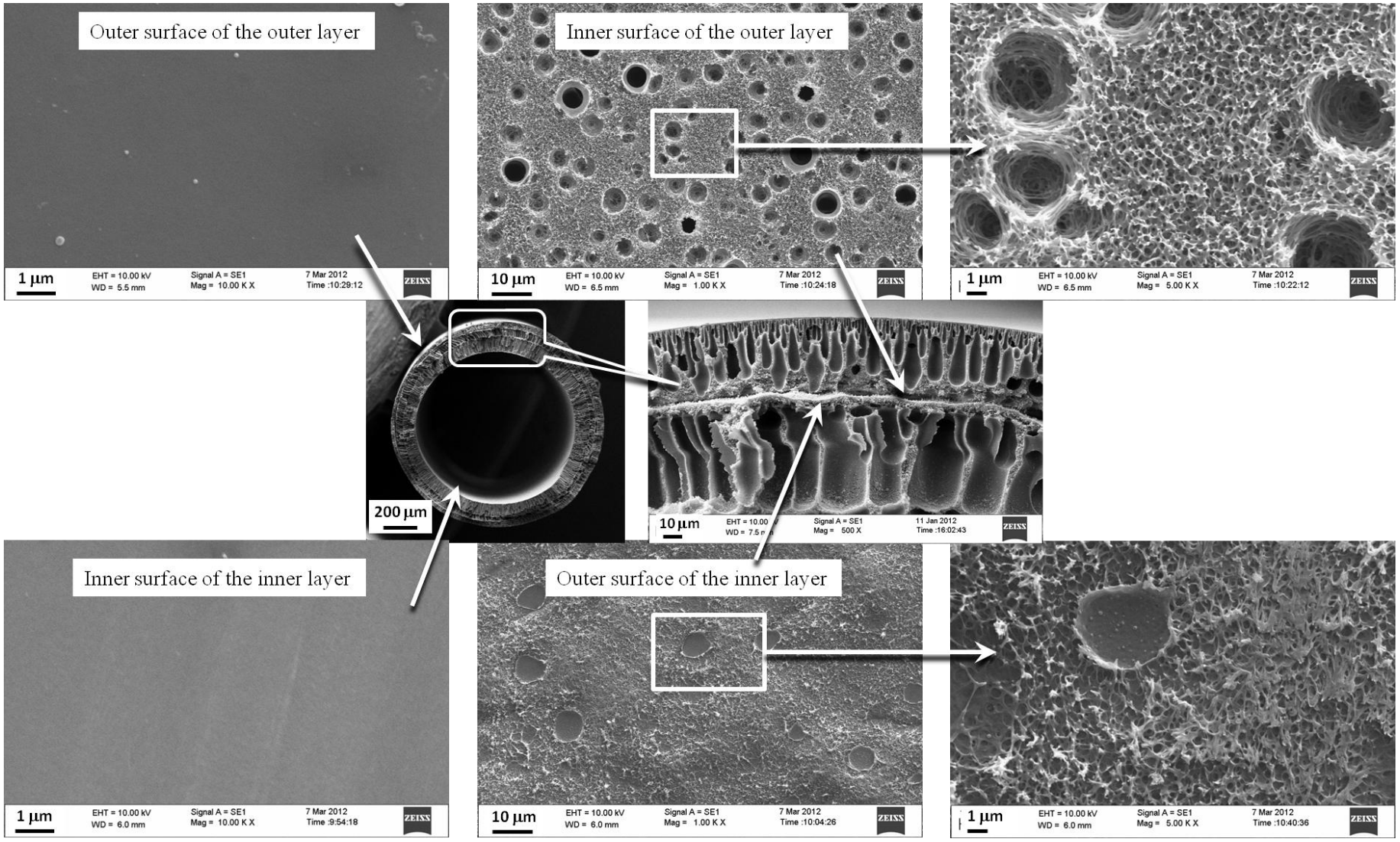

Figure 5.14. Surface morphology of the dual layer hollow fiber membrane made from DL-19-Li7 composition.

5.3.5. Effect of air gap

Figure 5.15 shows the cross-section of the PAI/PES dual layer hollow fiber membranes that were spun from the same composition for the inner layer (PES/NMP 16/84 wt.%) and the same PAI concentration (14 wt.%) without LiCl (a) and with 3.8% LiCl (b) as an additive at different air gaps from 1 to 10 cm. The DL-14-0 dual layer hollow fiber membrane spun with an air gap of 1 cm displayed a more severe delamination than the other fibers prepared with higher air gap distances. A higher air gap allows the outer and inner dope solutions to have a longer contact time for interpenetration (Pereira, Nobrega *et al.* 2003), and delays and slows down water diffusion through the outer layer. Hence, according to the first hypothesis, the delamination phenomenon will be mitigated.

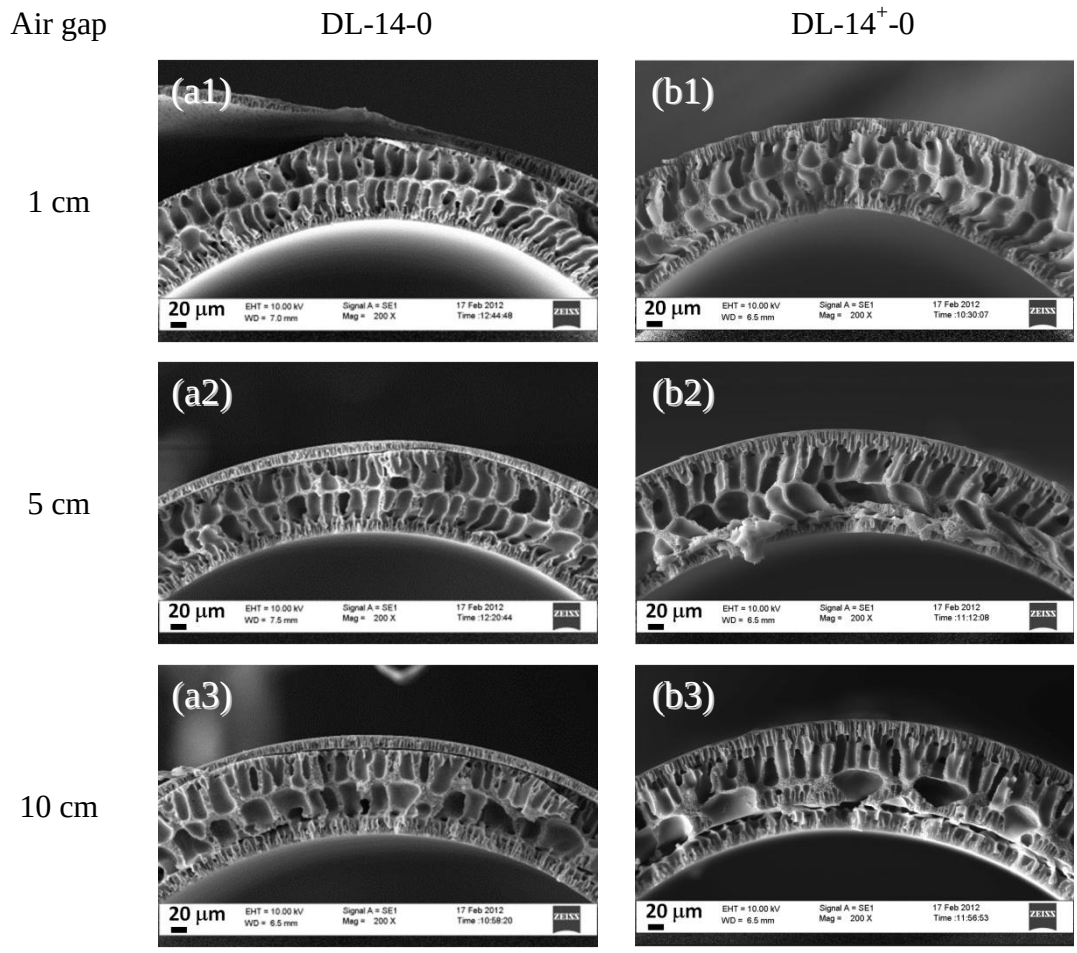

Figure 5.15. Cross-section morphology of dual layer hollow fiber membranes spun from compositions of (a) DL-14-0 and (b) DL-14^{+}-0 at different air gaps. Spinning conditions: outer dope flow rate: 1.7 g/min; inner dope flow rate: 4.6 g/min; bore fluid flow rate: 6 g/min; coagulation bath temperature: 25°C; bore fluid: water.

The interpenetration can be confirmed by examining the morphology at the interface. Figure 5.16 shows the SEM micrographs of the morphology at the interface of the DL-14-0 dual layer hollow fiber membranes at different air gaps. In general, both surfaces (the inner surface of the outer layer and the outer surface of the inner layer) are very porous. As the air gap is increased, the pore size becomes smaller for both surfaces. At a 1 cm air gap, the areas between the pores on the outer surface of the inner layer are very small and thin, and the surface is smooth (Figure 5.16-b1). Therefore, the adhesion between outer and inner layer is poor. As the air gap is increased, these areas become larger and the surface is covered by micro pores and spikes that might be due to the interaction of polymer from both the outer and inner layers (Figure 5.16-b3). There are more spikes covering the inner surface of the outer layer as well (Figure 5.16-a3).

The DL-14^{+}-0 membranes, on the other hand, have good attachment at all air gap distances (the outer layer cannot be peeled off) (as shown in Figure 5.15-b). However, it was found that in conjunction with increasing air gap distance, the macrovoids that developed outward from the lumen in the inner layer transformed from finger-like to tear-drop-like structures. This result can be explained by the second hypothesis. Increasing the air gap allows the phase inversion to occur much earlier and faster in the inner layer than in the outer layer. The macrovoid transformation occurs because the inner layer is unable to expand due to the robust attachment at the interface.

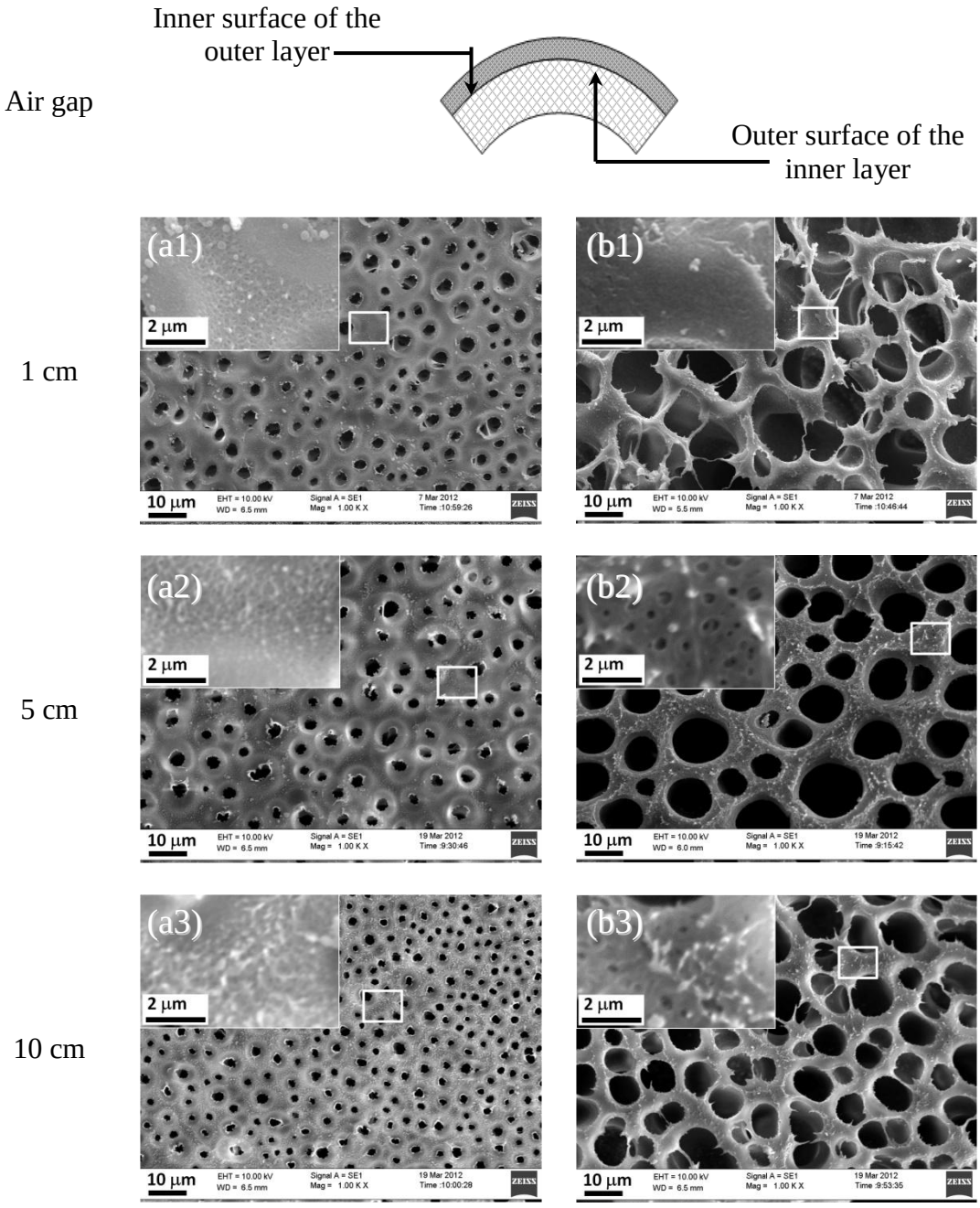

Figure 5.16. Surface morphology: (a) inner surface of the outer layer; (b) outer surface of the inner layer at the interface of DL-14-0 dual layer membranes spun at different air gaps: (1) 1 cm; (2) 5 cm; (3) 10 cm. Spinning conditions: outer dope flow rate: 1.7 g/min; inner dope flow rate: 4.6 g/min; bore fluid flow rate: 6 g/min; coagulation bath temperature: 25°C; bore fluid: water.

5.3.6. Effect of relative flow rates of polymer dopes

Figure 5.17 shows the cross-section and interface morphologies of the DL-19-Li7 membranes spun at different ratios of the outer to inner dope flow rates. The increase in outer dope flow rate results in a thicker outer layer. However, it does not help to improve the two-layer adhesion. It appears that the lamination/delamination is independent of the dope flow rates. As described previously, delamination occurs as the outer layer expands due to the large macrovoids. Increasing the dope flow rate increases the thickness of the outer layer but does not change the thermodynamic properties of the dope solution or the kinetics of phase inversion. Hence, the macrovoids are still present and thereby cause the expansion of the outer layer leading to delamination.

Figure 5.18 shows the cross-section and interface morphologies of the DL-14^{+}-Li6 membranes at different ratios of the outer to inner dope flow rates. In contrast to Figure 5.17, no delamination can be observed. As mentioned in Section 5.3.3, the 19% PAI system is more unstable than the system of 14% PAI with 3.8% LiCl. Therefore, the latter system has a slower phase separation rate. The formation of the relatively narrow finger-like structures that developed continuously from the outer to inner layer suggests a relatively small water penetration rate through the outer layer. However, increasing the outer dope flow rate promotes a non-uniform thickness of the hollow fiber membranes as the inner layer is unable to freely expand during the phase separation process due to a good adhesion of the outer and inner layers. This observation agrees with the second hypothesis.

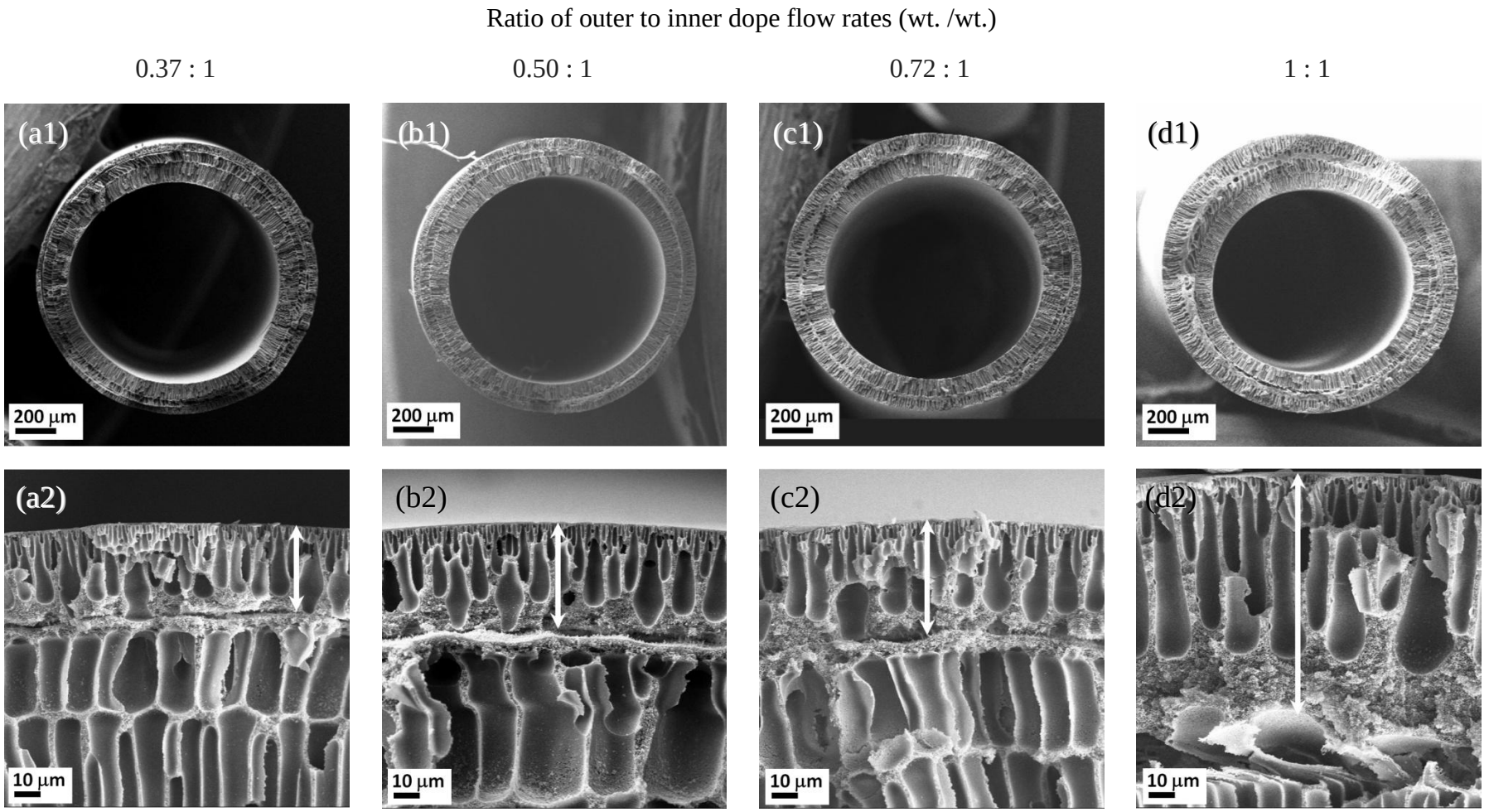

Figure 5.17. Cross-section morphology of dual layer hollow fiber membranes spun from composition of DL-19-Li7 at different ratios of outer to inner dope flow rates. Spinning conditions: bore fluid: water; bore fluid flow rate: 6 g/min; air gap: 1 cm; coagulation bath temperature: 25°C (white arrow indicates the outer layer).

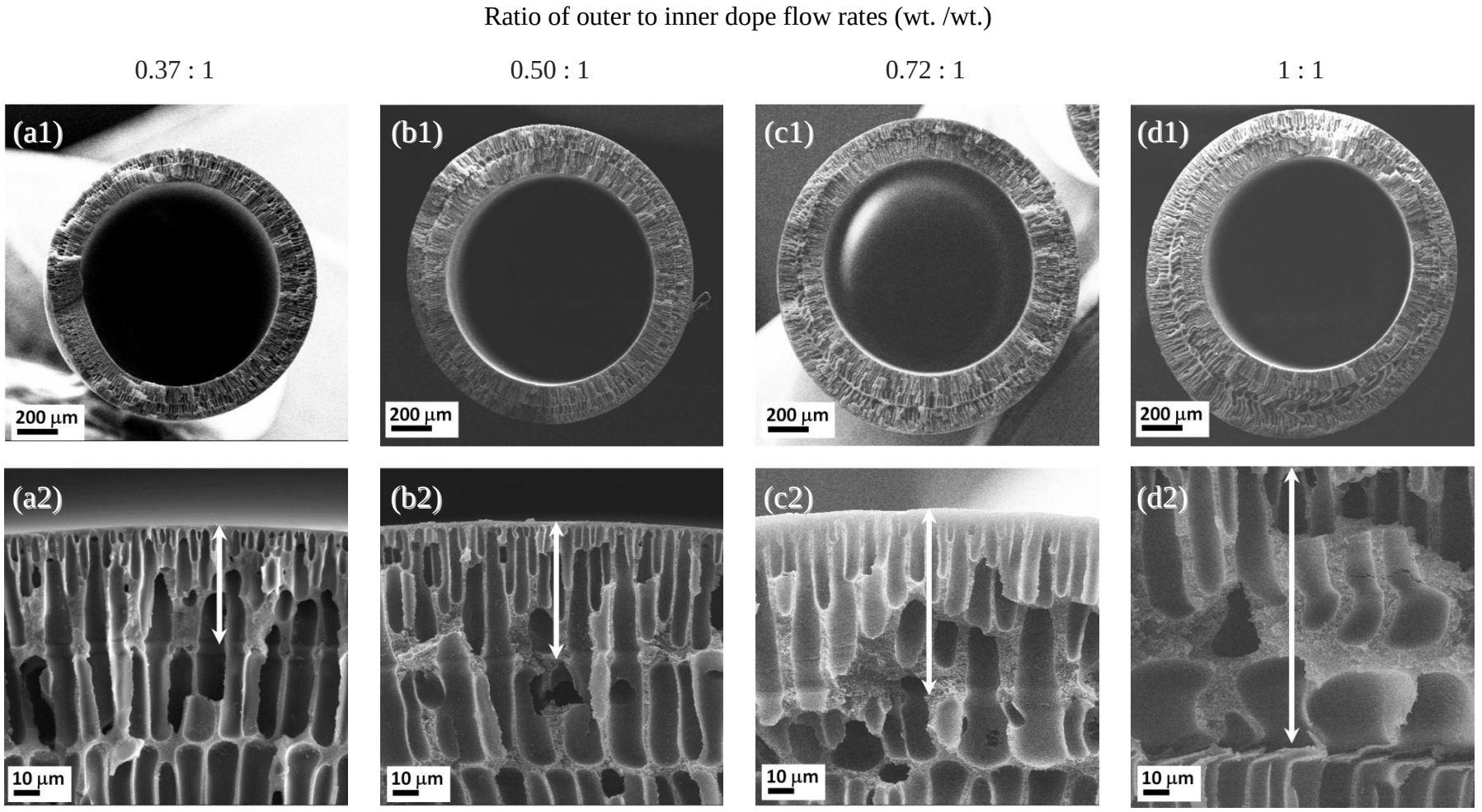

Figure 5.18. Cross-section morphology of dual layer hollow fiber membranes spun from composition of DL-14^{+}-Li6 at different ratios of outer to inner dope flow rates. Spinning conditions: bore fluid: water; bore fluid flow rate: 6 g/min; air gap: 1 cm; coagulation bath temperature: 25°C (white arrow indicates the outer layer).

5.3.7. Effect of solvent fraction in bore fluid and coagulation bath temperature

Figure 5.19 shows the cross-section morphology of the DL-18-Li6 dual layer hollow fiber membranes spun at 25 and 10°C for the external coagulation bath temperature in conjunction with different bore fluid compositions from 0% to 80% NMP in water. It can be seen that increasing the solvent concentration in the bore fluid up to 50% results in a slightly larger overall fiber diameter. This is due to delayed precipitation on the lumen side and decreased rigidity of the inner layer. Accordingly, die swell after the dope extrusion from the spinneret occurs (Shi, Wang *et al.* 2007; Widjojo, Chung *et al.* 2010). However, with a further increase to 80% NMP, the overall diameter of the fiber is reduced significantly (Figure 5.19 d1 and d2), which may be attributed to a longer delay of the precipitation at the inner surface such that the elongational stress on the fibers because of gravity results in a transverse shrinking (Khayet 2003).

In addition, it is found that the fibers spun at 25°C for the external coagulation bath temperature have a circular and regular inner contour at all bore fluid compositions (see Figure 5.19 a1-d1). Interestingly, as the external coagulation bath temperature is decreased to 10°C, the inner contour of the membranes becomes irregular when 0% to 50% NMP in water was used as the bore fluid. Decreasing the external coagulation bath temperature decreases the thermodynamic stability of the outer dope. Consequently, the precipitation at the outer layer becomes faster. Hence, the deformation of the inner contour occurs at 25 and 50% NMP concentration in the bore fluid as the inner layer is unable to freely expand due to good adhesion of the inner and outer layers, which is consistent with the second hypothesis.

The interfaces of the outer and inner layers of the DL-18-Li6 membranes shown in Figure 5.19 are enlarged and shown in Figure 5.20. It can be seen that the adhesion of the two layers was improved using a low water bath temperature and a softer bore fluid, as the finger-like structures were developed continuously from the outer layer to the inner layer. At the low external coagulation bath temperature, the water diffusion through the outer dope solution becomes slower resulting in an improvement in the attachment between the outer and inner layers. Regularity of the inner contour can be achieved when a very soft bore fluid (80% NMP in water) was used. Similar approaches to suppress inner contour deformation has been reported in literature (Duarte, Pereira *et al.* 2008).

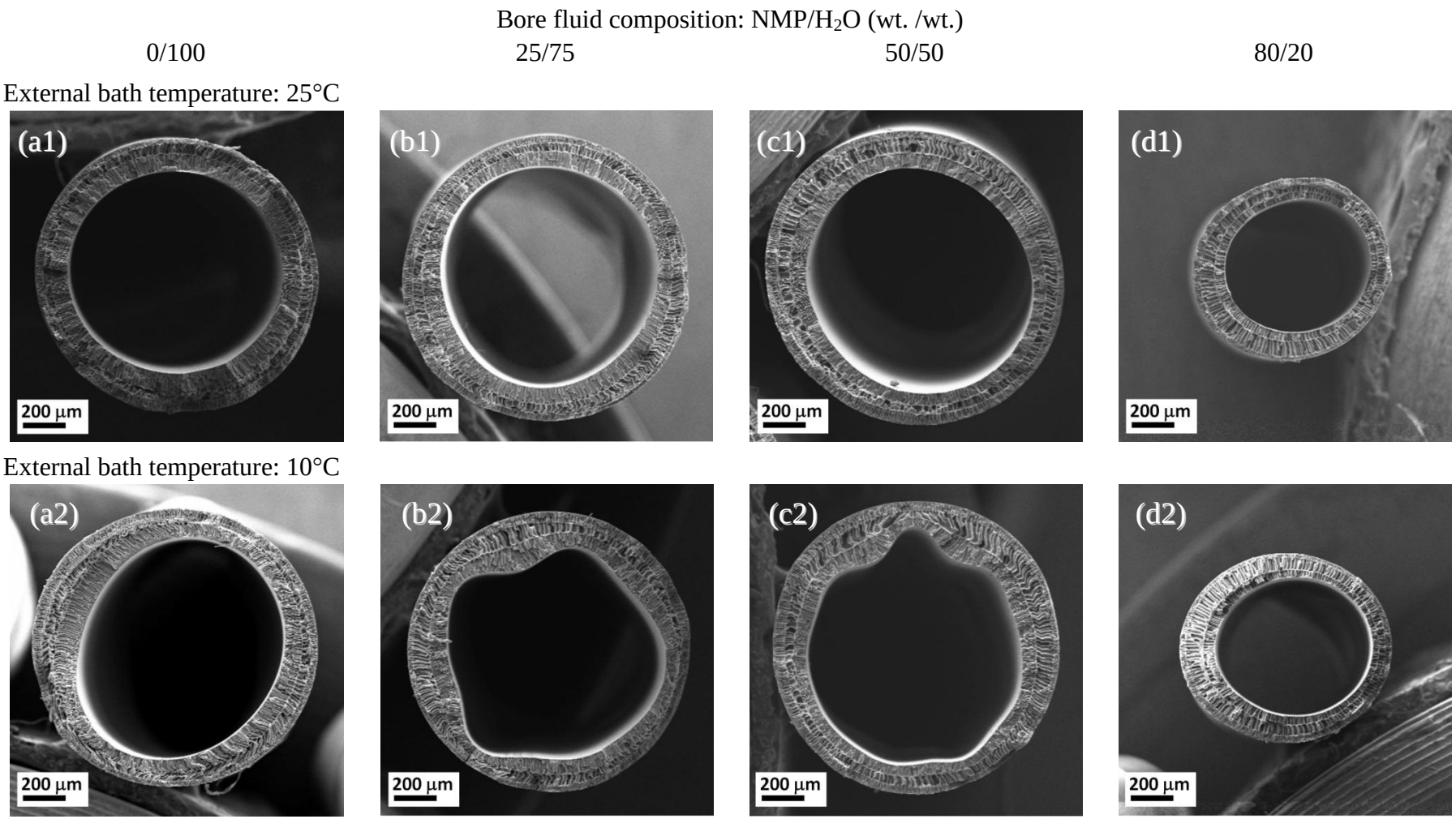

Figure 5.19. Cross-section morphology of DL-18-Li6 dual layer hollow fiber membranes spun at different coagulation bath temperatures. Spinning conditions: ratio of outer to inner dope flow rates: 0.37:1 (wt./wt.); bore fluid flow rate: 6 g/min; air gap: 1 cm; free fall take up speed.

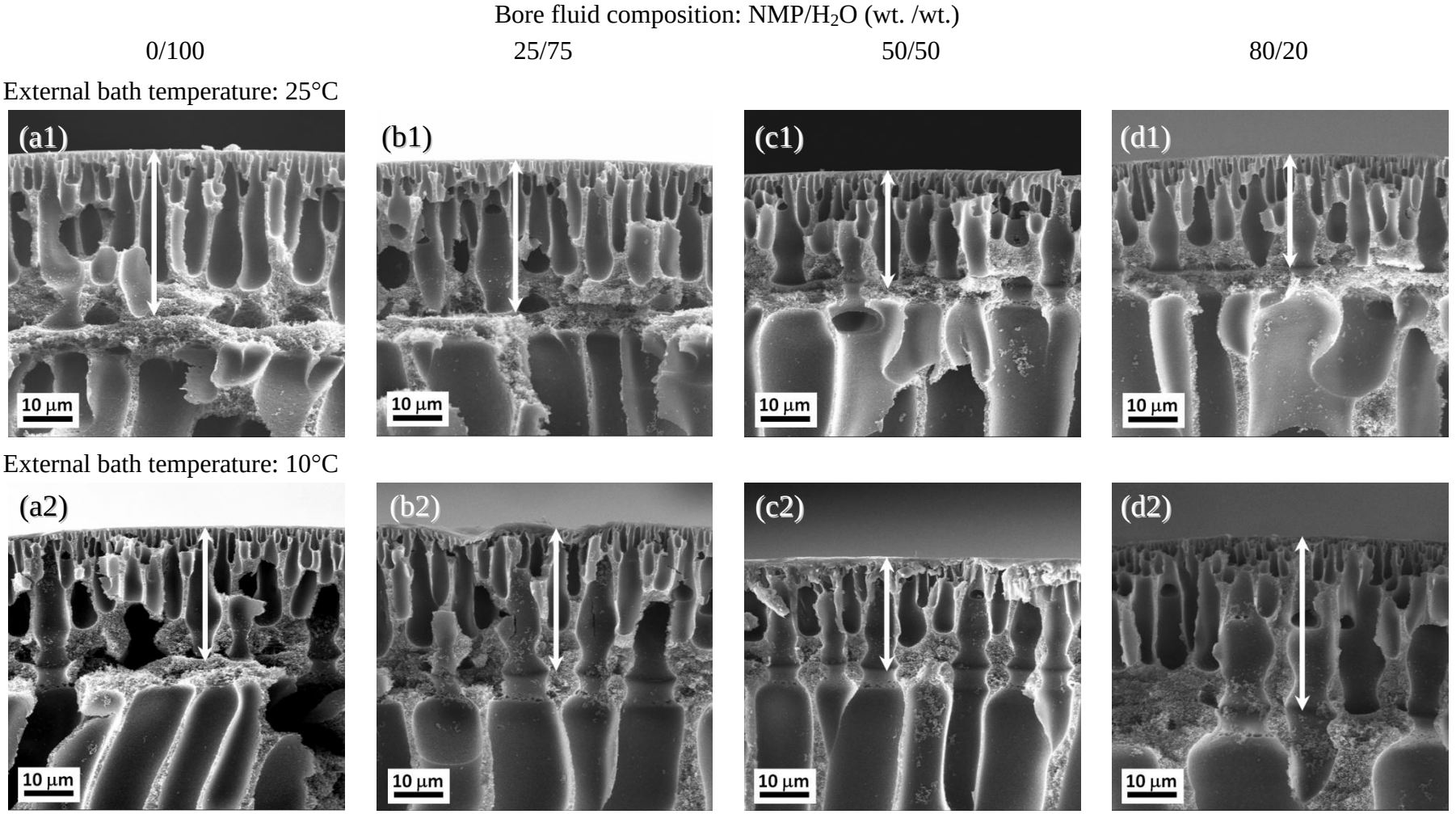

Figure 5.20. Outer and inner layer interface of DL-18-Li6 dual layer hollow fiber membranes spun at different coagulation bath temperatures. Spinning conditions: ratio of outer to inner dope flow rate: 0.37:1 (wt. /wt.); bore fluid flow rate: 6 g/min; air gap: 1 cm; free fall take up speed (white arrow indicates the outer layer).

5.4. Conclusions

A systematic study on the lamination/delamination and regular/irregular morphology of PAI-PES dual layer hollow fiber membranes has been done. The thermodynamic properties and phase separation kinetics of two polymer dope solutions as well as various spinning parameters were carefully tailored in order to investigate the evolution of the membrane morphology and structure. The morphology of the resultant dual layer fibers can vary from severe delamination to excellent adhesion between the two layers, from a distortion of finger-like structures and an irregular inner contour to an appropriate morphology of the polymer matrix.

The following conclusions can be drawn from this study:

- When the external coagulant, water, has a higher diffusion rate in the outer layer than in the inner layer, the outer layer tends to expand to form large macrovoids and to hold more water at the interface. As a result, the accumulated water impedes the adhesion of the two layers, leading to a delamination of two layers of the dual layer hollow fiber membranes.

- If water has a slower penetration rate through the outer layer dope than the inner layer dope, a good adhesion of these two layers is expected. Under this scenario, since macrovoids may form in the inner layer leading to the expansion of the inner layer, the distortion of the finger-like structures/macrovoids in the inner layer and irregularity of the inner contour may occur.

This study provides a solid foundation to develop superior dual layer hollow fiber membranes with an inter-penetrating dual layer structure.

CHAPTER 6

Novel Dual-layer Hollow Fiber Membranes Applied for FO Process

6.1. Introduction

A series of studies have been reported on the use of polymeric dual-layer hollow fiber membranes for specific applications, including gas separation (Ding, Cao *et al.* 2008; Peng, Chung *et al.* 2010), pervaporation (Wang, Goh *et al.* 2009), membrane distillation (Bonyadi and Chung 2007; Teoh, Chung *et al.* 2011), protein separation (Li and Chung 2008), nanofiltration (NF) (He, Mulder *et al.* 2002; Sun, Wang *et al.* 2010a) and forward osmosis (FO) (Yang, Wang *et al.* 2009a; b). For example, Yang *et al.* developed dual-layer hollow fiber NF membranes applied for FO process (Yang, Wang *et al.* 2009a; b). A polybenzimidazole (PBI) dope solution with a PBI concentration of 22.6 wt% was employed as the outer selective layer while polyethersulfone (PES) was used to form the inner support layer. The membranes showed a water flux of 33.8 $l/m^2.h$ using 5M $MgCl_2$ as the draw solution facing the outer active layer and de-ionized (DI) water as the feed facing the inner support layer. Considering that the draw solution concentration used was quite high, obviously, the water flux needs to be further improved. In the FO process, the low permeate flux is mainly due to internal concentration polarization (ICP) (Cath, Childress *et al.* 2006; Chou, Wang *et al.* 2012). The ICP can be mitigated by fabricating membrane with a porous substrate (Wang, Shi *et al.* 2010; Fang, Wang *et al.* 2012; Shi, Chou *et al.* 2012).

It is recognized that it is very challenging to make high performance dual-layer hollow fibers, as it involves a sophisticated spinning process in which two different phase inversion pathways occur simultaneously. The major problem in a dual-layer composite structure is the integrity and the adhesion of the two layers, which has been systematically studied in Chapter 5. A good interpenetration of outer and inner

polymer dope can be achieved to make dual layer membranes without two-layer delamination.

In Chapters 3, single-layer hollow fiber membrane with a NF-like selective layer was successfully fabricated by utilizing asymmetric microporous hollow fibers made of Torlon® polyamide-imide (PAI) material as the porous substrate followed by polyelectrolyte post-treatment using polyethyleneimine (PEI), which imparted positive charges to the membrane due to amine groups in PEI and densified the outer skin of the membrane. A further deposition of a polyelectrolyte layer was carried out in Chapter 4. However, the chemical cross-linking of entire PAI substrate resulted in a denser substrate which adversely affected the water flux. To overcome this drawback, a dual-layer hollow fiber with PAI polymer as the outer layer, supported by an inner layer made of polyethersulfone (PES) material that is inert to PEI polyelectrolyte, may be an option due to the selective cross-linking of the PAI layer.

The main purpose of Chapter 6 is to apply composite PAI-PES dual-layer hollow fiber membranes for FO application based on the studies in Chapters 3, 4 and 5. Microporous PAI-PES dual-layer hollow fibers were fabricated by one-step co-extrusion, followed by PEI polyelectrolyte post-treatment, resulting in a positively charged NF-like thin selective layer supported by a porous PES inner layer. The resultant membranes, subsequently, were further treated by multilayer polyelectrolyte deposition to tighten the selective layer. To the best of our knowledge, the cross-linking modification on microporous dual-layer hollow fiber membranes has not been explored previously as an alternative strategy to fabricate NF membranes applied for FO application.

6.2. Experimental

6.2.1. Materials

A series of different molecular weight (Mw) polyethylenimine (PEI; (1) ethylenediamine branched ~800, Aldrich; (2) ~2,000, 50 wt. % in H_2O, Aldrich; (3) branched ~25,000, Aldrich; (4) branched 50,000-100,000, Polysciences; (5) ~750,000, 50 wt.% in H_2O, Aldrich) were used to cross-link PAI-PES UF hollow fiber substrates.

Poly(styrenesulfonate) (PSS, Mw 70,000, Sigma Aldrich) and poly(allylamine hydrochloride) (PAH, Mw 120,000, Sigma Aldrich) were used in multilayer polyelectrolyte deposition. A series of different molecular weight polyethylene glycol (PEG, Mw 400; 600; 1,000; 2,000, Merck) were used to determine the pore size and pore size distribution of PEI cross-linked dual layer hollow fiber membranes. All the reagents were used as received. Other materials have been described in Chapter 3 Section 3.2.1 and Chapter 4 Section 4.2.1.

6.2.2. Fabrication of UF PAI-PES dual layer hollow fiber substrates

Dual layer PAI-PES UF hollow fiber substrates were fabricated based on method described in Chapter 5. The spinning conditions for each fiber are summarized in Table 6.1.

Table 6.1. Spinning conditions and parameters.

Parameters	DL-A	DL-B	DL-C
Outer dope, wt.%	PAI/LiCl/NMP 14/3.8/82.2		
Inner dope, wt.%	PES/PEG400/NMP 16/10/74		PES/LiCl/NMP 16/6/78
Bore fluid	DI water	DI water	DI water
Outer dope flow rate, g/min	1.7	1.7	2.0
Inner dope flow rate, g/min	5.3	5.3	5.3
Bore fluid flow rate, g/min	8	8	8
Air gap, cm	5	5	5
Take up speed	Free fall	Free fall	Free fall
External coagulant	Tap water	Tap water	Tap water
External coagulant bath temperature, °C	25	40	25

6.2.3. Modification of PAI-PES dual layer hollow fiber substrates

The cross-linking reaction between PAI-PEI dual layer hollow fiber substrates and PEI was conducted by immersing the substrates into a 500 ml of 1% (wt/wt) PEI aqueous solution at temperature of 70 °C for 75 min. The details of the procedures have been explained in Chapter 4 Section 4.2.3. The deposition of multilayer polyelectrolytes was done on the outer surface of the cross-linked PAI-PES dual layer hollow fiber membranes. Prior to the deposition, four of the cross-linked fibers were put together for each module. The polyelectrolyte solutions were prepared by dissolving 1 g polyelectrolyte (PSS/PAH) into 1 liter 0.5 M NaCl solution. The orientation of multilayer polyelectrolyte was PSS-PAH-PSS-glutaraldehyde. Multilayer polyelectrolyte deposition was carried out at ambient temperature of 20 °C by circulating the polyelectrolyte solution in the shell side of a hollow fiber module at a flow rate of 450 ml/min for 10 min each. The module was, subsequently, rinsed thoroughly by de-ionized water for approximately 1 min prior to the next deposition. At the end of deposition, a glutaraldehyde solution (1 wt%) was circulated through the membrane module as described in Chapter 4 Section 4.2.3. The membranes codes after modification are listed in Table 6.2.

Table 6.2. Modification condition and membrane code after modification.

Membrane code	PEI cross-linking*	Code after MLPE deposition
DL-C-800	1% PEI 800	DL-C-800-d
DL-C-2000	1% PEI 2,000	DL-C-2000-d
DL-C-25K	1% PEI 25,000	DL-C-25K-d
DL-C-50K	1% PEI 50,000	DL-C-50K-d
DL-C-750K	1% PEI 750,000	DL-C-750K-d

6.2.4. Characterization and analysis

- *Membrane morphology observation and surface chemistry analysis*

Membrane morphology observation by SEM and membrane dimension measurement by digital microscope has been described in Chapter 3 Section 3.2.4.

The cross-linking reaction between PAI and PEI was confirmed by fourier transform infrared spectroscopy using the attenuated total reflection (FTIR-ATR) with ZnSe crystal. PES was chosen as the inner layer material because it has no reaction with PEI during the cross-linking reaction. The confirmation of intact PES was analyzed by FTIR-ATR. The characterization was performed on PES flat sheet membrane prepared with the same dope concentration and modification condition as used for dual layer hollow fiber. The details procedures can be found in Chapter 4 Section 4.2.4.

- *Surface charge before and after modification*

The original and modified membrane surface charge (zeta potential) was observed based on the streaming potential measurement by using a SurPASS electrokinetic analyzer (AntonPaarGmbH, Austria) on the PAI flat sheet membranes. The zeta potential was measured at pH of 5-6 which is the pH of the feed and draw solution. The details procedures can be found in Chapter 4 Section 4.2.4.

- *Pure water permeability (PWP), salt rejection measurement, pore size* and pore size distribution

PWP experiments were performed before and after modification by using a bench-scale hollow fiber cross-flow filtration unit. Pore size and pore size distribution of hollow fiber substrates were measured by filtering a 2000 ppm dextran aqueous solution followed by GPC analysis. Salt rejection experiments were performed after PEI cross-linking as well as after polyelectrolyte deposition.

The determination of pore size and pore size distribution of the PEI-cross-linked membranes was carried out by filtering a 200 ppm PEG aqueous solution as the feed. Each molecular weight of PEG solutions was circulated for 30 min prior to collect the permeate. The total organic carbon (TOC) of feed and permeate was analyzed by a

TOC Analyzer (Shimadzu, Model: TOC-V CSH) which is equipped with a non-disperse infrared detector.

- *Performance in FO process*

Details of experiments have been described in Chapter 4 Section 4.2.4.

6.3. Results and discussion

6.3.1. Effects of coagulation bath temperature

Coagulation bath temperature has an effect on the structure and morphology of the resultant hollow fiber membranes. Thus, the membrane structure can be tailored simply by varying the system temperature (Cheng 1999). Figure 6.1 a and b shows the morphologies of DL-A and DL-B dual layer hollow fiber membranes spun at 25°C and 40°C coagulation bath temperatures. A significant change of the cross-section morphology has been observed when the coagulation bath temperature increased from 25 to 40°C. The twisted finger-like macrovoids formed at 25°C (Figure 6.1-a2) disappeared and became straight at 40°C (Figure 6.1-b2). As discussed in Chapter 5, at a higher air gap, the phase inversion in the inner (lumen) side occurs much earlier and faster than in the outer layer. Therefore, due to the perfect adhesion of outer and inner layers at the interface, the inner layer is unable to expand resulting in twisted finger-like macrovoids. The increase in coagulation bath temperature enhanced the thermodynamic stability of the outer dope solutions, leading to a slower demixing on the outer skin (Wongchitphimon, Wang *et al.* 2011). As a result, the pore size of the outer surface of DL-B is larger than that of DL-A which was spun at 25°C. However, the non-solvent diffusion through the outer layer to the inner layer seems faster which tends to freeze the structure at a low air gap and 25°C external coagulation bath temperature (see Figure 6.2).

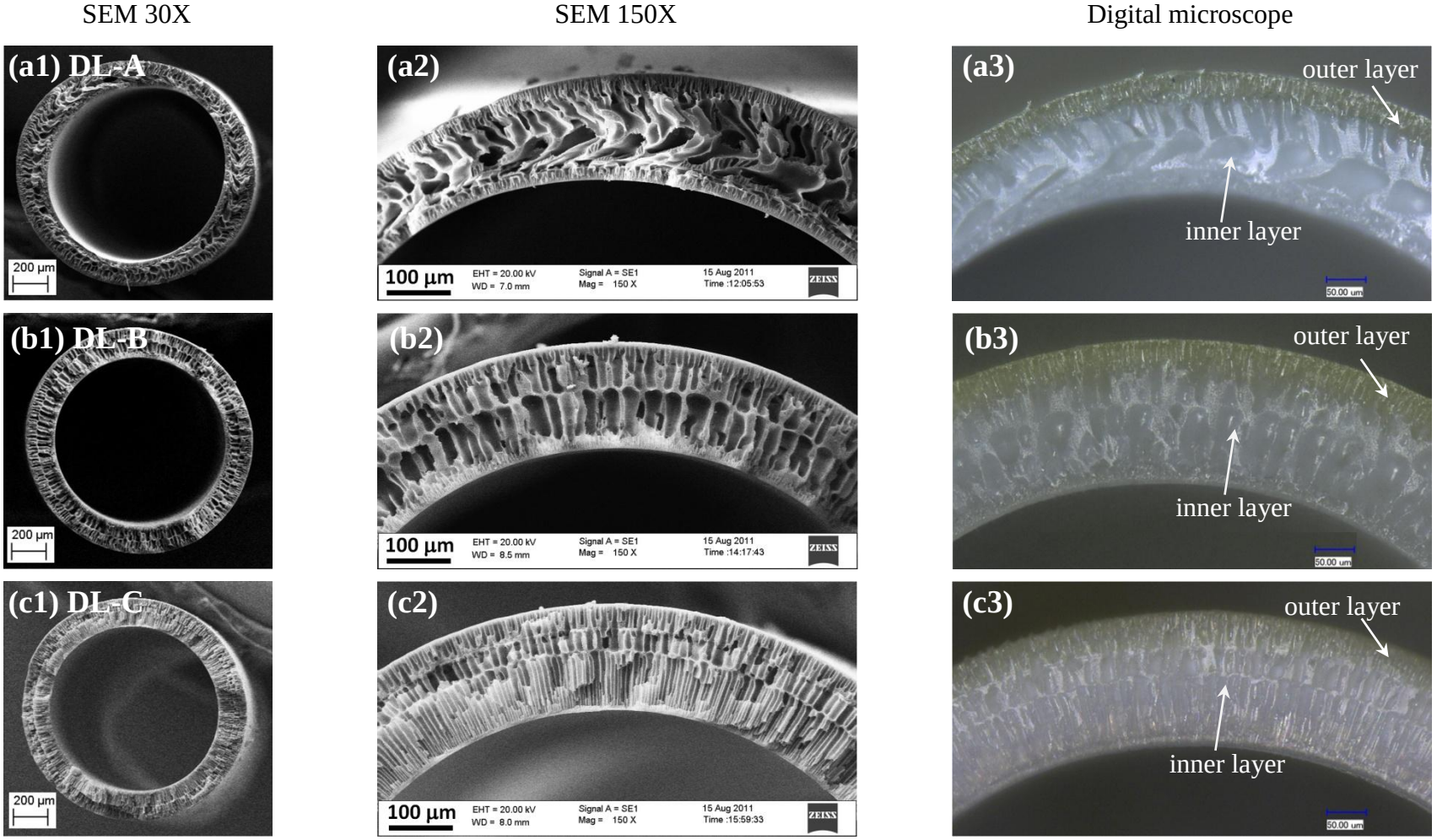

Figure 6.1.Cross-section morphology of dual layer hollow fiber membranes.

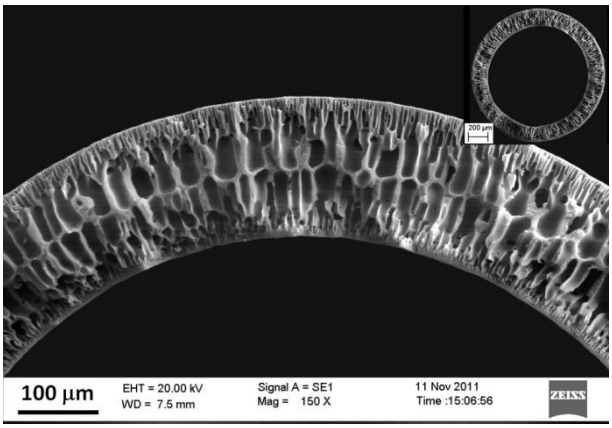

Figure 6.2. Cross-section morphology of dual layer hollow fiber membrane spun from outer and inner dope composition of PAI/LiCl/NMP 14/3.8/82.2 and PES/PEG400/NMP 16/10/74 at 1 cm air gap and external coagulation bath temperature of 25°C.

6.3.2. Effect of non-solvent additive on the morphology of the dual layer hollow fiber membranes

In order to examine the effect of additive on the inner layer macrovoids, two types of additives, PEG400 (Figure 6.1-a2) and LiCl (Figure 6.1-c2), were added into the PES solution as the inner dope individually. The fibers were spun with the same outer layer composition of PAI/LiCl/NMP 14/3.8/82.2. As shown in Figure 6.1-a2, using 10% PEG as an additive, the resultant dual layer hollow fibers exhibited large and twisted macrovoids in the inner layer. In contrast, when a small molecular additive, LiCl, was used, the large macrovoids in the inner layer was suppressed, as shown in Figure 6.1-c2 for 6% LiCl. These observations were believed to be associated with the change in the thermodynamic properties and phase inversion kinetics of the PES systems (Shi, Wang *et al.* 2008; Ahmed, Idris *et al.* 2010). PES systems with 10% PEG 400 as the additive have the total solubility parameter difference ($\Delta\delta t$) of 0.98 $(MPa)^{1/2}$. Total solubility parameter difference of PES/LiCl/NMP 16/6/78 is shown in Table 5.3. The addition of 6% LiCl significantly increases $\Delta\delta t$ to 11.9 $(MPa)^{1/2}$ which enhances the thermodynamic instability. However, the addition of 6% LiCl increased the viscosity of PES solution significantly to 6.9 Pa.s as listed in Table 5.3 due to the strong interaction of the additive with the solvent. The viscosity of PES system with 10% PEG400 is 0.8 Pa.s. A high viscosity of spinning dope slows down the non-solvent

diffusion into the polymer solution leading to a delayed demixing, and thus, suppresses the formation of big macrovoids (Shi, Wang *et al.* 2008).

6.3.3. Substrate characteristics: pure water permeability (PWP), MWCO, and pore size distribution

The dimension, PWP and MWCO of hollow fiber membranes prepared with different conditions are presented in Table 6.3. It can be seen that all fibers possessed quite large dimensions (OD/ID 1.40/1.05 mm/mm). A large fiber lumen is favorable for the fluid flow with less resistance. As the temperature of the coagulation bath increased from 25 to 40°C, the PWP and the outer skin MWCO also increased for fibers spun at the same air gap due to the increasing of the thermodynamic stability of the system. The pore size and pore size distribution of the three fibers are presented in Figure 6.3. Fiber DL-C spun with composition of PAI/LiCl/NMP 14/3.8/82.2 as the outer layer and PES/LiCl/NMP 16/6/78 as the inner layer has the narrowest pore size distribution. Therefore, the DL-C substrate was chosen for chemical cross-linking with PEI followed by multilayer polyelectrolyte deposition.

Table 6.3. Dimension, PWP and MWCO of dual-layer hollow fiber substrates spun at different conditions.

Substrate code	Outside diameter, mm	Inside diameter, mm	PWP, $l/m^2.h.bar$	Outer skin MWCO, KDa
DL-A	1.43	1.07	135 ± 3	16
DL-B	1.43	1.05	189 ± 27	43
DL-C	1.39	1.03	149 ± 16	31

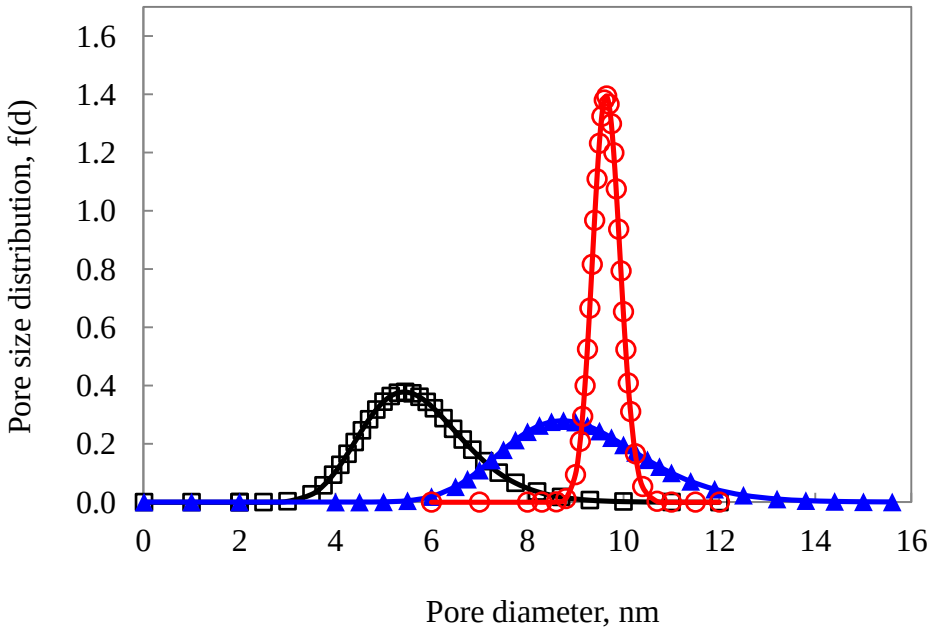

Figure 6.3. Pore size distributions (f(d)) of PAI-PES dual layer hollow fiber membranes ((□) DL-A; (▲) DL-B; (○) DL-C).

6.3.4. Surface morphology of the modified membranes

The PEI cross-linking reaction was taken place on the outer layer of the dual layer substrate. The details of the cross-linking reaction and charge characteristic can be found in Chapter 3. The surface morphology of the original and modified membranes by PEI 50 is shown in Figure 6.4. There is no obvious change in the morphology of the outer surface before and after PEI cross-linking using different molecular weights of PEI. However, the outer surface becomes rougher after multilayer polyelectrolyte deposition. Single layer PAI hollow fiber membranes also show similar results which have been discussed in Chapter 4. There is no significant change on the inner surface of the entire modified dual layer hollow fiber membranes. This suggests that the multilayer polyelectrolyte deposition only took place on the outer surface of the membranes.

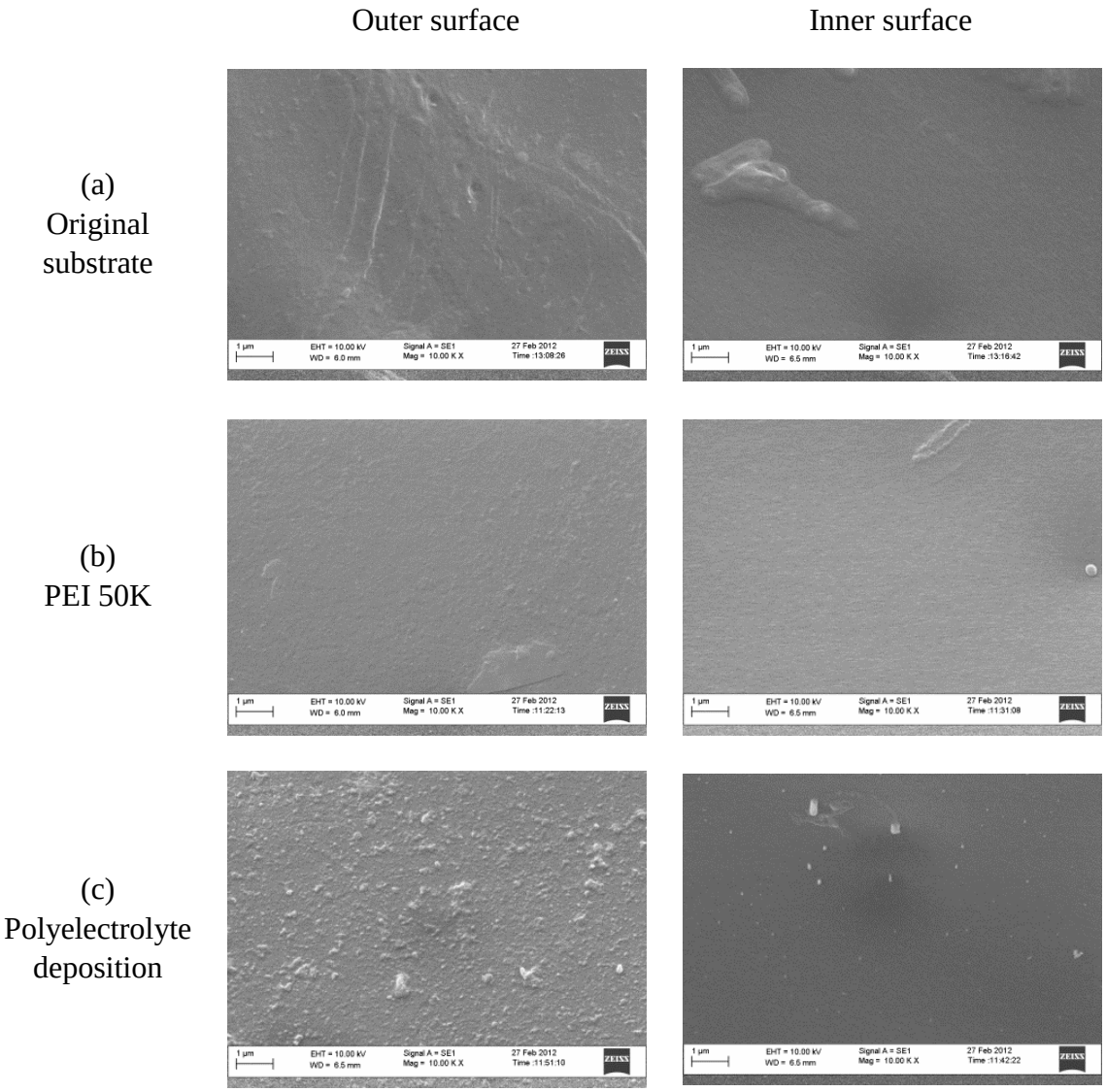

Figure 6.4. Surface morphology of DL-C dual layer: (a) original; (b) modified with PEI 50K; (c) multilayer polyelectrolyte deposition.

6.3.5. Characterization of modified membranes

- *PWP and salt rejection of cross-linked membranes*

Before PEI cross-linking, the original substrate of DL-C had the PWP of 149 l/m^2.h.bar as shown in Table 6.3. PWP and $MgCl_2$ rejection of the cross-linked membranes measured in a RO cross-flow filtration setup are tabulated in Table 6.4. As the molecular weight of PEI cross-linker increased, the PWP decreased from 22.6 l/m^2.h.bar when PEI with molecular weight of 800 was used to 11.7 l/m^2.h.bar when PEI with molecular weight of 750,000 was used. On the other hand, the salt rejection

to $MgCl_2$ increased from 58% to 89% due to a larger coverage of the surface pores by the PEI. Since the DL-C-800 membrane has the lowest $MgCl_2$ rejection, it has not been further modified by the multilayer polyelectrolyte deposition.

Table 6.4. PWP and salt rejection of PEI cross-linked membranes.

Membrane code	PWP, $l/m^2.h.bar$	Rej. $MgCl_2$, %
DL-C-800	22.6 ± 0.1	58 ± 3
DL-C-2000	19.9 ± 2.7	75 ± 6
DL-C-25K	12.4 ± 0.6	79 ± 12
DL-C-50K	15.4 ± 1.2	89 ± 3
DL-C-750K	11.7 ± 0.2	78 ± 8

- *Pore size and pore size distribution*

The pore size and pore size distribution of the PEI cross-linked membranes were determined based on the membrane rejection to PEG molecules. Figure 6.5 shows the relationship between the solute rejection and the stoke radius of the solute, whereas Figure 6.6 shows the pore size distribution of the outer surface after PEI cross-linking. The mean effective pore diameter is summarized in Table 6.5. It can be seen that DL-C-2000 has the largest effective pore diameter of 3.08 nm. The results of the membrane pore size correspond to the PWP results as shown in Table 6.4 where membrane with a higher mean effective pore diameter, D*, has a higher PWP.

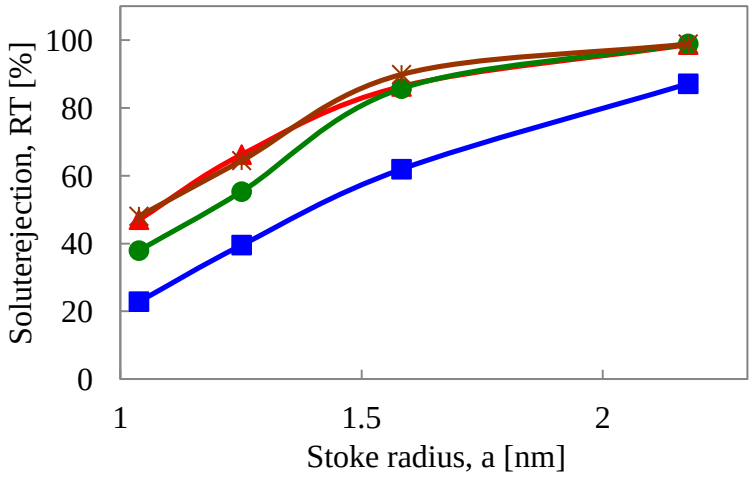

Figure 6.5. Effect of different molecular weight PEI as cross-linker on the rejection of neutral PEG solute (■ DL-C-2000; ▲ DL-C-25K; ● DL-C-50K; ✳ DL-C-750K).

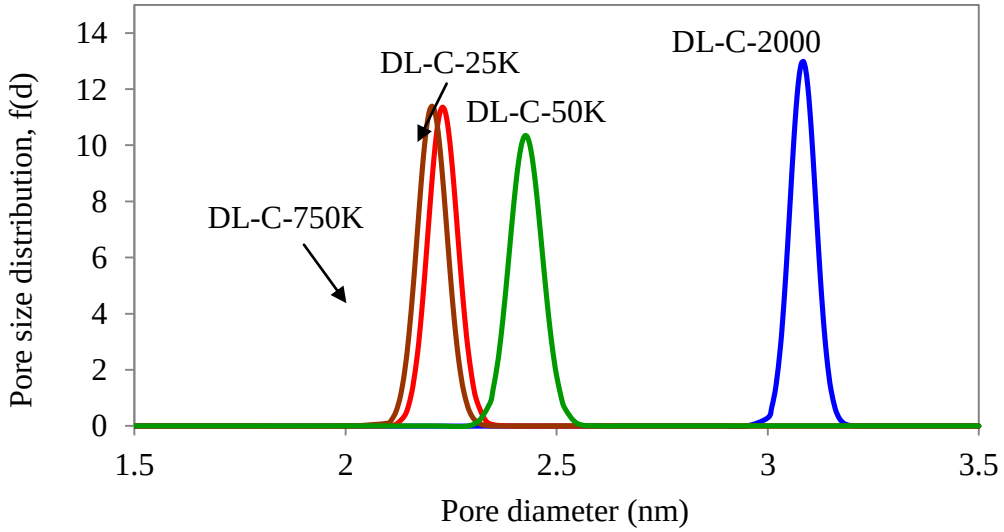

Figure 6.6. Plot of pore size and pore size distribution.

Table 6.5. Mean effective pore diameter (D^*) and geometric standard deviation (σ_p).

Membrane code	D^* (nm)	σ_p (nm)
DL-C-2000	3.08	1.01
DL-C-25K	2.23	1.02
DL-C-50K	2.43	1.02
DL-C-750K	2.21	1.02

- *Surface chemistry by FTIR*

The chemical reaction between the PAI and PEI was verified by FTIR-ATR measurements as discussed in Chapter 3. The FTIR spectra of the original substrate and the cross-linked membranes with different molecular weights of PEI are shown in Figure 6.7. It can be seen that after the cross-linking reaction with low-molecular-weight PEI (2000 and 25K), the imide peaks completely disappeared. However, when the PEI with high molecular weights (50K and 750K) was used, the imide peaks (1720 cm^{-1}) can still be observed which means that the substrate was partially cross-linked. This could be due to the fact that lower-molecular-weight PEI (1800 and 25K) can easily penetrate into the surface pores and cross-link the entire surface since they are smaller than the MWCO of the substrate as illustrated in Figure 6.8. The PES as the

inner layer remains intact as shown in Figure 6.9. There is no change in FTIR spectra before and after PEI cross-linking for PES.

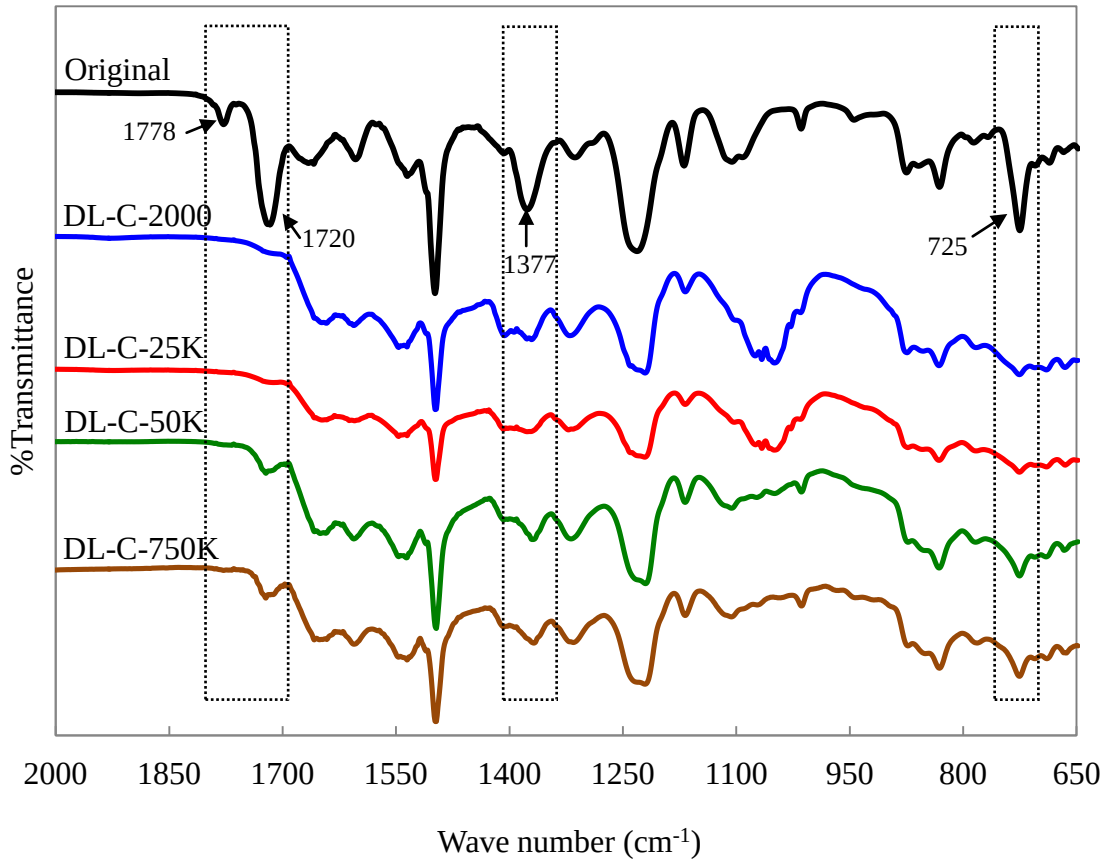

Figure 6.7. FTIR spectra of original substrate and PEI cross-linked membranes.

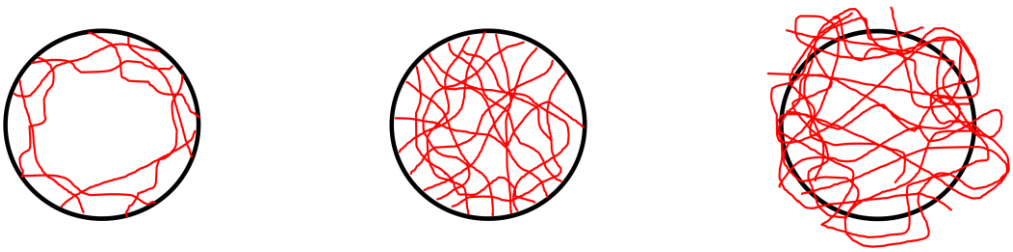

Figure 6.8. Illustration of PEI cross-linking on the surface pore with different molecular weights: (a) ~800 or ~2,000; (b) ~25K; (c) ~50K or ~750K.

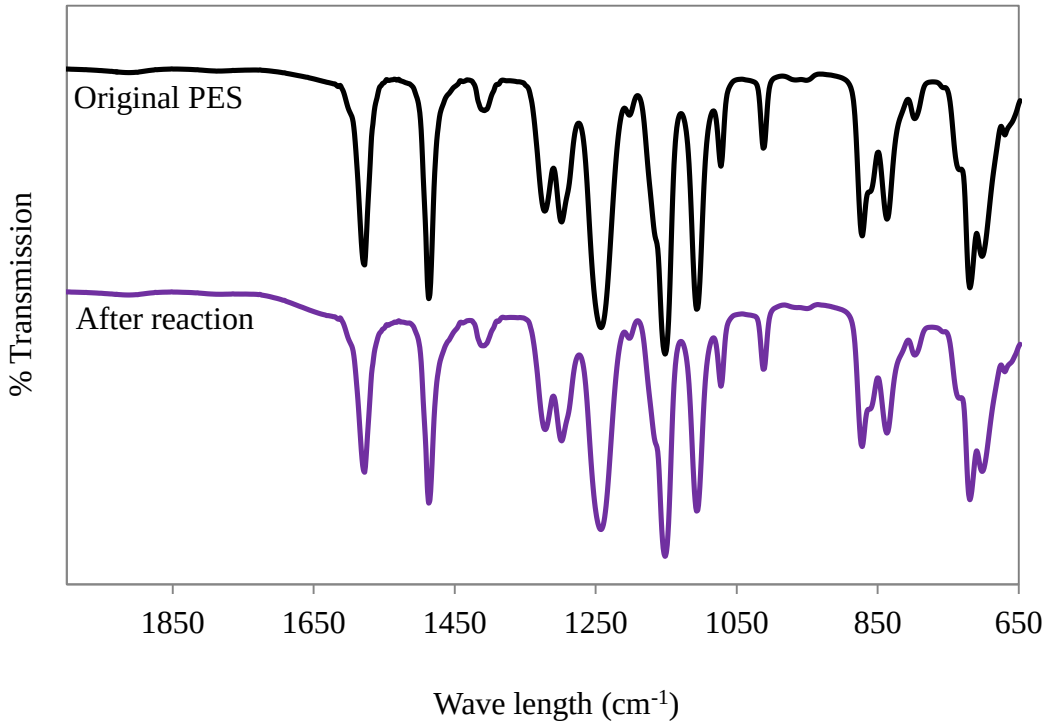

Figure 6.9. FTIR spectra of PES before (continuous line) and after PEI cross-linking.

Multilayer polyelectrolyte depositions were performed on the outer surface of positively charged PEI cross-linked membranes with the following sequences: PSS-PAH-PSS-glutaraldehyde. It is difficult to determine PAH spectra since it overlaps with PAI spectra. Therefore, polyelectrolyte depositions are confirmed by analyzing the characteristic peaks of sulfonate group from PSS. As shown in Figure 6.10, no obvious difference among the modified membranes after multilayer polyelectrolyte deposition. The sulfonate peak can be observed at wave length of 1028 and 1037 cm^{-1} throughout all the different PEI molecular weights. A clearer observation of the two characteristic peaks is shown in Figure 6.11.

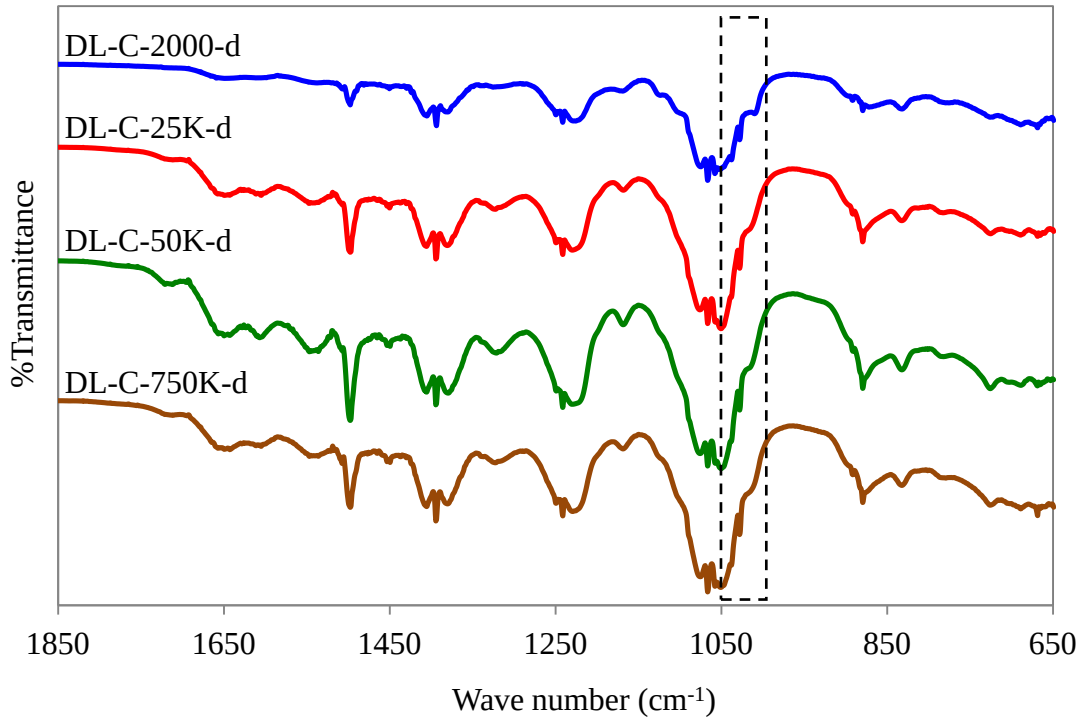

Figure 6.10. FTIR-ATR spectra of the cross-linked DL-C dual layer hollow fiber membranes modified by PEI cross-linking and multilayer polyelectrolyte deposition.

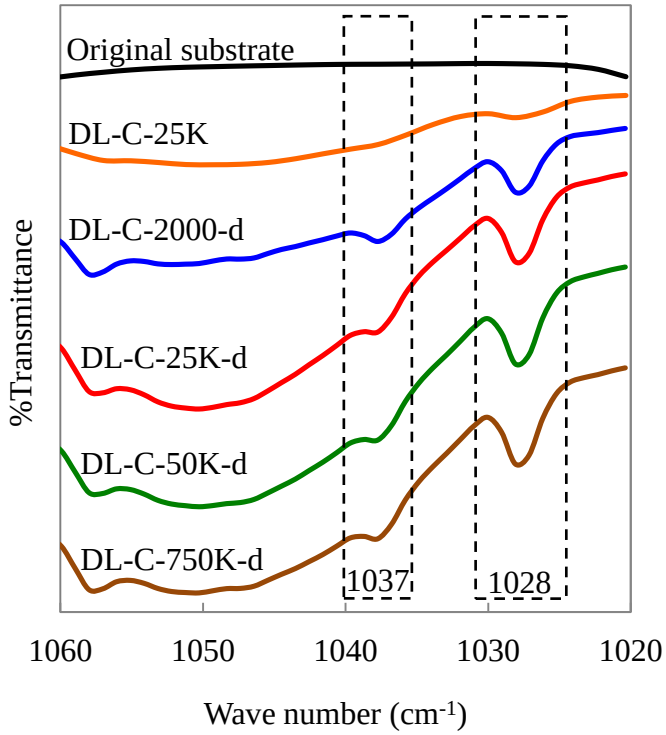

Figure 6.11. Characteristic peaks of sulfonate group at 1028 and 1037 cm-1 after multilayer polyelectrolyte deposition in comparison with original substrate and PEI cross-linking only.

- *Zeta potential*

The charge characteristics of modified membranes were determined in terms of zeta potential as shown in Table 6.6. As described in Chapter 3, the PAI substrate has negative charges at pH of 5-6. The chemical reaction between the PAI and PEI resulted in a positively charged membrane due to amine groups which bonded on the membrane outer surface as discussed earlier in Chapter 3. The effect of PEI molecular weight on the zeta potential of the cross-linked membranes before and after polyelectrolyte deposition can be seen clearly from Table 6.6. As the PEI molecular weight increases, the zeta potential of the cross-linked membranes increases since there are more amine groups attached on the surface. The positively charged surface of the PEI cross-linked membranes is desired to promote electrostatic interaction with PSS as polyanion as described previously in Chapter 4. Three layers of polyelectrolytes were deposited on the outer surface of the cross-linked membranes in the sequence of PSS-PAH-PSS. A decrease in the zeta potential is expected since the last layer was PSS polyanion.

Table 6.6. Zeta potential of various PEI cross-linked membranes before and after multilayer polyelectrolyte deposition (MLPE).

Membrane code	PEI cross-linked Zeta potential (mV)	MLPE Zeta potential (mV)
DL-C-2000	35.3	9.3
DL-C-25K	37.1	25.3
DL-C-50K	39.2	18.8
DL-C-750K	42.6	26.1

- *Contact angle*

Contact angle measurement shows the degree of hydrophilicity on the outer surface of the dual layer membranes. The effect of PEI cross-linking and multilayer polyelectrolyte deposition on the surface hydrophilicity is tabulated in Table 6.7. The original dual layer substrate has a contact angle of 71° on the outer surface. There is a slight decrease in the contact angle after PEI cross-linking as shown in Table 6.7 due to the contribution of amine groups from PEI. A further decrease in contact angle can

be observed after the depositions of multilayer polyelectrolytes. The sulfonate group in the PSS is believed to have a contribution to the increase in hydrophilicity.

Table 6.7. Contact angle of various PEI cross-linked membranes before and after multilayer polyelectrolyte deposition (MLPE).

Membrane code	Cross-linked Contact angle (°)	MLPE Contact angle (°)
DL-C-2000	66.2 ± 0.1	44.5 ± 4.3
DL-C-25K	61.8 ± 1.2	34.8 ± 1.2
DL-C-50K	70.0 ± 1.8	38.5 ± 0.4
DL-C-750K	69.9 ± 0.7	55.8 ± 0.9

* Substrate contact angle is 71.1±0.7°

6.3.6. Intrinsic properties of dual layer FO hollow fiber membranes

The modification of the substrate increases the thickness of the membrane selective layer which in turn increases the membrane resistance resulting in a decrease in the water permeability across the membrane. Table 6.8 shows the pure water permeability (PWP) and salt rejection of the polyelectrolyte membranes. After the deposition of multilayer polyelectrolytes, the PWP of all the membranes decreases to around 4 l/m^2.h.bar. The polyelectrolyte layers could have been very dense and thus significantly reduce the effective pore diameter. PWP is relatively constant for all polyelectrolyte membranes.

Table 6.8. Intrinsic properties of dual layer FO hollow fiber membranes after deposition of polyelectrolytes.

Membrane code	PWP, l/m^2.h.bar	Rej. $MgCl_2$, %
DL-C-2000-d	3.8 ± 0.4	92 ± 1.6
DL-C-25K-d	4.1 ± 0.3	97 ± 1.0
DL-C-50K-d	4.0 ± 0.3	96 ± 1.2
DL-C-750K-d	3.5 ± 0.4	97 ± 1.5

The deposition of multilayer polyelectrolytes on the outer layer of the PEI cross-linked membranes has increased the salt rejection to above 90%, though, the positive charges of the active layer after polyelectrolyte depositions decreased as shown in Table 6.6. This is because multilayer polyelectrolyte depositions form a dense network structure (Jin, Toutianoush *et al.* 2003). However, it can be seen that the salt rejection of the DL-C-2000-d is slightly lower than the other membranes. This could be due to the fact that the DL-C-2000-d membrane has the biggest effective pore size as compared to the rest of the membranes (Figure 6.6).

6.3.7. FO performance

The FO performances of dual layer membranes before and after polyelectrolyte deposition are shown in Table 6.9. It was found that the dual layer hollow fiber membranes modified by PEI cross-linking have a better performance in the AL-FW orientation than in the AL-DS orientation, similar to the results reported in Chapter 4. The J_s/J_v in the AL-FW for all membranes is much smaller compared with their counterparts in the AL-DS orientation. This might be due to the shielding effect occurred at the interface between the high concentration draw solution and the positively charged active layer in the AL-DS orientation by the counter ions (Peeters, Boom *et al.* 1998) as illustrated in Figure 6.12a and consequently, the active layer of the membrane was unable to reject the co-ions. However, in the AL-FW orientation (Figure 6.12b), the salt concentration at the interfaces between the outer layer and the inner support layer was lower than the bulk concentration of the draw solution due to water dilution. Therefore, the shielding effect may not be severe and the co-ions can be repelled by the positively charged outer layer of the membrane. In addition, the facilitated transport in the AL-DS orientation (salt flux and salt repulsion are in the same direction) and retarded transport in the AL-FW orientation (salt flux and salt repulsion are in the opposite direction) also played roles. Furthermore, the water flux in the orientation of AL-FW is higher than that in AL-DS as shown in Table 6.9. Normally, AL-FW is known to show lower flux due to more severe dilutive ICP. The lower than expected water flux in AL-DS might be due to the high salt flux. As a consequence, the salt concentration at the interface of selective layer and porous support increase leading to the decrease in the effective osmotic pressure difference as

the driving force. In addition, as compared to the wall thickness of single layer PAI hollow fiber membrane which is around 140 μm (refer to Chapter 3), the thickness of PAI layer in dual layer membrane is only 40 μm. Therefore, the amount of positive charge carried by the dual layer membrane is less than that in the single layer membrane.

Table 6.9. Performance of dual layer FO hollow fiber membranes applied in FO process*.

Membrane code	AL-DS		AL-FW	
	J_v (l/m^2.h)	J_s/J_v (g/l)	J_v (l/m^2.h)	J_s/J_v (g/l)
DL-C-2000	12.8	18.8	28.7	1.08
DL-C-25K	17.3	10.1	31.4	0.45
DL-C-50K	10.9	16.1	26.1	1.50
DL-C-750K	18.8	6.48	26.8	0.67
DL-C-2000-d	32.6	1.17	18.7	1.61
DL-C-25K-d	39.3	0.35	20.8	0.31
DL-C-50K-d	41.2	0.37	19.0	0.66
DL-C-750K-d	37.6	0.41	19.8	0.29

* Draw solution: 0.5M $MgCl_2$ and feed water: DI water

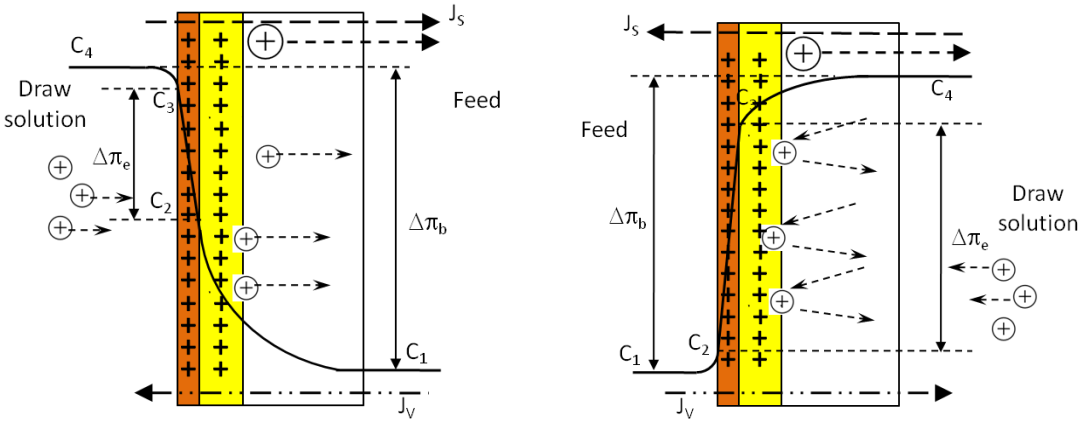

Figure 6.12. Illustration of effective osmotic pressure difference in a PEI cross-linked dual layer membrane (■ selective layer; ■ cross-linked PAI layer; □ PES layer) in the orientation of (a) AL-DS; (b) AL-FW.

The deposition of multilayer polyelectrolyte forms a dense layer over the PEI cross-linked membrane resulting in a tremendous increase of salt rejection and water flux as shown in Table 6.9. In this case, the salt rejection mechanism depends on both size exclusion and membrane charge. Since there are more ions retained by the selective layer in the orientation of AL-DS, the salt concentration at the interface of selective layer and porous support layer, C_2 (Figure 6.13-a) is lower as compared to the previous membranes (Figure 6.12-a). Therefore, the effective osmotic pressure difference across the membrane as the driving force is higher resulting in a higher FO water flux. In contrast, the FO water flux in the orientation of AL-FW is lower than that in the orientation of AL-DS. It is also lower than the FO water flux of PEI cross-linked membranes before multilayer deposition in the same orientation. This is due to the more severe internal concentration polarization in the orientation of AL-FW.

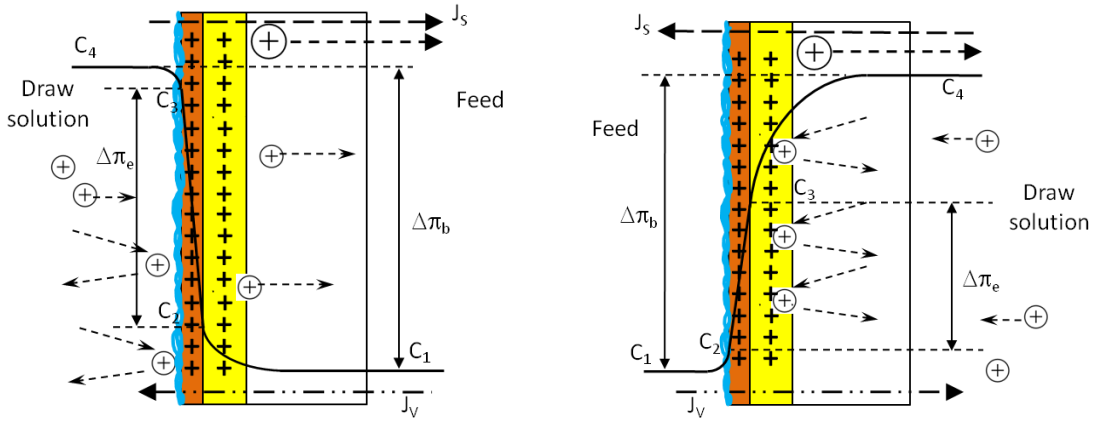

Figure 6.13. Illustration of effective osmotic pressure difference in a PEI cross-linked + MLPE deposition dual layer membrane (■ polyelectrolyte layer; ■ selective layer; ■ cross-linked PAI layer; □ PES layer) in the orientation of (a) AL-DS; (b) AL-FW.

An overall comparison of single layer and dual layer FO hollow fiber membranes is listed in Table 6.10. It is shown that there is an improvement in FO water flux for dual layer hollow fiber membranes made from PAI as the outer layer and PES as the inner layer. The PES inner layer remains intact during the cross-linking reaction with PEI resulting in a more porous support layer. In addition, the porosity of the inner layer can be easily tailored since the outer and inner layers are developed from different polymer dopes during dual layer hollow fiber spinning process.

Table 6.10. Overall comparison of single layer and dual layer FO hollow fiber membranes.

Membrane	PWP ($l/m^2.h.bar$)	Salt rej (%)	FO performances			FO conditions		Ref.
			Orientation	J_v ($l/m^2.h$)	J_s/J_v (g/l)	DS	FW	
Single layer PAI, ST#2	2.25	92.7 ($MgCl_2$)	AL-DS	13.1	0.73	0.5 M $MgCl_2$	DI-water	Ch.3
			AL-FW	8.40	0.29			
Single layer PAI, ST#3	2.19	91.1 ($MgCl_2$)	AL-DS	13.2	1.19	0.5 M $MgCl_2$	DI-water	Ch.3
			AL-FW	9.70	0.29			
Improved single layer PAI, ST#3	4.10	85.0 (Na_2SO_4)	AL-DS	29.0	0.30	0.5 M Na_2SO_4	DI-water	Ch.4
			AL-FW	13.0	0.20			
Improved single layer PAI, ST#4	4.30	69.0 (Na_2SO_4)	AL-DS	26.0	0.70	0.5 M Na_2SO_4	DI-water	Ch.4
			AL-FW	14.0	0.30			
Dual layer PAI-PES DL-C-25K-d	4.10	97.0 ($MgCl_2$)	AL-DS	39.3	0.35	0.5 M $MgCl_2$	DI-water	Ch 6
			AL-FW	20.8	0.31			
Dual layer PAI-PES DL-C-750K-d	3.50	97.0 ($MgCl_2$)	AL-DS	37.6	0.41	0.5 M $MgCl_2$	DI-water	Ch 6
			AL-FW	19.8	0.29			

6.4. Conclusions

Microporous dual layer hollow fiber membranes using PAI as the selective layer and PES as the inner support layer have been successfully fabricated with a delamination-free structure. The compositions of the inner polymer solutions, coagulation water bath temperature, etc. determine the morphology and structure of dual layer hollow fiber membranes.

A simple chemical cross-linking and multilayer polyelectrolytes depositions on the microporous dual layer hollow fiber have been carried out to develop a suitable FO membrane. The resultant novel FO membranes present promising performance in AL-DS and AL-FW configurations for FO application. A water flux of 40 l/m^2.h and J_s/J_v of 0.35 g/l were achieved using a 0.5 M $MgCl_2$ as draw solution and DI-water as feed at room temperature for AL-DS configuration. In the AL-FW configuration, the water flux of 20 l/m^2.h and J_s/J_v of 0.35 g/l were achieved using the same condition of the draw solution and the feed.

CHAPTER 7

Conclusions and Recommendations

7.1. Overall conclusions

This thesis presents the development of novel hollow fiber membranes for FO application. The current FO membranes are subjected to a lower than expected flux decline due to internal concentration polarization (ICP). Therefore, a membrane with a thin and porous support layer is needed to reduce the effect of ICP, meanwhile a dense ultra-thin selective layer with high water permeability and high salt reject is desirable. A series of novel FO hollow fiber membranes were developed by either single layer hollow fiber spinning followed by chemical cross-linking (Chapter 3) and further polyelectrolyte deposition (Chapter 4) or dual layer hollow fiber spinning (Chapter 5) followed by chemical modifications (Chapter 6).

Fabrication and modification of single layer FO hollow fiber membranes made from poly(amide-imide) (PAI) material have been investigated. The resulting membranes have a NF-like selective layer supported by a porous polymer matrix. The porous support, however, has been affected by the cross-linking reaction during the development of the NF-like selective layer. Further improvement has been proposed by fabricating a membrane with an inert support layer via dual layer hollow fiber spinning process. In the fabrication of dual layer hollow fiber membranes, the mechanisms associated with the lamination/delamination of the outer and inner layers as well as regular/irregular cross-section and macrovoids morphology were investigated systematically. All the membranes were characterized by the standard protocol in terms of structure and morphology, pore size and pore size distribution, pure water permeability, salt rejection, FO performance, etc.

The major findings and conclusions are summarized as follows:

- Single layer PAI FO hollow fiber membranes have been successfully fabricated by the phase inversion method followed by simple chemical cross-linking using a PEI solution to develop a positively charged NF-like selective layer. By varying the reaction parameters (e.g., temperature, time, and concentration), the pore size of the selective layer can be easily tailored.

- In the FO process, the positively charged single layer hollow fiber membrane has a FO water flux of 9.74 l/m^2.h and the ratio of salt to water flux ,J_s/J_v, less than 0.4 g/l when using 0.5 M $MgCl_2$ as a draw solution and DI water as the feed in the AL-FW configuration at 23°C.

- Different from a neutral membrane, the positively charged FO membrane provides double electric repulsions to the salt transfer through the membrane in the AL-FW configuration, leading to a reduction of salt penetration, while in the AL-DS configuration, the positive charges facilitate salt transportation.

- The positively charged membrane surface promotes the attachment of anionic polyelectrolytes such as polystyrene sulfonate (PSS) via electrostatic interactions. Different from the highly positively charged membranes, the PSS deposited membranes can maintain a steady water flux of 14 l/m^2.h when the feed contained 1000 ppm BSA and a 0.5 M Na_2SO_4 was used as the draw solution in the AL-FW configuration at ambient temperature of 23 °C.

- The morphology of the resultant dual layer fibers can vary from severe delamination to excellent adhesion between the two layers, from a distortion of finger-like structures and an irregular inner contour to an appropriate morphology of the polymer matrix. The thermodynamic properties and phase separation kinetics of two polymer dope solutions as well as various spinning parameters affect the evolution of the membrane morphology and structure.

- When the external coagulant, water, has a higher diffusion rate in the outer layer than in the inner layer, the outer layer tends to expand to form large macrovoids and to hold more water at the interface. As a result, the accumulated water

impedes the adhesion of the two layers, leading to a delamination of two layers of the dual layer hollow fiber membranes.

- If water has a slower penetration rate through the outer layer dope than the inner layer dope, a good adhesion of these two layers is expected. Under this scenario, since macrovoids may form in the inner layer leading to the expansion of the inner layer, the distortion of the finger-like structures/macrovoids in the inner layer and irregularity of the inner contour may occur.

- A simple chemical cross-linking and multilayer polyelectrolytes depositions on the microporous dual layer hollow fiber has been done to develop a suitable FO membrane. The resultant novel FO membranes present promising performance in AL-DS and AL-FW configurations for FO application. A water flux of 40 l/m^2.h and J_s/J_v of 0.35 g/l were achieved using 0.5 M $MgCl_2$ as the draw solution and DI-water as the feed at room temperature for AL-DS configuration. In the AL-FW configuration, the water flux of 20 l/m^2.h and J_s/J_v of 0.35 g/l were achieved using the same condition of the draw solution and feed. Significantly higher FO water flux can be achieved when an inert polymer to PEI cross-linking reaction is employed as the support layer.

7.2. Recommendations for future research

The following tasks are suggested as future projects to spring board from this work:

- Different pairs of polymer dope solutions can be used to make dual layer hollow fiber membranes to deepen the understanding and to further assess the hypothesis proposed in Chapter 5. As mentioned in Chapter 5, the rate of non-solvent diffusion through the outer and inner layer plays an important role in lamination/delamination of outer and inner layer as well as in regular/irregularity of cross-section morphology and macrovoids structure. Polymer/solvent/non-solvent system for either outer layer or inner layer can be varied to obtain a dual layer membrane with appropriate water and salt permeability.

- Other spinning parameters which are not studied in this thesis, which include temperature of bore fluid and polymer dopes, types of internal and external

coagulants (e.g., alcohols, etc), and take up speed, etc., are suggested to study in the future.

- Using a higher PAI concentration in the outer polymer dope solution to enhance the charge density after PEI cross-linking is the next step to further improve the selective layer of the membranes. A new system has to be designed precisely to avoid delamination as well as irregular morphology of cross-section and finger-like macrovoids.

- Polymers with a high hydrophilicity can be considered as the support layer of dual layer hollow fiber membranes to enhance water permeability. An option is to use sulfonated polymers such as sufonated polyethersulfone (SPES), sulfonated polyetherether ketone (SPEEK), etc. However, the major drawback of these polymers is that they can swell easily and have weak mechanical strength. Therefore, they can be blended with PES as the inner layer material to increase the membrane hydrophilicity, and hence water flux. In addition, polyacrylonitrile (PAN) is a potential candidate to substitute PES as the support layer due to its hydrophilicity and solvent resistance ability. PAN is widely used as the material of UF membrane prepared via the phase inversion technique (Wang, Yue *et al.* 2006; Qiu, Qi *et al.* 2011).

- FO process can be performed in two orientations. One is active layer facing draw solution (AL-DS) and the other one is active layer facing feed water (AL-FW). Normally, AL-DS orientation is favorable since it can produce higher water flux than AL-FW orientation as the latter suffers more severe dilutive ICP when the draw solution is inside the porous support layer (Wang, Shi *et al.* 2010). In the orientation of AL-DS, on the other hand, the feed flows against the porous support layer. When the feed contains particles/foulants, they can easily penetrate into the porous support and clog the pores. Pore clogging reduces the water flux and is difficult to clean. Therefore, double skinned FO membranes can be designed to retain the draw solutes and the particles/foulants from the feed solution.

- Mathematical equations can be developed to correlate the membrane fabrication parameters, membrane properties, operating and feed conditions as well as the

separation requirements. Fabrication parameters (such as characteristics and concentration of polymer, non-solvent additives and solvent, air gap/evaporation period, internal and external coagulants, temperature and take up speed) affect the properties of fabricated membrane as illustrated in Figure 7.1. Membrane properties (such as pore size, tortuosity, porosity, etc) as well as operating and feed conditions (such as cross-flow velocity, temperature, etc) influence the separation requirements (e.g. water flux and salt rejection)

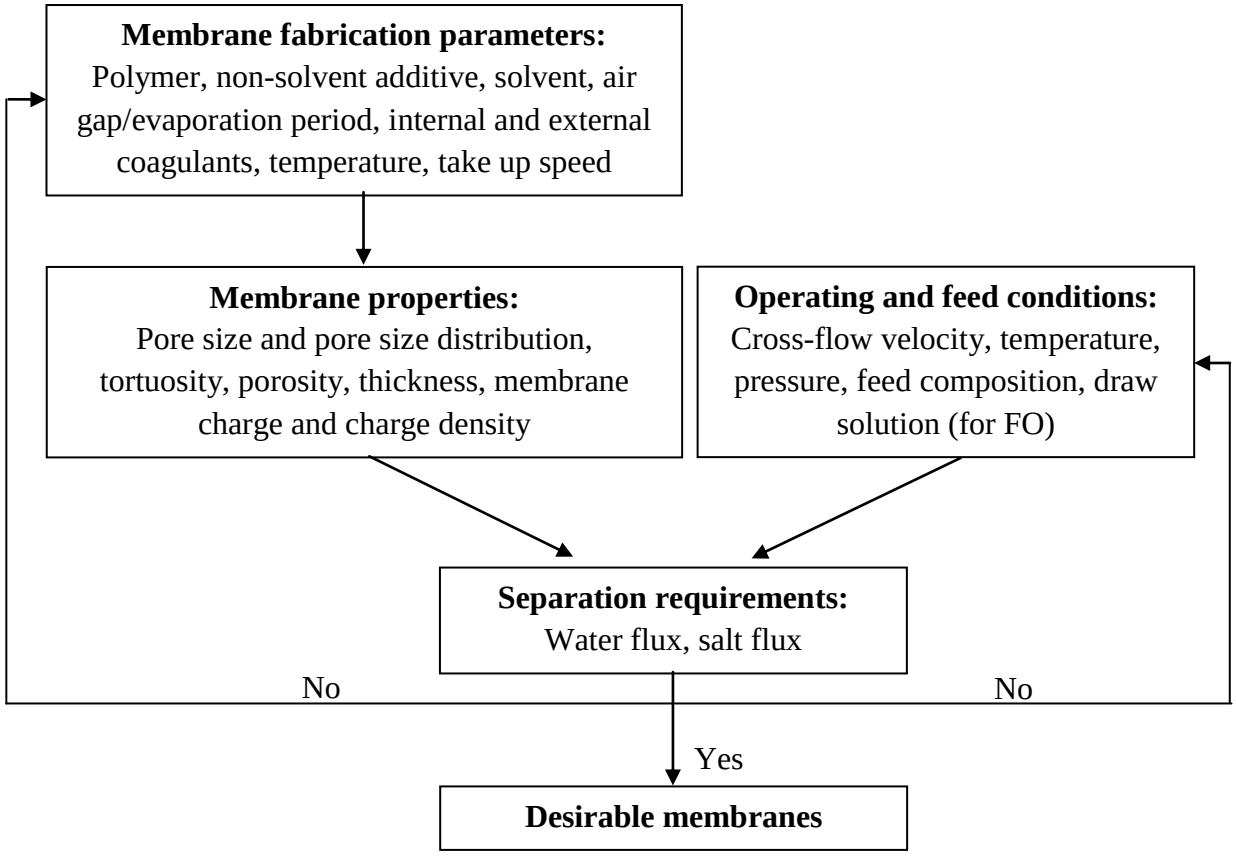

Figure 7.1. Correlation of membrane parameters involved in the desirable membrane fabrication

References

Achilli, A., Cath, T. Y. and Childress, A. E. (2009a), "Power generation with pressure retarded osmosis: an experimental and theoretical investigation", Journal of Membrane Science, Vol. 343, No. 1-2, pp. 42-52.

Achilli, A., Cath, T. Y. and Childress, A. E. (2010), "Selection of inorganic-based draw solutions for forward osmosis applications", Journal of Membrane Science, Vol. 364, No. 1-2, pp. 233-241.

Achilli, A., Cath, T. Y., Marchand, E. A. and Childress, A. E. (2009b), "The forward osmosis membrane bioreactor: a low fouling alternative to MBR processes", Desalination, Vol. 239, No. 1-3, pp. 10-21.

Ahmed, I., Idris, A. and Pa, N. F. C. (2010), "Novel method of synthesizing poly(ether sulfone) membranes containing two solvents and a lithium chloride additive and their performance", Journal of Applied Polymer Science, Vol. 115, No. 3, pp. 1428-1437.

Akbari, A., Desclaux, S., Rouch, J. C. and Remigy, J. C. (2007), "Application of nanofiltration hollow fibre membranes, developed by photografting, to treatment of anionic dye solutions", Journal of Membrane Science, Vol. 297, No. 1-2, pp. 243-252.

Al-Amoudi, A. S. (2010), "Factors affecting natural organic matter (NOM) and scaling fouling in NF membranes: A review", Desalination, Vol. 259, No. 1-3, pp. 1-10.

Alborzfar, M., Jonsson, G. and Grøn, C. (1998), "Removal of natural organic matter from two types of humic ground waters by nanofiltration", Water Research, Vol. 32, No. 10, pp. 2983-2994.

Albrecht, W., Weigel, T., Schossig-Tiedemann, M., Kneifel, K., Peinemann, K. V. and Paul, D. (2001), "Formation of hollow fiber membranes from poly(ether imide) at wet phase inversion using binary mixtures of solvents for the preparation of the dope", Journal of Membrane Science, Vol. 192, No. 1-2, pp. 217-230.

Anton-Paar (2009), Instruction Manual SurPASS Electrokinetic Analyzer, Anton Paar GmbH, Graz, Austria.

Ba, C., Langer, J. and Economy, J. (2009), "Chemical modification of P84 copolyimide membranes by polyethylenimine for nanofiltration", Journal of Membrane Science, Vol. 327, No. 1-2, pp. 49-58.

Balasubramanian, D. and Shaikh, R. (1973), "On the interaction of lithium salts with model amides", Biopolymers, Vol. 12, No. 7, pp. 1639-1650.

Barzin, J. and Sadatnia, B. (2008), "Correlation between macrovoid formation and the ternary phase diagram for polyethersulfone membranes prepared from two nearly similar solvents", Journal of Membrane Science, Vol. 325, No. 1, pp. 92-97.

Batchelder, G. W. (1965), Process for the demineralization of water. U. S. Patents. USA

Bonyadi, S. and Chung, T. S. (2007), "Flux enhancement in membrane distillation by fabrication of dual layer hydrophilic-hydrophobic hollow fiber membranes", Journal of Membrane Science, Vol. 306, No. 1-2, pp. 134-146.

Bonyadi, S., Chung, T. S. and Krantz, W. B. (2007), "Investigation of corrugation phenomenon in the inner contour of hollow fibers during the non-solvent induced phase-separation process", Journal of Membrane Science, Vol. 299, No. 1-2, pp. 200-210.

Boom, R. M., Wienk, I. M., Van Den Boomgaard, T. and Smolders, C. A. (1992), "Microstructures in phase inversion membranes. Part 2. The role of a polymeric additive", Journal of Membrane Science, Vol. 73, No. 2-3, pp. 277-292.

Bottino, A., Camera-Roda, G., Capannelli, G. and Munari, S. (1991), "The formation of microporous polyvinylidene difluoride membranes by phase separation", Journal of Membrane Science, Vol. 57, No. 1, pp. 1-20.

Bruening, M. L., Dotzauer, D. M., Jain, P., Ouyang, L. and Baker, G. L. (2008), "Creation of functional membranes using polyelectrolyte multilayers and polymer brushes", Langmuir, Vol. 24, No. 15, pp. 7663-7673.

Cabasso, I., Klein, E. and Smith, J. K. (1976), "Polysulfone hollow fibers. I. Spinning and properties", Journal of Applied Polymer Science, Vol. 20, No. 9, pp. 2377-2394.

Cath, T. Y., Childress, A. E. and Elimelech, M. (2006), "Forward osmosis: principles, applications, and recent developments", Journal of Membrane Science, Vol. 281, No. 1-2, pp. 70-87.

Cheng, L.-P. (1999), "Effect of Temperature on the Formation of Microporous PVDF Membranes by Precipitation from 1-Octanol/DMF/PVDF and Water/DMF/PVDF Systems", Macromolecules, Vol. 32, No. 20, pp. 6668-6674.

Cheng, S., Oatley, D. L., Williams, P. M. and Wright, C. J. (2011), "Positively charged nanofiltration membranes: Review of current fabrication methods and introduction of a novel approach", Advances in Colloid and Interface Science, Vol. 164, No. 1-2, pp. 12-20.

Childress, A. E. and Elimelech, M. (2000), "Relating Nanofiltration Membrane Performance to Membrane Charge (Electrokinetic) Characteristics", Environmental Science & Technology, Vol. 34, No. 17, pp. 3710-3716.

Chiu, T. Y. and James, A. E. (2007), "Electrokinetic characterisation techniques on asymmetric microfiltration membranes", Colloids and Surfaces A: Physicochemical and Engineering Aspects, Vol. 301, No. 1-3, pp. 281-288.

Choi, J. and Rubner, M. F. (2005), "Influence of the degree of ionization on weak polyelectrolyte multilayer assembly", Macromolecules, Vol. 38, No. 1, pp. 116-124.

Choo, C. G., Rychnovsky, S. D. and Etter, M. C. (1994), "Crystal and Molecular Studies of Succinimide-Lithium Salt Complexes", Chemistry of Materials, Vol. 6, No. 8, pp. 1200-1205.

Chou, S., Shi, L., Wang, R., Tang, C. Y., Qiu, C. and Fane, A. G. (2010), "Characteristics and potential applications of a novel forward osmosis hollow fiber membrane", Desalination, Vol. 261, No., pp. 365-372.

Chou, S., Wang, R., Shi, L., She, Q., Tang, C. and Fane, A. G. (2012), "Thin-film composite hollow fiber membranes for pressure retarded osmosis (PRO) process with high power density", Journal of Membrane Science, Vol. 389, No., pp. 25-33.

Chung, T.-S. (1997), "A Critical Review of Polybenzimidazoles -- Historical Development and Future R&D", Polymer Review, Vol. 37, No. 2, pp. 277 - 301.

Chung, T.-S., Qin, J.-J. and Gu, J. (2000), "Effect of shear rate within the spinneret on morphology, separation performance and mechanical properties of ultrafiltration polyethersulfone hollow fiber membranes", Chemical Engineering Science, Vol. 55, No. 6, pp. 1077-1091.

Chung, T. S., Kafchinski, E. R. and Foley, P. (1992), "Development of asymmetric hollow fibers from polyimides for air separation", Journal of Membrane Science, Vol. 75, No. 1-2, pp. 181-195.

Cornelissen, E. R., Harmsen, D., De Korte, K. F., Ruiken, C. J., Qin, J. J., Oo, H. and Wessels, L. P. (2008), "Membrane fouling and process performance of forward osmosis membranes on activated sludge", Journal of Membrane Science, Vol. 319, No. 1-2, pp. 158-168.

Decher, G. (1997), "Fuzzy nanoassemblies: Toward layered polymeric multicomposites", Science, Vol. 277, No. 5330, pp. 1232-1237.

Ding, X., Cao, Y., Zhao, H., Wang, L. and Yuan, Q. (2008), "Fabrication of high performance Matrimid/polysulfone dual-layer hollow fiber membranes for O2/N2 separation", Journal of Membrane Science, Vol. 323, No. 2, pp. 352-361.

Duarte, L. T., Pereira, C. C., Habert, A. C. and Borges, C. P. (2008), "Polyurethane/polyethersulphone composite hollow fibers produced by simultaneous spinning of two polymer solutions", Journal of Membrane Science, Vol. 311, No. 1-2, pp. 12-22.

Elimelech, M. and Mc Cutcheon, J. (2008), Method for designing membranes for osmotically driven membrane processes: Yale University (Two Whitney Avenue, New Haven, CT, 06511, US), Elimelech, Menachem (39 Brookwood Drive, Woodbridge, CT, 06525, US), Mc Cutcheon, Jeffrey (31 Branch Lane, East Setauket, NY, 11733, US)

Evans, C. D., Monteith, D. T. and Cooper, D. M. (2005), "Long-term increases in surface water dissolved organic carbon: Observations, possible causes and environmental impacts", Environmental Pollution, Vol. 137, No. 1, pp. 55-71.

Fang, W., Wang, R., Chou, S., Setiawan, L. and Fane, A. G. (2012), "Composite forward osmosis hollow fiber membranes: Integration of RO- and NF-like selective layers to enhance membrane properties of anti-scaling and anti-internal concentration polarization", Journal of Membrane Science, Vol. 394-395, No. 0, pp. 140-150.

Frank, B. S. (1972), Desalination of sea water. U. S. Patents. USA

Frank, M., Bargeman, G., Zwijnenburg, A. and Wessling, M. (2001), "Capillary hollow fiber nanofiltration membranes", Separation and Purification Technology, Vol. 22-23, No., pp. 499-506.

Garcia-Castello, E. M., McCutcheon, J. R. and Elimelech, M. (2009), "Performance evaluation of sucrose concentration using forward osmosis", Journal of Membrane Science, Vol. 338, No. 1-2, pp. 61-66.

Gray, G. T., McCutcheon, J. R. and Elimelech, M. (2006), "Internal concentration polarization in forward osmosis: role of membrane orientation", Desalination, Vol. 197, No. 1-3, pp. 1-8.

Greene, G. and Tannenbaum, R. (2004), "Adsorption of polyelectrolyte multilayers on plasma-modified porous polyethylene", Applied Surface Science, Vol. 233, No. 1-4, pp. 336-342.

Hancock, N. T. and Cath, T. Y. (2009), "Solute coupled diffusion in osmotically driven membrane processes", Environmental Science and Technology, Vol. 43, No. 17, pp. 6769-6775.

He, T., Frank, M., Mulder, M. H. V. and Wessling, M. (2008), "Preparation and characterization of nanofiltration membranes by coating polyethersulfone hollow fibers with sulfonated poly(ether ether ketone) (SPEEK)", Journal of Membrane Science, Vol. 307, No. 1, pp. 62-72.

He, T., Mulder, M. H. V., Strathmann, H. and Wessling, M. (2002), "Preparation of composite hollow fiber membranes: co-extrusion of hydrophilic coatings onto porous hydrophobic support structures", Journal of Membrane Science, Vol. 207, No. 2, pp. 143-156.

Herron, J. C., or, Us) (2008), Asymmetric forward osmosis membranes. United States: Hydration Technologies Inc. (Albany, OR, US)

Higuchi, A., Yoshikawa, M., Guiver, M. D. and Robertson, G. P. (2005), "Vapor permeation and pervaporation of aqueous 2-propanol solutions through the Torlon® poly(amide imide) membrane", Separation Science and Technology, Vol. 40, No. 13, pp. 2697-2707.

Hoffmann, K. and Tieke, B. (2009), "Layer-by-layer assembled membranes containing hexacyclen-hexaacetic acid and polyethyleneimine N-acetic acid and their ion selective permeation behaviour", Journal of Membrane Science, Vol. 341, No. 1-2, pp. 261-267.

Hong, S. U. and Bruening, M. L. (2006), "Separation of amino acid mixtures using multilayer polyelectrolyte nanofiltration membranes", Journal of Membrane Science, Vol. 280, No. 1-2, pp. 1-5.

Hong, S. U., Malaisamy, R. and Bruening, M. L. (2006), "Optimization of flux and selectivity in Cl^-/SO_4^{2-} separations with multilayer polyelectrolyte membranes", Journal of Membrane Science, Vol. 283, No. 1-2, pp. 366-372.

Hong, S. U., Malaisamy, R. and Bruening, M. L. (2007), "Separation of fluoride from other monovalent anions using multilayer polyelectrolyte nanofiltration membranes", Langmuir, Vol. 23, No. 4, pp. 1716-1722.

Hong, S. U., Ouyang, L. and Bruening, M. L. (2009), "Recovery of phosphate using multilayer polyelectrolyte nanofiltration membranes", Journal of Membrane Science, Vol. 327, No. 1-2, pp. 2-5.

Jiang, L., Chung, T.-S., Li, D. F., Cao, C. and Kulprathipanja, S. (2004), "Fabrication of Matrimid/polyethersulfone dual-layer hollow fiber membranes for gas separation", Journal of Membrane Science, Vol. 240, No. 1-2, pp. 91-103.

Jin, W., Toutianoush, A. and Tieke, B. (2003), "Use of polyelectrolyte layer-by-layer assemblies as nanofiltration and reverse osmosis membranes", Langmuir, Vol. 19, No. 7, pp. 2550-2553.

Kang, J. S. and Lee, Y. M. (2002), "Effects of molecular weight of polyvinylpyrrolidone on precipitation kinetics during the formation of asymmetric polyacrylonitrile membrane", Journal of Applied Polymer Science, Vol. 85, No. 1, pp. 57-68.

Kang, Y. S., Kim, H. J. and Kim, U. Y. (1987), "Asymmetric membrane formation via immersion precipitation method. I. Kinetic effect", Journal of Membrane Science, Vol. 60, No. 2-3, pp. 219-232.

Khayet, M. (2003), "The effects of air gap length on the internal and external morphology of hollow fiber membranes", Chemical Engineering Science, Vol. 58, No. 14, pp. 3091-3104.

Khayet, M., Feng, C. Y., Khulbe, K. C. and Matsuura, T. (2002), "Preparation and characterization of polyvinylidene fluoride hollow fiber membranes for ultrafiltration", Polymer, Vol. 43, No. 14, pp. 3879-3890.

Khulbe, K. C., Feng, C. Y., Hamad, F., Matsuura, T. and Khayet, M. (2004), "Structural and performance study of micro porous polyetherimide hollow fiber membranes prepared at different air-gap", Journal of Membrane Science, Vol. 245, No. 1-2, pp. 191-198.

Klitzing, R. V. and Tieke, B. (2004), Polyelectrolyte Membranes. Advances in Polymer Science. 165**:** 177-210 p.

Kneifel, K. and Peinemann, K. V. (1992), "Preparation of hollow fiber membranes from polyetherimide for gas separation", Journal of Membrane Science, Vol. 65, No. 3, pp. 295-307.

Kong, J. and Li, K. (2001), "Preparation of PVDF hollow-fiber membranes via immersion precipitation", Journal of Applied Polymer Science, Vol. 81, No. 7, pp. 1643-1653.

Kosuri, M. R. and Koros, W. J. (2008), "Defect-free asymmetric hollow fiber membranes from Torlon®, a polyamide-imide polymer, for high-pressure CO2 separations", Journal of Membrane Science, Vol. 320, No. 1-2, pp. 65-72.

Krasemann, L. and Tieke, B. (1999), "Composite membranes with ultrathin separation layer prepared by self-assembly of polyelectrolytes", Materials Science and Engineering C, Vol. 8-9, No., pp. 513-518.

Krasemann, L. and Tieke, B. (2000), "Selective ion transport across self-assembled alternating multilayers of cationic and anionic polyelectrolytes", Langmuir, Vol. 16, No. 2, pp. 287-290.

Krasemann, L., Toutianoush, A. and Tieke, B. (2001), "Self-assembled polyelectrolyte multilayer membranes with highly improved pervaporation separation of ethanol/water mixtures", Journal of Membrane Science, Vol. 181, No. 2, pp. 221-228.

Kravath, R. E. and Davis, J. A. (1975), "Desalination of sea water by direct osmosis", Desalination, Vol. 16, No. 2, pp. 151-155.

Kuo, C.-H., Chang, H.-Y., Liu, C.-P., Lee, S.-H., You, Y.-W. and Shyue, J.-J. (2011), "Effect of surface chemical composition on the surface potential and iso-electric point of silicon substrates modified with self-assembled monolayers", Physical Chemistry Chemical Physics, Vol. 13, No. 9, pp. 3649-3653.

Kurth, C. J. and Burk, R. L. (2009), Thin film membranes with additives for forward and pressure retarded osmosis. United States: NANOH20 INC. (Los Angeles, CA, US)

Lajimi, R. H., Abdallah, A. B., Ferjani, E., Roudesli, M. S. and Deratani, A. (2004), "Change of the performance properties of nanofiltration cellulose acetate membranes

by surface adsorption of polyelectrolyte multilayers", Desalination, Vol. 163, No. 1-3, pp. 193-202.

Lee, K. L., Baker, R. W. and Lonsdale, H. K. (1981), "Membranes for power generation by pressure-retarded osmosis", Journal of Membrane Science, Vol. 8, No. 2, pp. 141-171.

Li, D., Chung, T.-S. and Wang, R. (2004), "Morphological aspects and structure control of dual-layer asymmetric hollow fiber membranes formed by a simultaneous co-extrusion approach", Journal of Membrane Science, Vol. 243, No. 1-2, pp. 155-175.

Li, X., Goyens, W., Ahmadiannamini, P., Vanderlinden, W., De Feyter, S. and Vankelecom, I. (2010), "Morphology and performance of solvent-resistant nanofiltration membranes based on multilayered polyelectrolytes: Study of preparation conditions", Journal of Membrane Science, Vol. 358, No. 1-2, pp. 150-157.

Li, Y. and Chung, T.-S. (2008), "Exploration of highly sulfonated polyethersulfone (SPES) as a membrane material with the aid of dual-layer hollow fiber fabrication technology for protein separation", Journal of Membrane Science, Vol. 309, No. 1-2, pp. 45-55.

Lin, Y.-C., Yu, B.-Y., Lin, W.-C., Lee, S.-H., Kuo, C.-H. and Shyue, J.-J. (2009), "Tailoring the surface potential of gold nanoparticles with self-assembled monolayers with mixed functional groups", Journal of Colloid and Interface Science, Vol. 340, No. 1, pp. 126-130.

Ling, M. M., Wang, K. Y. and Chung, T.-S. (2010), "Highly Water-Soluble Magnetic Nanoparticles as Novel Draw Solutes in Forward Osmosis for Water Reuse", Industrial & Engineering Chemistry Research, Vol. 49, No. 12, pp. 5869-5876.

Liu, J.-Q., Xu, Z.-L., Li, X.-H., Zhang, Y., Zhou, Y., Wang, Z.-X. and Wang, X.-J. (2007), "An improved process to prepare high separation performance PA/PVDF hollow fiber composite nanofiltration membranes", Separation and Purification Technology, Vol. 58, No. 1, pp. 53-60.

Liu, R. X., Qiao, X. Y. and Chung, T.-S. (2007), "Dual-layer P84/polyethersulfone hollow fibers for pervaporation dehydration of isopropanol", Journal of Membrane Science, Vol. 294, No. 1-2, pp. 103-114.

Liu, T., Xu, S., Zhang, D., Sourirajan, S. and Matsuura, T. (1991), "Pore size and pore size distribution on the surface of polyethersulfone hollow fiber membranes", Desalination, Vol. 85, No. 1, pp. 1-12.

Liu, Y., Koops, G. H. and Strathmann, H. (2003), "Characterization of morphology controlled polyethersulfone hollow fiber membranes by the addition of polyethylene glycol to the dope and bore liquid solution", Journal of Membrane Science, Vol. 223, No. 1-2, pp. 187-199.

Loeb, S. and Sourirajan, S. (1963), "Seawater demineralisation by means of an osmotic membrane", Advances in Chemistry Series, Vol. 38, No., pp. 117-132.

Loeb, S., Titelman, L., Korngold, E. and Freiman, J. (1997), "Effect of porous support fabric on osmosis through a Loeb-Sourirajan type asymmetric membrane", Journal of Membrane Science, Vol. 129, No. 2, pp. 243-249.

Loh, C. H., Wang, R., Shi, L. and Fane, A. G. (2011), "Fabrication of high performance polyethersulfone UF hollow fiber membranes using amphiphilic Pluronic block copolymers as pore-forming additives", Journal of Membrane Science, Vol. 380, No. 1-2, pp. 114-123.

Malaisamy, R. and Bruening, M. L. (2005), "High-flux nanofiltration membranes prepared by adsorption of multilayer polyelectrolyte membranes on polymeric supports", Langmuir, Vol. 21, No. 23, pp. 10587-10592.

Mansourizadeh, A. and Ismail, A. F. (2010), "Effect of additives on the structure and performance of polysulfone hollow fiber membranes for CO2 absorption", Journal of Membrane Science, Vol. 348, No. 1-2, pp. 260-267.

McCutcheon, J. R. and Elimelech, M. (2006), "Influence of concentrative and dilutive internal concentration polarization on flux behavior in forward osmosis", Journal of Membrane Science, Vol. 284, No. 1-2, pp. 237-247.

McCutcheon, J. R. and Elimelech, M. (2008), "Influence of membrane support layer hydrophobicity on water flux in osmotically driven membrane processes", Journal of Membrane Science, Vol. 318, No. 1-2, pp. 458-466.

McCutcheon, J. R., McGinnis, R. L. and Elimelech, M. (2005), "A novel ammonia-carbon dioxide forward (direct) osmosis desalination process", Desalination, Vol. 174, No. 1, pp. 1-11.

McCutcheon, J. R., McGinnis, R. L. and Elimelech, M. (2006), "Desalination by ammonia-carbon dioxide forward osmosis: Influence of draw and feed solution concentrations on process performance", Journal of Membrane Science, Vol. 278, No. 1-2, pp. 114-123.

McGinnis, R. L. (2002), Osmotic desalinization process. U. S. Patents. USA

McGinnis, R. L. and Elimelech, M. (2007), "Energy requirements of ammonia-carbon dioxide forward osmosis desalination", Desalination, Vol. 207, No. 1-3, pp. 370-382.

McGinnis, R. L., McCutcheon, J. R. and Elimelech, M. (2007), "A novel ammonia-carbon dioxide osmotic heat engine for power generation", Journal of Membrane Science, Vol. 305, No. 1-2, pp. 13-19.

Miao, J., Chen, G. H. and Gao, C. J. (2005), "A novel kind of amphoteric composite nanofiltration membrane prepared from sulfated chitosan (SCS)", Desalination, Vol. 181, No. 1-3, pp. 173-183.

Miller, M. D. and Bruening, M. L. (2004), "Controlling the nanofiltration properties of multilayer polyelectrolyte membranes through variation of film composition", Langmuir, Vol. 20, No. 26, pp. 11545-11551.

Moriya, A., Maruyama, T., Ohmukai, Y., Sotani, T. and Matsuyama, H. (2009), "Preparation of poly(lactic acid) hollow fiber membranes via phase separation methods", Journal of Membrane Science, Vol. 342, No. 1-2, pp. 307-312.

Mulder, M. (1996), Basic Principles of Membrane Technology, 2. Springer,

Nanda, D., Tung, K.-L., Hsiung, C.-C., Chuang, C.-J., Ruaan, R.-C., Chiang, Y.-C., Chen, C.-S. and Wu, T.-H. (2008), "Effect of solution chemistry on water softening using charged nanofiltration membranes", Desalination, Vol. 234, No. 1-3, pp. 344-353.

Nightingale, E. R. (1959), "Phenomenological theory of ion solvation. Effective radii of hydrated ions", The Journal of Physical Chemistry, Vol. 63, No. 9, pp. 1381-1387.

Nijdam, W., De Jong, J., Van Rijn, C. J. M., Visser, T., Versteeg, L., Kapantaidakis, G., Koops, G. H. and Wessling, M. (2005), "High performance micro-engineered hollow fiber membranes by smart spinneret design", Journal of Membrane Science, Vol. 256, No. 1-2, pp. 209-215.

Niwa, M., Kawakami, H., Nagaoka, S., Kanamori, T. and Shinbo, T. (2000), "Fabrication of an asymmetric polyimide hollow fiber with a defect-free surface skin layer", Journal of Membrane Science, Vol. 171, No. 2, pp. 253-261.

Ohya, H., Shiki, S. and Kawakami, H. (2009), "Fabrication study of polysulfone hollow-fiber microfiltration membranes: Optimal dope viscosity for nucleation and growth", Journal of Membrane Science, Vol. 326, No. 2, pp. 293-302.

Ouyang, L., Malaisamy, R. and Bruening, M. L. (2008), "Multilayer polyelectrolyte films as nanofiltration membranes for separating monovalent and divalent cations", Journal of Membrane Science, Vol. 310, No. 1-2, pp. 76-84.

Peeters, J. M. M., Boom, J. P., Mulder, M. H. V. and Strathmann, H. (1998), "Retention measurements of nanofiltration membranes with electrolyte solutions", Journal of Membrane Science, Vol. 145, No. 2, pp. 199-209.

Peng, N., Chung, T.-S., Chng, M. L. and Aw, W. (2010), "Evolution of ultra-thin dense-selective layer from single-layer to dual-layer hollow fibers using novel Extem® polyetherimide for gas separation", Journal of Membrane Science, Vol. 360, No. 1-2, pp. 48-57.

Pereira, C. C., Nobrega, R., Peinemann, K. V. and Borges, C. P. (2003), "Hollow fiber membranes obtained by simultaneous spinning of two polymer solutions: a morphological study", Journal of Membrane Science, Vol. 226, No. 1-2, pp. 35-50.

Persson, K. M., Gekas, V. and Trägårdh, G. (1995), "Study of membrane compaction and its influence on ultrafiltration water permeability", Journal of Membrane Science, Vol. 100, No. 2, pp. 155-162.

Petersen, R. J. (1993), "Composite reverse osmosis and nanofiltration membranes", Journal of Membrane Science, Vol. 83, No. 1, pp. 81-150.

Phillip, W. A., Yong, J. S. and Elimelech, M. (2010), "Reverse Draw Solute Permeation in Forward Osmosis: Modeling and Experiments", Environmental Science & Technology, Vol. 44, No. 13, pp. 5170-5176.

Qiao, X. and Chung, T.-S. (2006), "Diamine modification of P84 polyimide membranes for pervaporation dehydration of isopropanol", AIChE Journal, Vol. 52, No. 10, pp. 3462-3472.

Qin, J. and Chung, T. S. (1999), "Effect of dope flow rate on the morphology, separation performance, thermal and mechanical properties of ultrafiltration hollow fibre membranes", Journal of Membrane Science, Vol. 157, No. 1, pp. 35-51.

Qiu, C., Qi, S. and Tang, C. Y. (2011), "Synthesis of high flux forward osmosis membranes by chemically crosslinked layer-by-layer polyelectrolytes", Journal of Membrane Science, Vol. 381, No. 1-2, pp. 74-80.

Ren, J. and Wang, R. Preparation of polymeric membranes. In: L. K.Wang, J. P. Chen, Y.-T. Hung and N. K. Shammas (Ed.). Membrane and desalination technologies. Totowa, NJ, USA: Humana Press, Inc., Vol.13, 2010. Preparation of polymeric membranes

Ren, J., Wang, R., Zhang, H.-Y., Li, Z., Liang, D. T. and Tay, J. H. (2006), "Effect of PVDF dope rheology on the structure of hollow fiber membranes used for CO2 capture", Journal of Membrane Science, Vol. 281, No. 1-2, pp. 334-344.

Reuvers, A. J. and Smolders, C. A. (1987), "Formation of membranes by means of immersion precipitation : Part II. the mechanism of formation of membranes prepared from the system cellulose acetate-acetone-water", Journal of Membrane Science, Vol. 34, No. 1, pp. 67-86.

Robertson, G. P., Guiver, M. D., Yoshikawa, M. and Brownstein, S. (2004), "Structural determination of Torlon® 4000T polyamide-imide by NMR spectroscopy", Polymer, Vol. 45, No. 4, pp. 1111-1117.

Sablani, S. S., Goosen, M. F. A., Al-Belushi, R. and Wilf, M. (2001), "Concentration polarization in ultrafiltration and reverse osmosis: a critical review", Desalination, Vol. 141, No. 3, pp. 269-289.

Sairam, M., Sereewatthanawut, E., Li, K., Bismarck, A. and Livingston, A. G. (2011), "Method for the preparation of cellulose acetate flat sheet composite membranes for forward osmosis-desalination using MgSO4 draw solution", Desalination, Vol. 273, No. 2-3, pp. 299-307.

Santoso, Y. E., Chung, T. S., Wang, K. Y. and Weber, M. (2006), "The investigation of irregular inner skin morphology of hollow fiber membranes at high-speed spinning and the solutions to overcome it", Journal of Membrane Science, Vol. 282, No. 1-2, pp. 383-392.

Schaep, J., Van Der Bruggen, B., Vandecasteele, C. and Wilms, D. (1998), "Influence of ion size and charge in nanofiltration", Separation and Purification Technology, Vol. 14, No. 1-3, pp. 155-162.

Schafer, A. I., Fane, A. G. and Waite, T. D. (1998), "Nanofiltration of natural organic matter: removal, fouling and the influence of multivalent ions", Desalination, Vol. 118, No. 1-3, pp. 109-122.

Schafer, A. I., Fane, A. G. and Waite, T. D. (2005), Nanofiltration - Principles and Applications, Elsevier Advanced Technology, Oxford, UK.

Setiawan, L., Wang, R., Li, K. and Fane, A. G. (2011), "Fabrication of novel poly(amide-imide) forward osmosis hollow fiber membranes with a positively charged nanofiltration-like selective layer", Journal of Membrane Science, Vol. 369, No. 1-2, pp. 196-205.

Shan, W., Bacchin, P., Aimar, P., Bruening, M. L. and Tarabara, V. V. (2010), "Polyelectrolyte multilayer films as backflushable nanofiltration membranes with tunable hydrophilicity and surface charge", Journal of Membrane Science, Vol. 349, No. 1-2, pp. 268-278.

Shen, L. Q., Xu, Z. K., Yang, Q., Sun, H. L., Wang, S. Y. and Xu, Y. Y. (2004), "Preparation and characterization of sulfonated polyetherimide/polyetherimide blend membranes", Journal of Applied Polymer Science, Vol. 92, No. 3, pp. 1709-1715.

Shi, L., Chou, S. R., Wang, R., Fang, W. X., Tang, C. Y. and Fane, A. G. (2012), "Effect of substrate structure on the performance of thin-film composite forward osmosis hollow fiber membranes", Journal of Membrane Science, Vol. 382, No. 1-2, pp. 116-123.

Shi, L., Wang, R., Cao, Y., Feng, C., Liang, D. T. and Tay, J. H. (2007), "Fabrication of poly(vinylidene fluoride-co-hexafluropropylene) (PVDF-HFP) asymmetric microporous hollow fiber membranes", Journal of Membrane Science, Vol. 305, No. 1-2, pp. 215-225.

Shi, L., Wang, R., Cao, Y., Liang, D. T. and Tay, J. H. (2008), "Effect of additives on the fabrication of poly(vinylidene fluoride-co-hexafluropropylene) (PVDF-HFP) asymmetric microporous hollow fiber membranes", Journal of Membrane Science, Vol. 315, No. 1-2, pp. 195-204.

Stache, K. (1989), Apparatus for transforming sea water, brackish water, polluted water or the like into a nutrious drink by means of osmosis. U. S. Patents. USA: DD-dynamics Devices Ltd., London, England

Stanton, B. W., Harris, J. J., Miller, M. D. and Bruening, M. L. (2003), "Ultrathin, multilayered polyelectrolyte films as nanofiltration membranes", Langmuir, Vol. 19, No. 17, pp. 7038-7042.

Strathmann, H. and Kock, K. (1977), "The formation mechanism of phase inversion membranes", Desalination, Vol. 21, No. 3, pp. 241-255.

Su, J., Chung, T. S., Helmer, B. J. and De Wit, J. S. (2012), "Enhanced double-skinned FO membranes with inner dense layer for wastewater treatment and macromolecule recycle using Sucrose as draw solute", Journal of Membrane Science, Vol. 396, No., pp. 92-100.

Su, J., Yang, Q., Teo, J. F. and Chung, T. S. (2010), "Cellulose acetate nanofiltration hollow fiber membranes for forward osmosis processes", Journal of Membrane Science, Vol. 355, No. 1-2, pp. 36-44.

Sukitpaneenit, P. and Chung, T.-S. (2012), "High Performance Thin-Film Composite Forward Osmosis Hollow Fiber Membranes with Macrovoid-Free and Highly Porous Structure for Sustainable Water Production", Environmental Science & Technology, Vol. 46, No. 13, pp. 7358-7365.

Sun, S. P., Wang, K. Y., Peng, N., Hatton, T. A. and Chung, T.-S. (2010a), "Novel polyamide-imide/cellulose acetate dual-layer hollow fiber membranes for nanofiltration", Journal of Membrane Science, Vol. 363, No. 1-2, pp. 232-242.

Sun, S. P., Wang, K. Y., Rajarathnam, D., Hatton, T. A. and Chung, T.-S. (2010b), "Polyamide-imide nanofiltration hollow fiber membranes with elongation-induced nano-pore evolution", AIChE Journal, Vol. 56, No. 6, pp. 1481-1494.

Suryanarayan, S., Mika, A. M. and Childs, R. F. (2006), "Gel-filled hollow fiber membranes for water softening", Journal of Membrane Science, Vol. 281, No. 1-2, pp. 397-409.

Tang, C. Y., Chong, T. H. and Fane, A. G. (2011), "Colloidal interactions and fouling of NF and RO membranes: A review", Advances in Colloid and Interface Science, Vol. 164, No. 1-2, pp. 126-143.

Tang, C. Y., She, Q., Lay, W. C. L., Wang, R. and Fane, A. G. (2010), "Coupled effects of internal concentration polarization and fouling on flux behavior of forward osmosis membranes during humic acid filtration", Journal of Membrane Science, Vol. 354, No. 1-2, pp. 123-133.

Tang, W. and Ng, H. Y. (2008), "Concentration of brine by forward osmosis: Performance and influence of membrane structure", Desalination, Vol. 224, No. 1-3, pp. 143-153.

Tasselli, F. and Drioli, E. (2007), "Tuning of hollow fiber membrane properties using different bore fluids", Journal of Membrane Science, Vol. 301, No. 1-2, pp. 11-18.

Temmel, S., Kern, W., Luxbacher, T., Grundke, K., Stamm, M. and Adler, H.-J. R. Zeta Potential of Photochemically Modified Polymer Surfaces-Characterization of Polymer Surfaces and Thin Films. In: (Ed.): Springer, Berlin, Heidelberg, Vol.132, 2006. Zeta Potential of Photochemically Modified Polymer Surfaces-Characterization of Polymer Surfaces and Thin Films, pp.54-61. (Progress in Colloid and Polymer Science)

Teoh, M. M., Chung, T.-S. and Yeo, Y. S. (2011), "Dual-layer PVDF/PTFE composite hollow fibers with a thin macrovoid-free selective layer for water production via membrane distillation", Chemical Engineering Journal, Vol. 171, No. 2, pp. 684-691.

Tieke, B., Toutianoush, A. and Jin, W. (2005), "Selective transport of ions and molecules across layer-by-layer assembled membranes of polyelectrolytes, p-sulfonato-calix[n]arenes and Prussian Blue-type complex salts", Advances in Colloid and Interface Science, Vol. 116, No. 1-3, pp. 121-131.

Tiraferri, A., Yip, N. Y., Phillip, W. A., Schiffman, J. D. and Elimelech, M. (2011), "Relating performance of thin-film composite forward osmosis membranes to support layer formation and structure", Journal of Membrane Science, Vol. 367, No. 1-2, pp. 340-352.

Ulbricht, M. (2006), "Advanced functional polymer membranes", Polymer, Vol. 47, No. 7, pp. 2217-2262.

United-Nations (2004), WORLD POPULATION TO 2300. New York: United Nations Department of Economic and Social Affairs Population Division

Van Ackern, F., Krasemann, L. and Tieke, B. (1998), "Ultrathin membranes for gas separation and pervaporation prepared upon electrostatic self-assembly of polyelectrolytes", Thin Solid Films, Vol. 327-329, No. 1-2, pp. 762-766.

Veríssimo, S., Peinemann, K. V. and Bordado, J. (2005a), "New composite hollow fiber membrane for nanofiltration", Desalination, Vol. 184, No. 1-3, pp. 1-11.

Veríssimo, S., Peinemann, K. V. and Bordado, J. (2005b), "Thin-film composite hollow fiber membranes: An optimized manufacturing method", Journal of Membrane Science, Vol. 264, No. 1-2, pp. 48-55.

Veríssimo, S., Peinemann, K. V. and Bordado, J. (2006), "Influence of the diamine structure on the nanofiltration performance, surface morphology and surface charge of the composite polyamide membranes", Journal of Membrane Science, Vol. 279, No. 1-2, pp. 266-275.

Wang, D., Li, K. and Teo, W. K. (2000), "Highly permeable polyethersulfone hollow fiber gas separation membranes prepared using water as non-solvent additive", Journal of Membrane Science, Vol. 176, No. 2, pp. 147-158.

Wang, J., Yao, Y., Yue, Z. and Economy, J. (2009), "Preparation of polyelectrolyte multilayer films consisting of sulfonated poly (ether ether ketone) alternating with selected anionic layers", Journal of Membrane Science, Vol. 337, No. 1-2, pp. 200-207.

Wang, J., Yue, Z. and Economy, J. (2008), "Novel method to make a continuous micro-mesopore membrane with tailored surface chemistry for use in nanofiltration", Journal of Membrane Science, Vol. 308, No. 1-2, pp. 191-197.

Wang, J., Yue, Z., Ince, J. S. and Economy, J. (2006), "Preparation of nanofiltration membranes from polyacrylonitrile ultrafiltration membranes", Journal of Membrane Science, Vol. 286, No. 1-2, pp. 333-341.

Wang, K. Y. and Chung, T.-S. (2006), "Fabrication of polybenzimidazole (PBI) nanofiltration hollow fiber membranes for removal of chromate", Journal of Membrane Science, Vol. 281, No. 1-2, pp. 307-315.

Wang, K. Y., Chung, T.-S. and Qin, J.-J. (2007), "Polybenzimidazole (PBI) nanofiltration hollow fiber membranes applied in forward osmosis process", Journal of Membrane Science, Vol. 300, No. 1-2, pp. 6-12.

Wang, K. Y., Fei Li, D., Chung, T.-S. and Bor Chen, S. (2004), "The observation of elongation dependent macrovoid evolution in single- and dual-layer asymmetric hollow fiber membranes", Chemical Engineering Science, Vol. 59, No. 21, pp. 4657-4660.

Wang, K. Y., Ong, R. C. and Chung, T. S. (2010), "Double-skinned forward osmosis membranes for reducing internal concentration polarization within the porous sublayer", Industrial and Engineering Chemistry Research, Vol. 49, No. 10, pp. 4824-4831.

Wang, K. Y., Yang, Q., Chung, T.-S. and Rajagopalan, R. (2009), "Enhanced forward osmosis from chemically modified polybenzimidazole (PBI) nanofiltration hollow fiber membranes with a thin wall", Chemical Engineering Science, Vol. 64, No. 7, pp. 1577-1584.

Wang, R., Shi, L., Tang, C. Y., Chou, S., Qiu, C. and Fane, A. G. (2010), "Characterization of novel forward osmosis hollow fiber membranes", Journal of Membrane Science, Vol. 355, No. 1-2, pp. 158-167.

Wang, Y., Goh, S. H., Chung, T. S. and Na, P. (2009), "Polyamide-imide/polyetherimide dual-layer hollow fiber membranes for pervaporation dehydration of C1-C4 alcohols", Journal of Membrane Science, Vol. 326, No. 1, pp. 222-233.

Wei, J., Qiu, C., Tang, C. Y., Wang, R. and Fane, A. G. (2011), "Synthesis and characterization of flat-sheet thin film composite forward osmosis membranes", Journal of Membrane Science, Vol. 372, No. 1-2, pp. 292-302.

Widjojo, N., Chung, T.-S., Arifin, D. Y., Weber, M. and Warzelhan, V. (2010), "Elimination of die swell and instability in hollow fiber spinning process of hyperbranched polyethersulfone (HPES) via novel spinneret designs and precise spinning conditions", Chemical Engineering Journal, Vol. 163, No. 1â€“2, pp. 143-153.

Widjojo, N., Chung, T. S. and Krantz, W. B. (2007), "A morphological and structural study of Ultem/P84 copolyimide dual-layer hollow fiber membranes with delamination-free morphology", Journal of Membrane Science, Vol. 294, No. 1-2, pp. 132-146.

Wienk, I. M., Teunis, H. A., Boomgaard, T. V. D. and Smolders, C. A. (1993), "A new spinning technique for hollow fiber ultrafiltration membranes", Journal of Membrane Science, Vol. 78, No. 1â€“2, pp. 93-100.

Wijmans, J. G., Kant, J., Mulder, M. H. V. and Smolders, C. A. (1985), "Phase separation phenomena in solutions of polysulfone in mixtures of a solvent and a nonsolvent: relationship with membrane formation", Polymer, Vol. 26, No. 10, pp. 1539-1545.

Wilkinson, A. D. M. A. (1997), IUPAC. Compendium of Chemical Terminology, 2. Blackwell Scientific Publications, Oxford.

Wongchitphimon, S., Wang, R., Jiraratananon, R., Shi, L. and Loh, C. H. (2011), "Effect of polyethylene glycol (PEG) as an additive on the fabrication of polyvinylidene fluoride-co-hexafluropropylene (PVDF-HFP) asymmetric microporous hollow fiber membranes", Journal of Membrane Science, Vol. 369, No. 1-2, pp. 329-338.

Xu, Z.-K., Shen, L.-Q., Yang, Q., Liu, F., Wang, S.-Y. and Xu, Y.-Y. (2003), "Ultrafiltration hollow fiber membranes from poly(ether imide): preparation, morphologies and properties", Journal of Membrane Science, Vol. 223, No. 1-2, pp. 105-118.

Xu, Z. L. and Qusay, F. A. (2004), "Effect of polyethylene glycol molecular weights and concentrations on polyethersulfone hollow fiber ultrafiltration membranes", Journal of Applied Polymer Science, Vol. 91, No. 5, pp. 3398-3407.

Yang, F., Zhang, S., Yang, D. and Jian, X. (2007), "Preparation and characterization of polypiperazine amide/PPESK hollow fiber composite nanofiltration membrane", Journal of Membrane Science, Vol. 301, No. 1-2, pp. 85-92.

Yang, Q., Wang, K. Y. and Chung, T.-S. (2009a), "Dual-Layer Hollow Fibers with Enhanced Flux As Novel Forward Osmosis Membranes for Water Production", Environmental Science & Technology, Vol. 43, No. 8, pp. 2800-2805.

Yang, Q., Wang, K. Y. and Chung, T.-S. (2009b), "A novel dual-layer forward osmosis membrane for protein enrichment and concentration", Separation and Purification Technology, Vol. 69, No. 3, pp. 269-274.

Yang, Y., Jian, X., Yang, D., Zhang, S. and Zou, L. (2006), "Poly(phthalazinone ether sulfone ketone) (PPESK) hollow fiber asymmetric nanofiltration membranes: Preparation, morphologies and properties", Journal of Membrane Science, Vol. 270, No. 1-2, pp. 1-12.

Yeow, M. L., Liu, Y. T. and Li, K. (2003), "Isothermal phase diagrams and phase-inversion behavior of poly(vinylidene fluoride)/solvents/additives/water systems", Journal of Applied Polymer Science, Vol. 90, No. 8, pp. 2150-2155.

Yeow, M. L., Liu, Y. T. and Li, K. (2004), "Morphological study of poly(vinylidene fluoride) asymmetric membranes: Effects of the solvent, additive, and dope temperature", Journal of Applied Polymer Science, Vol. 92, No. 3, pp. 1782-1789.

Yip, N. Y., Tiraferri, A., Phillip, W. A., Schiffman, J. D. and Elimelech, M. (2010), "High performance thin-film composite forward osmosis membrane", Environmental Science and Technology, Vol. 44, No. 10, pp. 3812-3818.

Yoon, K., Hsiao, B. S. and Chu, B. (2009), "High flux nanofiltration membranes based on interfacially polymerized polyamide barrier layer on polyacrylonitrile nanofibrous scaffolds", Journal of Membrane Science, Vol. 326, No. 2, pp. 484-492.

Yu, D.-G., Chou, W.-L. and Yang, M. C. (2006), "Effect of bore liquid temperature and dope concentration on mechanical properties and permeation performance of polyacrylonitrile hollow fibers", Separation and Purification Technology, Vol. 51, No. 1, pp. 1-9.

Zhang, G., Gao, X., Ji, S. and Liu, Z. (2009), "One-step dynamic assembly of polyelectrolyte complex membranes", Materials Science and Engineering: C, Vol. 29, No., pp. 1877-1884.

Zhang, G., Ruan, Z., Ji, S. and Liu, Z. (2009), "Construction of Metal-Ligand-Coordinated Multilayers and Their Selective Separation Behavior", Langmuir, Vol. 26, No. 7, pp. 4782-4789.

Zhang, G., Song, X., Ji, S., Wang, N. and Liu, Z. (2008), "Self-assembly of inner skin hollow fiber polyelectrolyte multilayer membranes by a dynamic negative pressure layer-by-layer technique", Journal of Membrane Science, Vol. 325, No. 1, pp. 109-116.

Zhang, S., Wang, K. Y., Chung, T.-S., Chen, H., Jean, Y. C. and Amy, G. (2010), "Well-constructed cellulose acetate membranes for forward osmosis: minimized internal concentration polarization with an ultra-thin selective layer", Journal of Membrane Science, Vol. 360, No. 1-2, pp. 522-535.

Zhang, S., Wang, K. Y., Chung, T.-S., Jean, Y. C. and Chen, H. (2011), "Molecular design of the cellulose ester-based forward osmosis membranes for desalination", Chemical Engineering Science, Vol. 66, No. 9, pp. 2008-2018.

Zularisam, A. W., Ismail, A. F. and Salim, R. (2006), "Behaviours of natural organic matter in membrane filtration for surface water treatment - a review", Desalination, Vol. 194, No. 1-3, pp. 211-231.